Circulating biomarkers in

cancer progression and treatment

Eveline Emma Vietsch

Circulating biomarkers in
cancer progression and treatment

Circulerende biomarkers in kanker progressie en therapie

Thesis

to obtain the degree of Doctor from the
Erasmus University Rotterdam
by command of the rector magnificus
Prof.dr. R.C.M.E. Engels
and in accordance with the decision of the Doctorate Board.

The public defence shall be held on
Wednesday 12 December 2018 at 13.30 hours

by

Eveline Emma Vietsch
born in Seria, Brunei

Erasmus University Rotterdam

Doctoral Committee

Promotors: Prof. dr. C.H.J. van Eijck

Prof. dr. A. Wellstein

Other members: Prof. dr. J.M. Kros

Prof. dr. J.G.J.V. Aerts

Prof. dr. H.W.M. van Laarhoven

Table of contents

CHAPTER 1

Introduction

Adapted from:

Circulating biomarkers to monitor cancer progression and treatment.

Suthee Rapisuwon[1]
Eveline E. Vietsch[1,2]
Anton Wellstein[1]

and

Circulating DNA and Micro-RNA in Patients with Pancreatic Cancer.

Eveline E. Vietsch[1,2]
Casper H.J. van Eijck[2]
Anton Wellstein[1]

1 Department of Oncology, Georgetown University, Washington, DC, USA
2 Department of Surgery, Erasmus Medical Center, Rotterdam, the Netherlands

INTRODUCTION

Tumor Heterogeneity

Cancer presents with dynamic intratumoral and interlesional heterogeneity [1,2]. This process is driven by the genomic instability and rapid proliferation of cancer cells. Over time, cancer cell populations become even more diverse, known as temporal heterogeneity [3]. Tumor heterogeneity follows Darwinian evolutionary principles, where cancer cell subpopulations with optimal phenotypes including distinct surface marker expression, metabolism, proliferation, apoptosis, invasion, angiogenesis, drug sensitivity, and antigen presentation survive in a given tumor [4,5]. Tumor heterogeneity that enables malignant progression and metastatic spread by evolutionary selection is also the major cause of emergent resistance during cancer treatment. Yet, we rely on few standard diagnostic tumor biopsies for the characterization of a given cancer. These biopsies will provide only a partial characterization of the overall makeup of the dynamic systemic disease.

Circulating biomarkers

Tissue biopsies are invasive, expensive and represent a single snapshot in time of an evolving disease. The capturing and analysis of blood-based biomarkers is an alternative method to gain insight into the molecular makeup of cancer in a given patient. The major strength of circulating biomarkers is the possibility to compare serial samples from the same patient and thus generate a molecular readout of disease progression and therapy resistance in real time. Technologies have been rapidly developed over the past decade enabling the assessment of cell free nucleic acids. Extracellular nucleic acids, such as DNA and microRNAs (miRs), are found in almost all human bodily fluids and the circulation provides an attractive alternative to tumor tissue biopsies (Figure 1). The term "circulating" refers to the portion of extracellular molecules that are transported in the cell-free blood compartment. Identification of patient specific cancer markers is crucial for the improvement of controlling this disease. It is conceivable that blood samples can reflect the molecular profile of a primary tumor as well as residual cancer cells that are not accessible physically or below detection on radio graphical imaging. Liquid biopsies can be taken repeatedly to follow evolution of the disease. Circulating DNA and miRs are relatively stable in plasma and serum samples, and easy to quantitate by PCR or sequencing methods. Still, the interpretation of circulating nucleic acids remains challenging. Extensive validation and protocol standardization is required before circulating nucleic acid analysis can be used as clinically approved markers. Circulating miRs represent the tumor and the host response to malignant lesions. In contrast, circulating tumor-specific DNA harbors the molecular characteristics from the cancer cells such as mutations.
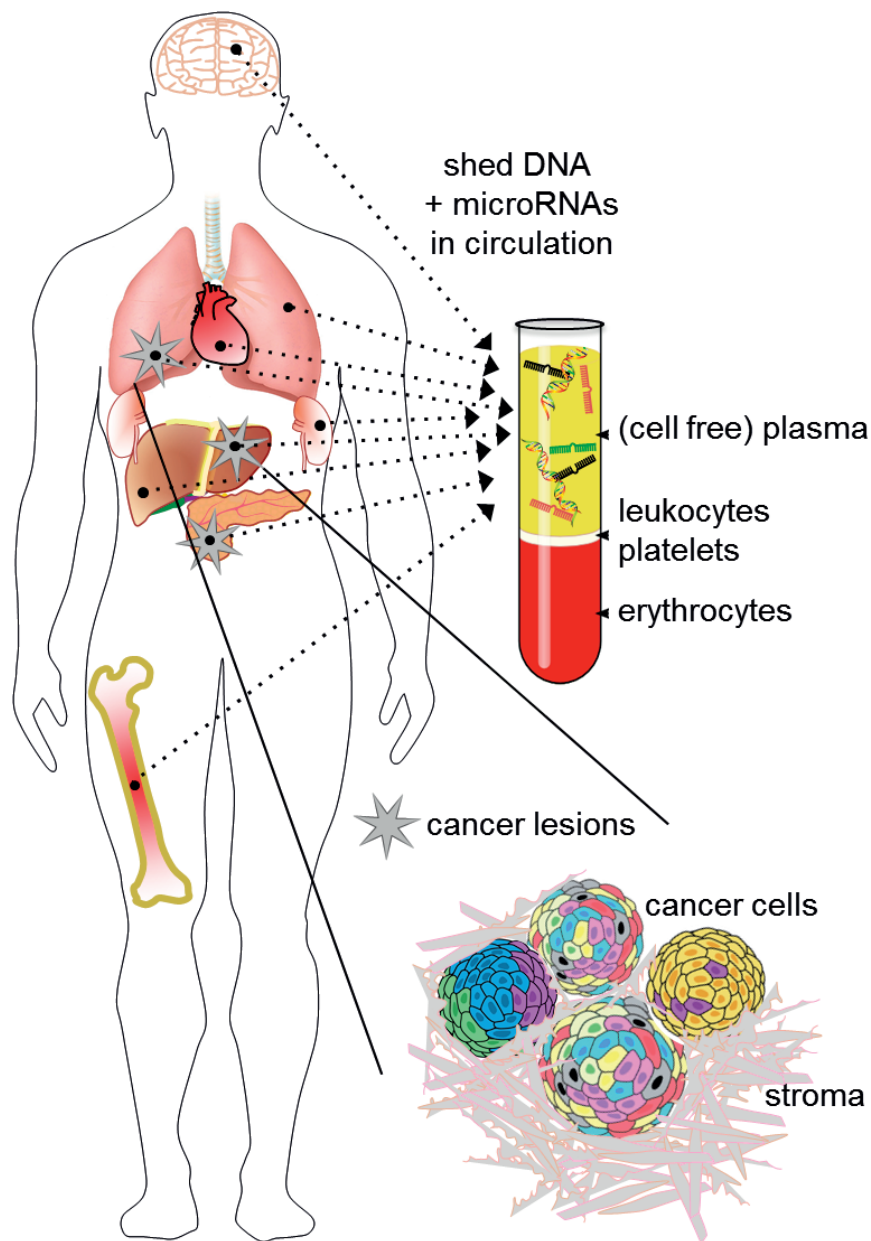
Figure 1. Release of cell free DNA and miR into the circulation. Healthy organs e.g. brain, lung, heart, kidney, liver, bone marrow shed wild type DNA and microRNAs into the bloodstream as indicated by the dotted arrows. The cancer lesions contain cancer cells (colored) and stromal cells (grey). Tumor-derived mutated DNA originates from the heterogeneous cancer cell populations and is shed into the circulation as cell-free (cf) DNA. MicroRNAs derived from blood cells, normal and tumor tissues reflect the composite of signaling in cancer cells, stroma and normal tissues. Double helices in the plasma compartment indicate cfDNA, short, single-stranded nucleic acids in different colors indicate miRNAs.

Circulating DNA

Cell-free DNA

All human cells can release DNA into their extracellular environment. Extracellular DNA has been detected in saliva, mucus, pancreatic juice, lymph, breast milk, cerebrospinal fluid, urine, amniotic fluid, and blood. Necrosing or apoptosing cells are thought to be the major source of cell-free DNA, however active DNA release via extracellular vesicles or protein complexes has been observed in cells such as lymphocytes and cancer cells[6,7]. DNA in the cell-free compartment of the blood, i.e., the plasma or serum, is called ccfDNA. In order to study ccfDNA, blood samples collected with standard collection tubes must be rapidly processed, to allow for reproducible assessments of ccfDNA levels. If plasma or serum are not separated from the cells within short order (~2 hours), dying cells can shed their DNA as well as DNA degrading enzymes and thus bias the levels of ccfDNA. Some collection tubes that capture and fixate the blood components appear to mitigate this problem and allow for shipping and later (within 72 hours) separation by centrifugation [8]. CcfDNA can be encapsulated in lipid membrane microvesicles, trapped by leukocytes, bound to nucleosomes, serum- and/or lipoproteins. Studies on the half-life of ccfDNA have described times ranging from minutes to 13 hours. This discrepancy is not surprising, given the multitude of possible ccfDNA carriers and factors involved in ccfDNA clearance. When ccfDNA is bound to protein complexes, or inside membrane vesicles, the DNA is less vulnerable to degradation. Phagocytes clean up dead cells and nucleases in the blood and rapidly degrade ccfDNA, whereas the liver and kidneys metabolize it. These events occur at different rates, depending on (patho)physiological conditions of the individual at that time. As the knowledge on ccfDNA has dramatically increased over the past decade, it became clear that levels of DNA in the blood are a comprehensive indication of the present physiological and pathological processes throughout the body. CcfDNA can impact the immune system and signals through Toll-like receptors on dendritic cells and macrophages. Both ccfDNA from the host and from microbial invaders can elicit inflammatory responses [9-11]. In the case of the autoimmune disease systemic lupus erythematosus (SLE), DNA-specific antibodies bind to the abundant extracellular, double stranded ccfDNA and form immune complexes that elicit inflammation. Moreover, patients with DNAse deficiency have increased susceptibility to autoimmune diseases such as SLE [12], due to the increased levels of ccfDNA. In the blood of healthy individuals, the vast majority of ccfDNA originates from erythrocytes, leukocytes, and endothelial cells [13,14]. In addition, ccfDNA is shed from cells of organs that incurred damage by hypoxia, trauma, inflammation, etc. [15,16]. CcfDNA levels are elevated after physical exercise [17-19], surgery [20], myocardial infarction [21], and many other disorders. Especially in patients with cancer, ccfDNA levels rise dramatically [22-24]. Ever since this observation was made in the late 1970s, ccfDNA has become a major player in the field of cancer biomarkers.

Circulating DNA levels in patients with cancer

The levels of ccfDNA in patients with cancer can be increased due to higher rates of cellular turnover and cell death in tumor tissues. Tumor-derived ccfDNA is termed circulating cell-free tumor DNA, in short 'ctDNA'. Cancer cells are not the only cells in tumors that contribute to the high levels of ctDNA: activated tumor-associated fibroblasts, endothelial cells, and immune cells also shed DNA. It is well established that ctDNA does not originate from intact circulating tumor cells: cell-free ctDNA levels are 100-1000 times more abundant than the intracellular DNA content of circulating tumor cells and the typical number of circulating tumor cells per mL of blood (<10), cannot account for the numerous micrograms of ctDNA per mL of blood observed in cancer patients [25,26]. CtDNA is smaller in size than ccfDNA from healthy individuals [27,28]. The sizes of ctDNA fragments range from 120-180 base pairs (bp) and peak below 150 bp [27,29,30]. The packaging of extracellular DNA is different for cancer cells from different origin and also depends on the extent of phagocytosis by immune cells. A small portion of ctDNA is packaged into exosomes and can measure 100-2500 bp; even larger DNA strands can bind to the outer membrane of exosomes [31]. Aside from the release mechanisms and packaging of ctDNA, the quantity of ctDNA is dependent on the type, location, vascularity, and size of the tumor. For instance, hypoxia is a major driver of ctDNA release [32]. Thus, tumor load and ctDNA levels do not necessary correlate with each other. Instead of quantitating the levels of ctDNA, many studies focus on cancer cell-specific, qualitative characteristics of ccfDNA in cancer patients. Because ctDNA refers to the cell-free DNA portion in blood that is derived from the tumor it harbors the hallmark genomic alterations of the cancer cells from which the DNA is shed.

Circulating Mutant Tumor DNA

Mutations in ctDNA are often studied as qualitative and quantitative biomarkers in cancer patients. Advances in PCR-based detection assays have allowed for relatively easy mutant ctDNA measurements. When quantitating known mutations, methods such as droplet digital PCR allow for mutation detection as low as 1 per 10.000 copies of wildtype DNA. Similar detection thresholds are met when screening for a broader range of genomic alterations, using targeted panels of amplicon deep sequencing. The number of mutations vary by up to 1000-fold among specimens from a given cancer type [33]. Although mutant ctDNA originates from cancer cells, tumors consist of heterogeneous cancer subpopulations. This intratumoral heterogeneity implies that different cancer cells harbor different sets of mutations. Therefore it is prudent to monitor more than one gene mutation when attempting to correlate clinical outcomes to mutant ctDNA levels. Moreover, the stroma component of cancers is important to consider when quantitating mutant ctDNA. The highly reactive stroma in pancreatic cancers for instance, could lead to a shift in the mutant ctDNA fraction compared to wildtype ctDNA. In contrast to studies in pancreatic cancer, which have shown that fewer myofibroblasts in tumors are associated with poor survival [34], in colorectal

cancer it has been shown that a lower cancer cell-to-stroma ratio is associated with worse outcomes [35]. Likewise, high levels of cancer-associated fibroblasts in esophageal cancer are correlated with a worse clinical outcome [36].The levels of mutant ctDNA in the background of wildtype ctDNA could be misleading when correlations are made between clinical outcomes and mutant fractions of ctDNA [16]. In early stages of cancer, mutant ctDNA may be below the detection limit due to a low tumor load. Also, missed ctDNA can be caused by clonal heterogeneity of a tumor, or because a subpopulation carrying the mutation has a low apoptosis rate. In some cases the total ctDNA level is the superior marker of cancer load [37], though a particular mutant ctDNA can be informative if an abundant gene mutation is assessed [22]. As discussed above, biological factors such as tumor vascularity, phagocytosis of dead cells, ctDNA clearance by the kidneys and liver, as well as the sensitivity of the detection assay will affect the measurements of mutant DNA. Even copy numbers of the mutant allele can be different in cancer cells from the same tumor. In colorectal cancer patients with detectable mutant KRAS and BRAF ctDNA, mutant allele fractions in plasma can range from 0.13% to 68.77%, as determined by Intplex PCR [38]. Therefore, most studies separate patients based on the presence or absence of mutant ctDNA for the cancer related genes monitored rather than the abundance of the mutant allele fraction.

Circulating microRNAs

MiR biogenesis

Mature microRNAs (miRs) are highly conserved short strands of non-coding RNA, derived from hairpin precursor transcripts [39]. After cleavage of primary microRNA (pri-miRNA) transcripts by the Drosha/DCGR8 complex, nuclear-to-cytoplasmic transport, and maturation with DICER1[40,41], 21–24 nucleotide long, double stranded mature miRs are formed. One of the mature miR strands binds predominantly to the 3' untranslated region (UTR) region of mRNA to regulate protein translation. Additionally, miRs can also bind to the open reading frame (ORF) or 5'UTR of target mRNAs to repress or activate translational efficiency [42-44]. The discovery of small RNAs that are involved in translation regulation via an antisense RNA-RNA interaction was first described in Caenorhabditis elegans [45]. To date, more than 2600 human mature miRNAs have been identified and annotated [46], with more than half of human protein-coding genes likely regulated by a miR [47].

MiR expression alterations in cancer

MiRs are dysregulated in cancer and play crucial roles in cell proliferation, apoptosis, metastasis, angiogenesis and tumor-stroma interactions [48]. Dysregulated miRs can function both as oncogenes (e.g. miR-155; miR-21, miR-221; miR-222, miR-106b-93-25 cluster; the miR-17-92 cluster) and tumor suppressors (e.g. miR-15; miR-16; let-7; miR-34; miR-29; miR-122, miR-125a-5p and miR-1343-3p), depending on their downstream targets [49,50]. Many human miR genes are located on chromosomal sites that are susceptible to

chromosome breakage, amplification and fusion with other chromosomes [51]. Additionally, alterations in RNA binding proteins and cell signaling pathways contribute to cancer through miRNA expression changes as well as mutations in core components of the miR biogenesis machinery that can promote oncogenesis [40]. It has recently been shown that mutant KRAS in colon cancer cell lines leads to decreased Ago2 secretion in exosomes and Ago2 knockdown resulted in decreased secretion of let-7a and miR-100 in exosomes whilst cellular levels of the respective miRs remained unchanged compared to control cells [52]. A systematic expression analysis of 217 mammalian miRs from 334 samples, including multiple human cancers revealed extensive diversity in miR expression across cancers, and a large amount of diagnostic information encoded in a relatively small number of miRs. More than half of the miR (129 out of 217) had lower expression levels in tumors compared to normal tissues, irrespective of cell types [53]. miR expression profiles allows classification of poorly differentiated cancers and identify tumors of unknown tissue origin [53]. In subsequent studies, profiling miR expression improved cancer diagnosis and helped identify the tissue of origin in carcinoma with unknown primary site by standard histology or immunohistological analyses [54,55].

Cell-free miRs

MiRs are present and stable in the peripheral circulation. The first report on miR expression in the circulation in 2008 described detection of four placenta-associated miRs (miR-141, miR-149, miR-299-5p, and miR-135b) in maternal plasma during pregnancy, after which the level decreased following delivery [56]. In 2008, a study demonstrated increased levels of circulating miR-21, miR-155 and miR-210 expression in patients with diffuse large B-cell lymphoma (DLBCL) compared to healthy controls [57]. Mitchell et al. also showed that circulating serum miR-141 could distinguish patients with advanced prostate cancer from healthy controls [58]. The vast majority of research on circulating miR signatures in oncology is focused on diagnostics [59], in which patients with cancer are compared to healthy individuals. Given the profuse inter-individual differences in genetic background of individual patients in addition to the heterogeneous nature of cancer, using cf-miR as cancer diagnostic biomarkers will remain challenging. Data from a number of laboratories suggest that different RNA species can be specifically packaged into microvesicles by active sorting mechanisms which have not been fully elucidated [60]. The origin of cf-miR is heterogeneous. miR-21 is a good example to illustrate this point. Although the release of miR-21 into the circulation is correlated with a multitude of cancer types, it is also highly expressed in activated T-cells and associated with inflammation and wound healing [61,62]. Elevated circulating miR-21 levels do not merely reflect tumor presence. They can also reflect the host response to the tumor, which is important in predicting disease progression. Moreover, there are often discordances between cf-miRNA signatures and the paired tumor tissue [59]. Assuming that the quality of miRNA measurements is not determined by the

efficacy of RNA extraction, this suggests that cancer-associated cf-miRNA deregulations is more likely to reflect the systemic response to the presence of cancer. Indeed, several studies have shown that cf-miRNAs are predominantly derived from blood cells [63] and the endothelium [64] in addition to the tumor.

Cell-free miRs as prognostic biomarkers

Cancer progression and systemic drug therapy involve many organ systems and are not limited to the primary tumor. This makes cf-miRNA attractive biomarkers for cancer progression and drug efficacy monitoring. For instance, in serum obtained pre-surgically from patients with early stage colorectal cancers, a panel of 6 circulating miRNAs can predict cancer recurrence [65]. In pancreatic cancer patients, an expression signature of 6 plasma miRs was associated with worse overall survival [66]. Changes in cf-miRNA patterns within the same patients can be monitored over time during therapy. The growing evidence of the utility of cf-miRNA as cancer therapy response indicators has been accumulating during the last few years [67-69]. Cf-miRNAs are likely to surpass the clinical utility of conventional protein markers such as CA-125, CA19-9, PSA and radiographical imaging, which have low sensitivity and specificity for detection of minimal residual disease and are not designed to characterize cancer at the host response level.

OUTLINE OF THIS THESIS

Cancer is a heterogeneous disease which is constantly evolving. Cancer cell subpopulations have distinct genomic and phenotypic properties and respond differently to treatment. **Chapter 2** assesses clonal subpopulations of pancreatic cancer from a transgenic mouse that develops pancreatic cancer induced by mutations in *Kras* and *Trp53*. We characterized the clonal cells on the genomic, phenotypic and drug-sensitivity level. More importantly, we studied the sensitivity of the clonal cells to different types of anti-cancer drugs in the context of the mixed heterogeneous tumors in the presence of an intact immune system.

In contrast to tumor biopsies, 'liquid biopsies' are new in the field of biomarkers and can be obtained repeatedly by blood draws to follow cancer evolution. In order to follow the dynamics of cancer over time we studied the mutation patterns in circulating tumor DNA over the course of cancer progression in patients with colon and pancreatic cancer in **Chapter 3.** Plasma DNA mutations in 56 cancer-associated genes before surgical removal were compared to the mutations found in the primary tumors. Moreover, at time of metastatic disease, the plasma DNA mutations were compared to those at time of the primary disease.

MiRs control genes in cellular processes such as apoptosis, proliferation and inflammation and miRs are dysregulated in in diseases such as cancer. In contrast to circulating

tumor DNA, which can indicate presence of cancer cells, circulating miRs could provide information about the host's response to cancer. In **Chapter 4** we analyzed the changes in serum miRs in patients with pancreatic cancer after resection, and compared the serum miR expression of patients with short versus long progression free survival. The results were compared to circulating miRs that are altered in KPC transgenic mice that developed metastatic pancreatic cancer. We further assessed the expression of two miRs that are associated to cancer progression in the patients' tumor tissues by in situ hybridization.

In **Chapter 5** we studied circulating miRs in patients with breast cancer undergoing kinase inhibitor treatment. Dovitinib is a multi-kinase inhibitor impacting angiogenesis and the tumor-stroma crosstalk. We measured serum miR expression over the course of dovitinib therapy to assess whether circulating miRs could indicate drug response or resistance.

The work presented in this thesis is summarized and discussed in **Chapter 6.**

REFERENCES

1   Swanton, C. (2012) Intratumor heterogeneity: evolution through space and time. *Cancer Res* 72, 4875-4882

2   Nowell, P. C. (1976) The clonal evolution of tumor cell populations. *Science* 194, 23-28

3   Dagogo-Jack, I. & Shaw, A. T. (2018) Tumour heterogeneity and resistance to cancer therapies. *Nat Rev Clin Oncol* 15, 81-94

4   Heppner, G. H. (1984) Tumor heterogeneity. *Cancer Res* 44, 2259-2265

5   Nicolson, G. L. (1984) Generation of phenotypic diversity and progression in metastatic tumor cells. *Cancer Metastasis Rev* 3, 25-42

6   Anker, P., Stroun, M. & Maurice, P. A. (1976) Spontaneous extracellular synthesis of DNA released by human blood lymphocytes. *Cancer Res* 36, 2832-2839

7   Gahan, P. B., Anker, P. & Stroun, M. (2008) Metabolic DNA as the origin of spontaneously released DNA? *Ann N Y Acad Sci* 1137, 7-17

8   Alidousty, C. et al. (2017) Comparison of Blood Collection Tubes from Three Different Manufacturers for the Collection of Cell-Free DNA for Liquid Biopsy Mutation Testing. *J Mol Diagn* 19, 801-804

9   Ishii, K. J. et al. (2001) Genomic DNA released by dying cells induces the maturation of APCs. *J Immunol* 167, 2602-2607

10 Kawashima, A. et al. (2011) Fragments of genomic DNA released by injured cells activate innate immunity and suppress endocrine function in the thyroid. *Endocrinology* 152, 1702-1712

11 Pisetsky, D. S. (2012) The origin and properties of extracellular DNA: from PAMP to DAMP. *Clin Immunol* 144, 32-40

12 Martinez-Valle, F. et al. (2009) DNase 1 activity in patients with systemic lupus erythematosus: relationship with epidemiological, clinical, immunological and therapeutical features. *Lupus* 18, 418-423

13 Lui, Y. Y. et al. (2002) Predominant hematopoietic origin of cell-free DNA in plasma and serum after sex-mismatched bone marrow transplantation. *Clin Chem* 48, 421-427

14 Snyder, M. W., Kircher, M., Hill, A. J., Daza, R. M. & Shendure, J. (2016) Cell-free DNA Comprises an In Vivo Nucleosome Footprint that Informs Its Tissues-Of-Origin. *Cell* 164, 57-68

15 Mittra, I., Nair, N. K. & Mishra, P. K. (2012) Nucleic acids in circulation: are they harmful to the host? *J Biosci* 37, 301-312

16 Mouliere, F. & Thierry, A. R. (2012) The importance of examining the proportion of circulating DNA originating from tumor, microenvironment and normal cells in colorectal cancer patients. *Expert Opin Biol Ther* 12 Suppl 1, S209-215

17 Breitbach, S., Sterzing, B., Magallanes, C., Tug, S. & Simon, P. (2014) Direct measurement of cell-free DNA from serially collected capillary plasma during incremental exercise. *J Appl Physiol* (1985) 117, 119-130

18 Fatouros, I. G. et al. (2010) Time of sampling is crucial for measurement of cell-free plasma DNA following acute aseptic inflammation induced by exercise. *Clin Biochem* 43, 1368-1370

19 Helmig, S., Fruhbeis, C., Kramer-Albers, E. M., Simon, P. & Tug, S. (2015) Release of bulk cell free DNA during physical exercise occurs independent of extracellular vesicles. *Eur J Appl Physiol* 115, 2271-2280

20 McIlroy, D. J. et al. (2015) Cell necrosis-independent sustained mitochondrial and nuclear DNA release following trauma surgery. *J Trauma Acute Care Surg* 78, 282-288

21 Chang, C. P. et al. (2003) Elevated cell-free serum DNA detected in patients with myocardial infarction. *Clin Chim Acta* 327, 95-101

22 El Messaoudi, S. et al. (2016) Circulating DNA as a Strong Multimarker Prognostic Tool for Metastatic Colorectal Cancer Patient Management Care. *Clin Cancer Res* 22, 3067-3077

23   Kuroi, K., Tanaka, C. & Toi, M. (2001) Clinical significance of plasma nucleosome levels in cancer patients. *Int J Oncol* 19, 143-148

24   Leon, S. A., Shapiro, B., Sklaroff, D. M. & Yaros, M. J. (1977) Free DNA in the serum of cancer patients and the effect of therapy. *Cancer Res* 37, 646-650

25   Bettegowda, C. et al. (2014) Detection of circulating tumor DNA in early- and late-stage human malignancies. *Sci Transl Med* 6, 224ra224

26   Crowley, E., Di Nicolantonio, F., Loupakis, F. & Bardelli, A. (2013) Liquid biopsy: monitoring cancer-genetics in the blood. *Nat Rev Clin Oncol* 10, 472-484

27   Mouliere, F. et al. (2011) High fragmentation characterizes tumour-derived circulating DNA. *PLoS One* 6, e23418

28   Thierry, A. R. et al. (2010) Origin and quantification of circulating DNA in mice with human colorectal cancer xenografts. *Nucleic Acids Res* 38, 6159-6175

29   Diehl, F. et al. (2005) Detection and quantification of mutations in the plasma of patients with colorectal tumors. *Proc Natl Acad Sci U S A* 102, 16368-16373

30   Jiang, P. et al. (2015) Lengthening and shortening of plasma DNA in hepatocellular carcinoma patients. *Proc Natl Acad Sci U S A* 112, E1317-1325

31   Thakur, B. K. et al. (2014) Double-stranded DNA in exosomes: a novel biomarker in cancer detection. *Cell Res* 24, 766-769

32   Cortese, R., Almendros, I., Wang, Y. & Gozal, D. (2015) Tumor circulating DNA profiling in xeno-grafted mice exposed to intermittent hypoxia. *Oncotarget* 6, 556-569

33   Alexandrov, L. B. et al. (2013) Signatures of mutational processes in human cancer. *Nature* 500, 415-421

34   Ozdemir, B. C. et al. (2014) Depletion of carcinoma-associated fibroblasts and fibrosis induces immunosuppression and accelerates pancreas cancer with reduced survival. *Cancer Cell* 25, 719-734

35   West, N. P. et al. (2010) The proportion of tumour cells is an independent predictor for survival in colorectal cancer patients. *Br J Cancer* 102, 1519-1523

36   Ha, S. Y., Yeo, S. Y., Xuan, Y. H. & Kim, S. H. (2014) The prognostic significance of cancer-associated fibroblasts in esophageal squamous cell carcinoma. *PLoS One* 9, e99955

37   Thierry, A. R., El Messaoudi, S., Gahan, P. B., Anker, P. & Stroun, M. (2016) Origins, structures, and functions of circulating DNA in oncology. *Cancer Metastasis Rev* 35, 347-376

38   Mouliere, F. et al. (2013) Circulating Cell-Free DNA from Colorectal Cancer Patients May Reveal High KRAS or BRAF Mutation Load. *Transl Oncol* 6, 319-328

39   Bartel, D. P. (2004) MicroRNAs: genomics, biogenesis, mechanism, and function. Cell 116, 281-297

40   Lin, S. & Gregory, R. I. (2015) MicroRNA biogenesis pathways in cancer. *Nat Rev Cancer* 15, 321-333

41   Suzuki, H. I. & Miyazono, K. (2011) Emerging complexity of microRNA generation cascades. *J Biochem* 149, 15-25

42   Bartel, D. P. (2009) MicroRNAs: target recognition and regulatory functions. *Cell* 136, 215-233

43   Hock, J. & Meister, G. (2008) The Argonaute protein family. *Genome Biol* 9, 210

44   Vasudevan, S., Tong, Y. & Steitz, J. A. (2007) Switching from repression to activation: microRNAs can up-regulate translation. *Science* 318, 1931-1934

45   Lee, R. C., Feinbaum, R. L. & Ambros, V. (1993) The C. elegans heterochronic gene lin-4 encodes small RNAs with antisense complementarity to lin-14. *Cell* 75, 843-854

46   Griffiths-Jones, S., Grocock, R. J., van Dongen, S., Bateman, A. & Enright, A. J. (2006) miRBase: microRNA sequences, targets and gene nomenclature. *Nucleic Acids Res* 34, D140-144

47   Krol, J., Loedige, I. & Filipowicz, W. (2010) The widespread regulation of microRNA biogenesis, function and decay. *Nat Rev Genet* 11, 597-610

48   Di Leva, G., Garofalo, M. & Croce, C. M. (2014) MicroRNAs in cancer. *Annu Rev Pathol* 9, 287-314

49   Yuan, T. et al. (2016) Plasma extracellular RNA profiles in healthy and cancer patients. *Sci Rep* 6, 19413

50   Garofalo, M. & Croce, C. M. (2011) microRNAs: Master regulators as potential therapeutics in cancer. *Annu Rev Pharmacol Toxicol* 51, 25-43

51   Calin, G. A. et al. (2004) Human microRNA genes are frequently located at fragile sites and genomic regions involved in cancers. *Proc Natl Acad Sci U S A* 101, 2999-3004

52   McKenzie, A. J. et al. (2016) KRAS-MEK Signaling Controls Ago2 Sorting into Exosomes. *Cell Rep* 15, 978-987

53   Lu, J. et al. (2005) MicroRNA expression profiles classify human cancers. *Nature* 435, 834-838

54   Rosenfeld, N. et al. (2008) MicroRNAs accurately identify cancer tissue origin. *Nat Biotechnol* 26, 462-469

55   Sokilde, R. et al. (2014) Efficient identification of miRNAs for classification of tumor origin. *J Mol Diagn* 16, 106-115

56   Chim, S. S. et al. (2008) Detection and characterization of placental microRNAs in maternal plasma. *Clin Chem* 54, 482-490

57   Lawrie, C. H. et al. (2008) Detection of elevated levels of tumour-associated microRNAs in serum of patients with diffuse large B-cell lymphoma. *Br J Haematol* 141, 672-675

58   Mitchell, P. S. et al. (2008) Circulating microRNAs as stable blood-based markers for cancer detection. *Proc Natl Acad Sci U S A* 105, 10513-10518

59   Jarry, J., Schadendorf, D., Greenwood, C., Spatz, A. & van Kempen, L. C. (2014) The validity of circulating microRNAs in oncology: five years of challenges and contradictions. *Mol Oncol* 8, 819-829

60   Kosaka, N. et al. (2010) Secretory mechanisms and intercellular transfer of microRNAs in living cells. *J Biol Chem* 285, 17442-17452

61   Dong, L. et al. (2014) Decreased expression of microRNA-21 correlates with the imbalance of Th17 and Treg cells in patients with rheumatoid arthritis. *J Cell Mol Med* 18, 2213-2224

62   Iliopoulos, D., Kavousanaki, M., Ioannou, M., Boumpas, D. & Verginis, P. (2011) The negative co-stimulatory molecule PD-1 modulates the balance between immunity and tolerance via miR-21. *Eur J Immunol* 41, 1754-1763

63   Pritchard, C. C. et al. (2012) Blood cell origin of circulating microRNAs: a cautionary note for cancer biomarker studies. *Cancer Prev Res (Phila)* 5, 492-497

64   Williams, Z. et al. (2013) Comprehensive profiling of circulating microRNA via small RNA sequencing of cDNA libraries reveals biomarker potential and limitations. *Proc Natl Acad Sci U S A* 110, 4255-4260

65   Shivapurkar, N. et al. (2014) Recurrence of early stage colon cancer predicted by expression pattern of circulating microRNAs. *PLoS One* 9, e84686

66   Zhou, X. et al. (2018) Plasma miRNAs in diagnosis and prognosis of pancreatic cancer: A miRNA expression analysis. *Gene* 673, 181-193

67   Zhang, Y. C., Xu, Z., Zhang, T. F. & Wang, Y. L. (2015) Circulating microRNAs as diagnostic and prognostic tools for hepatocellular carcinoma. *World J Gastroenterol* 21, 9853-9862

68   Schwarzenbach, H. (2015) The potential of circulating nucleic acids as components of companion diagnostics for predicting and monitoring chemotherapy response. *Expert Rev Mol Diagn* 15, 267-275

69   Odenthal, M. et al. (2015) Serum microRNA profiles as prognostic/predictive markers in the multi-modality therapy of locally advanced adenocarcinomas of the gastroesophageal junction. *Int J Cancer* 137, 230-237

CHAPTER 2

Intratumoral heterogeneity and tumor-host crosstalk alter drug sensitivity of clonal subpopulations in a pancreatic cancer model

Eveline E. Vietsch[1]
Sarah Martinez Roth[1]
John K. Simmons[2]
Aamir Javaid[1]
Matthew D. Park[1]
Marianne H.B.C. Stenstra[1]
Justine N. McCutcheon[1]
Eric B. Berens[1]
Ivana Peran[1]
Maha Moussa[1]
Marta Catalfamo[1]
Beverly A. Mock[2]
Giuseppe Giaccone[1]
Marcel O. Schmidt[1]
Anna T. Riegel[1]
Anton Wellstein[1]

[1] Lombardi Comprehensive Cancer Center, Georgetown University, 3970 Reservoir Road NW, Washington DC 20007, USA

[2] Laboratory of Cancer Biology and Genetics, National Cancer Institute, Bethesda, MD 20892, USA

ABSTRACT

Cancers consist of heterogeneous cell subpopulations that survived selection during tumor evolution. Interactions between these subpopulations and the host impact as well as their impact on drug responses are poorly understood. We established a model of tumor heterogeneity using clonal cell lines isolated from a KPC (*Kras*^G12D/+^; *Trp53*^R172H/+^; *P48-Cre*) mouse pancreatic tumor. Deep sequencing of unique mutations characteristic for cancer subpopulations was used to monitor clonal abundance after various anti-cancer therapies in heterogeneous tumors that were reconstituted from cell mixtures. We found that the composition of heterogeneous tumors is affected by the crosstalk amongst the cancer subpopulations and the host environment that includes the immune system as a major player. Some cancer cell subpopulations showed sensitivity to anti-PD-1 immune checkpoint inhibitor treatment in vivo. This sensitivity was mirrored in vitro by the level of activation of T-cells isolated from caecal patches of tumor bearing mice. We provide a platform that comprises the crosstalk between cancer cell subpopulations and the host and reveals the impact on drug efficacy.

INTRODUCTION

Pancreatic ductal adenocarcinoma (PDAC) is a lethal disease for which no curative drug therapy currently exists [1]. The approved drug treatment with the antimetabolite gemcitabine extends disease-free survival after surgery by 6.5 months but does not improve overall survival [2]. Mutant *KRAS*, the major oncogenic driver in PDAC, is present in >90% of tumor specimen [3,4], and acts in part via its downstream effector pathway RAF, MEK and ERK. MEK kinase inhibitors such as trametinib reduce both RAS-dependent MEK and ERK phosphorylation [5]. However, initial studies show that treatment with MEK inhibitors does not provide discernible benefit in patients with PDAC [6], indicating that alternative pathways downstream of KRAS take over during malignant progression [7,8]

DNA sequence and functional analyses revealed that tumors of diverse histological types are composed of clonal cell subpopulations [9-11]. Evolution of these subpopulations is driven by an aggregate of mutations and epigenetic changes as well as selective pressure by the tumor environment [12-17] that is enhanced by the recruitment of cancer-associated stroma and immune cells [18]. Stromal desmoplasia, one of the histologic signatures of PDAC, can inhibit the invasion of cancer cells [19,20] but also plays a role in reducing the efficacy of chemotherapy [21-24] and in suppressing the activity of the immune system [25]. In addition to the stromal / cancer cell interactions, phenotypically different cancer cell populations can influence each other's growth behavior [26-28] as well as treatment responses [29,30].

To establish a model that can track cooperation and competition between cancer subpopulations and the host in response to drug treatment, we generated a series of clonal cancer cell lines from the well-established *LSL-Kras*[G12D/+]; *LSL-Trp53*[R172H/+]; *P48-Cre* driven PDAC model [31]. Genomic analysis revealed that each of the clonal cell lines carries a distinct set of signature mutations. Rather than exogenously tagging cells, we employed these molecular signatures to quantitate the abundance of the clones in reconstituted cell mixtures by deep sequencing of DNA extracted from cells in culture or from allograft tumors in compatible, immune-competent mice. Here we show that growth of subpopulations of cancer cells in heterogeneous mixtures in culture and in tumors and the effects of treatment with an anti-metabolite chemotherapeutic drug (gemcitabine), a MEK kinase inhibitor (trametinib) or an immune checkpoint inhibitor (α-PD-1 antibody) revealed distinct sensitivity of the clonal subpopulations that was affected by intratumoral, stromal and immune cell interactions.

MATERIALS AND METHODS

Mouse experiments

The animal study protocols were approved by the Georgetown University Animal Care and Use Committee. The transgenic KPC mouse model was originally described by Hingorani et al [31]. Mice were aged 3-6 months at time of the experiments and both sexes were used randomly.

KPC derived pancreatic cancer clonal cell line culture

A female KPC mouse 135 days of age was euthanized for tumor harvesting. Fresh mouse pancreatic tumor tissue was minced for 5 minutes and shaken at 150 rpm for 1 hour at 37ºC in a Dulbecco's Modified Eagle Medium/Nutrient Mixture F-12 (DMEM/F-12, Gibco Life) with 5% fetal bovine serum (FBS), 2 mg/mL collagenase (Sigma), 4 mg/mL trypsin (Sigma), 50 μg/mL gentamicin (Gibco Life), and 1 IU/mL penicillin/streptomycin (Gibco Life). The cell pellet was washed and centrifuged at 600 g in 4ºC in DMEM / F-12, four times. The cell pellet was suspended in primary cell culture media (F-12, 10% FBS, 16 μg/mL insulin (Gibco Life), 10 ng/mL epidermal growth factor, 1 μg/mL hydrocortisone (Sigma), 4 ng/mL cholera toxin (Sigma), 50 μg/mL gentamicin, and 0.5 IU/mL penicillin/streptomycin). The cells were placed in a 37ºC, 5% CO_2, humidified incubator on a Collagen-1 coated 10 cm culture dish (Corning BioCoat) in primary cell culture media for 40 minutes to let fibroblasts attach. Subsequently, the unattached cancer cells were transferred to a regular 10 cm dish. Primary cell culture media was changed every 48 hours. Pictures were taken with the Olympus IX71 inverted microscope. After one week, the primary cancer cells were trypsinized, and resuspended in primary cell media in the dilution of a single cell per 200 μL well plated in a 96-well plate. After 3 weeks incubation, eleven wells contained clonal cell populations. The eleven clones were expanded individually to stable clonal cell lines and were grown in DMEM/10% FBS from passage 4 onwards.

3D growth in collagen

One thousand clonal cells were embedded in 40 μL of either neutralized rat tail type-1 collagen (Millipore) / DMEM10% FBS mixture. Cells were left in a 37ºC, 5% CO2, humidified incubator for 10 days. Images were taken with using an Olympus IX71 inverted microscope.

Western blot analysis

Protein lysates from cells were obtained using a buffer with 50 mM Tris pH 8.0, 150 mM NaCl, 40 mM β-glycerophoshpate, 0.25% Na-deoxycholate, 1% NP40, 50 mM NaF, 20 mM NaPPi, 1 mM EGTA. Before use of the lysis buffer, 1 mM of Na-orthovanadate and protease inhibitor cocktail (cOmplete, Roche) was added. Protein lysates were prepared for denaturing Bis-Tris gels by adding NuPAGE lithium dodecyl sulfate buffer and Reducing

Agent (Novex, Life), followed by 10 minutes incubation at 70 °C. Proteins were separated in Bis-Tris gels (Novex, Life) by electrophoresis in NuPAGE MOPS SDS Running buffer (Novex, Life). Gels were transferred to polyvinylidene fluoride membranes by the use of the iBlot system (Invitrogen). Membranes were blocked with 5% non-fat dry milk in PBS-T for 1 hour, washed once with PBS-T (0.1% Tween20 in PBS). Primary antibodies (total ERK1/2, Cell Signaling #9102 Rabbit pAb) and phospho T202/Y204 ERK1/2, (Cell Signaling #9101 Rabbit pAb) were diluted to 1:1000 in 5% milk PBS-T. Membranes were incubated at 4 °C overnight. Next, membranes were washed 3 times with PBS-T and incubated with second-ary Horseradish peroxidase-linked anti-rabbit antibody (GE Healthcare, NA934V) in 5% milk in PBS-T for 1 hour at room temperature. Membranes were washed 3 times and signals were visualized with Immobilon Western Chemoluminescent HRP Substrate (Millipore) on HyBlot CL autoradiography film (Denville Scientific). Band intensities were estimated using Adobe Photoshop.

RNA sequencing of clonal cell lines

Total RNA was extracted from six clonal cell lines that were grown in DMEM 10% FBS using the RNeasy kit (Qiagen) following the manufacturers' instructions. RNA quality was assessed and all samples had a RNA integrity number (RIN) value higher than 7.0, verified using the 2100 Bioanalyzer (Agilent Technologies). Truseq Stranded RNA libraries were constructed after the depletion of ribosomal RNA using RiboZero. The libraries were then sequenced using the Illumina HiSeq 4000 with paired-end 75 nucleotide reads. Gene expression data in fragments per kilobase of transcript per million reads (FPKM) for every gene in each sample set was analyzed by Gene Set Enrichment Analysis (GSEA), resulting in an enrichment score for each gene when each individual clone was compared to the rest. The scored genes of the experimental data sets were organized into functionality-specific families. The Hallmark family sets represent specific, well-defined biological states or pro-cesses based on the Molecular Signatures Database (MSigDB) hallmark gene set collection.

Exome sequencing of clonal cell lines

Genomic DNA from eight samples was analyzed: Six mouse pancreatic cancer clonal cell lines, the corresponding parental KPC mouse tumor tissue and a healthy pancreas from a female p48-Cre littermate mouse. Exome sequencing was performed by Otogenetics (Nor-cross, GA). In short, mouse exons were captured with an Aligent V4 kit and paired-end 100 nucleotide reads were obtained from the HiSeq2000 (Illumina) with a 30X coverage. Whole exome sequencing data were analyzed was mapped to the MM9 assembly using BWA (v0.7.16a) [32] and the variant calling analysis was performed with HaplotypeCaller as part of the Genome Analysis Toolkit (GATK v3.8-0) [33]. Genetic variants within a given pancreatic cancer clone were then detected by comparison to pancreatic tissue from a the matched, healthy littermate. We focused on non-synonymous mutations only, known

dbSNPs were subtracted. Mutations with less than 5 reads, variant allele frequency less than 0.2, MQ less than 40.00 and genes with more than one mutation were discarded. Unique, clone-specific mutations were validated by Sanger sequencing before using them as clonal signature mutations in later allograft tumor experiments.

Endpoint PCR

DNA from clonal cells and tissue was isolated using the PrepEase Genomic DNA Isolation Kit (Usb), following the manufacturer's protocol. DNA from mouse tissues from different treatment groups was pooled at equimolarity. Per 50 μL of PCR reaction 200 ng of DNA from cells or tissues were used. Endpoint PCR was performed using the Platinum Taq DNA Polymerase Kit (Invitrogen 10966-034), with PCR buffer containing 1.5 mM $MgCl_2$, 0.2 mM dNTP, 0.2 μM primers and 1 U Platinum *Taq* DNA polymerase, using the Epgradient Mastercycler (Eppendorf). The cycling consisted of 2 min at 95 ^{o}C for initial denaturation, 40 cycles of 95 ^{o}C for 30 sec, 61 ^{o}C for 30 sec, and 72 ^{o}C for 40 sec. PCR amplicon products were purified using the QIAquick PCR Purification Kit (Qiagen), removing primers, nucleotides, enzymes, mineral oil, salts, and other impurities from the PCR products. Amplicons were examined by electrophoresis in 2% agarose gel with 1X TAE buffer, and visualized with ethidium bromide and xylene cyanol dye. As a size marker the 1 kb DNA ladder (Invitrogen) was used. The gel was examined under UV light for amplicon bands.

Primers used for PCR amplification of *Kras* and *Trp53* for LoxP genotyping clonal cell lines:

gene	primer	sequence	amplicon size wildtype allele	amplicon size recombined allele
Kras	forward reverse	5'-GGGTAGGTGTTGGGATAGCTG-3' 5'-TCCGAATTCAGTGACTACAGATGTACA-3'	270 bp	304 bp
Trp53	forward reverse	5'- TGACAAGCCTTGCACCTTTCCAAC-3' 5'- CCACAGAGGCTGGATGTGTAA-3'	239 bp	273 bp

Droplet digital PCR for *Kras*[G12D] allele frequency quantification

DNA from six clonal cell lines was used for PrimePCR ddPCR Mutation Detection (Bio-Rad). Per 20 μL reaction 20 ng DNA were used with ddPCR supermix for probes (no dUTP), 450 nM primers and 250 nM of both *Kras* probes. Probes used for *Kras*[G12D] allele frequency quantification with ddPCR using genomic DNA from clonal cell lines:

Kras allele	primer	sequence	probe	dye / quencher
wildtype	forward reverse	5'-TATCGTCAAGGCGCTC-3' 5'-GCTGAAAATGACTGAGTATAAA-3'	TGGAGCTGGTGGCG	5'– HEX / 3' – Iowa Black FQ
G12D mutant	forward reverse	5'-TATCGTCAAGGCGCTC-3' 5'-GCTGAAAATGACTGAGTATAAA-3'	TGGAGCTGATGGCGT	5'– 6-FAM / 3' – Iowa Black FQ

The PCR mixture was combined with 40 μL Droplet Generation oil for Probes, and placed in Cartridges in the Droplet Generator (Bio-Rad). Endpoint PCR was performed with the following protocol: Enzyme activation at 95 $^{\circ}$C for 10 minutes, 40 cycles of 94 $^{\circ}$C for 30 seconds, 58 $^{\circ}$C for 1 minute. Enzyme deactivation was achieved at 98 $^{\circ}$C for 10 minutes, hold at 4 $^{\circ}$C. After PCR, the samples were analyzed in the QX200 Droplet Reader to quantify *Kras* allele frequency.

In vitro growth assays

To monitor clonal growth dynamics in vitro, the xCELLigence Real Time Cell Analysis was used as described earlier [34] with 1000 clonal cells/well in DMEM/10% FBS in 16-well E-plates (ACEA Biosciences). All cell lines were measured in quadruplicate wells. For dose response curves the IncuCyte ZOOM system (Essen Bioscience) was used with 250 clonal cells/well plated in 384-well plates in DMEM/10% FBS. After overnight cell attachment, trametinib (Selleckchem) or gemcitabine (LC Laboratories), were added in triplicate wells at different concentrations as indicated in the respective figures. The IncuCyte Zoom system measured Cell Confluence every 12 hours. Growth inhibition was normalized to DMSO control and the respective IC_{50} values were derived by non-linear curve fitting using log [inhibitor] vs. normalized response with variable slope (Prism GraphPad 5.0).

Treatment of pooled mixture of clones in vitro for deep sequencing

Twenty thousand cells per clonal line, to make a mixture of 6 cell lines, were plated in T175 flasks in DMEM10%FBS and allowed to attach for 6 hours. 25 nM of gemcitabine (LC Laboratories) or 100 nM of trametinib (Selleckchem) or DMSO in PBS as a control were added respectively. Cells were allowed to grow to confluency (4 days for the DMSO, 7 days for the trametinib and 11 days for the gemcitabine treated cells). Floating cells were washed away and DNA was isolated from the remaining attached cells after trypsinization.

Growth assay with conditioned media in vitro

Two hundred thousand cells from each of the six clonal cell lines mixed together, or 1.2 million clonal cells alone, were plated in T175 flasks in DMEM10%FBS. After 48 hours, the conditioned media was collected and centrifuged in 0.22 μM membrane vacuum filtration columns (Millipore) to sterilize and remove debris. The conditioned media was stored in 4° Celsius until use. For the growth assay, clonal cell lines G8 and C8 were plated in 16-well xCelligene E-Plates (see above). The cells were plated at a 1:1 ratio of the conditioned media (c.m.) from the clone mix, together with fresh DMEM/10%FBS, or in c.m. from the respective clones (C8 or G8) and fresh DMEM/10%FBS. Different concentrations of trametinib (Selleckchem) or DMSO in PBS as a control were added after cells had attached for 6 hours. The cell index was monitored every 5 hours and dose response curves were generated in Prism Graphpad 5.0.

Allograft tumors

The mouse PDAC cells were tested for mycoplasma contamination and are negative. One million clonal PDAC cells were injected subcutaneously into the flanks of immune competent, compatible wildtype mice (relatives of the KPC mouse). Drug treatments were initiated when tumors had established after ~1 week: 250 μg of rat monoclonal anti-mouse-PD-1 (clone BE0146, BioXCell, New Hampshire, USA) in 50 μL PBS via intraperitoneal injection twice a week, or isotype mAb in PBS as a control; Gemcitabine (LC Laboratories) at 40 mg/kg in sterile water, or water as a control, with 5 doses in week 1 and 2 doses in week 2 by intraperitoneal injections; trametinib (GSK1120212, Selleckchem) by oral gavage at 0.5 mg/kg in 3% DMSO dissolved in 0.5% methylcellulose / 0.2% Tween80 (Sigma) daily for 2 weeks, the carrier mix served as a control.

Histopathology and Immunohistochemistry

Immunohistochemical staining of tumor tissue was performed for α-Smooth Muscle Actin (Rabbit α–SMA monoclonal antibody, Abcam ab124964). Five micron sections from formalin fixed paraffin embedded tissues were de-paraffinized with xylenes and rehydrated through a graded alcohol series. Heat induced epitope retrieval was performed by immersing the tissue sections at 98 °C for 20 minutes in 10 mM citrate buffer (pH 6.0) with 0.05% Tween. Staining was performed using the VectaStain Kit from Vector Labs according to manufacturer's instructions. Briefly, slides were treated with 3% hydrogen peroxide and 10% normal (animal) serum and exposed to 1:1000 Rabbit α–SMA (Abcam ab124964), or α–PD-L1 (Cell Signaling Technology #64988) in Normal antibody diluent (MP Bio-medicals) overnight at 4 °C. Slides were exposed to anti-rabbit biotin-conjugated secondary antibody (Vector Labs), Vectastain ABC reagent and DAB chromagen (Dako). Slides were counterstained with Hematoxylin (Fisher, Harris Modified Hematoxylin), dehydrated and mounted with Acrymount. Images were captured using an Olympus IX71 inverted microscope. Histopathological evaluations were done with advice from pathologist Dr. Bhaskar Kallakury.

Amplicon deep sequencing

The six genes with clonal signature mutations were PCR amplified and validated by Sanger sequencing (MCLab). Purified PCR amplicons of these clonal signature genes plus mutant *Kras* and mutant *Trp53* for all cancer cells were from DNA from allograft tumors that were pooled in equimolarity. PCR amplicons were quantified using the Quantifluor ONE dsDNA kit on the GloMax-Multi-Plus Microplate Reader (Promega) by following the manufacturer's protocol. Amplicons were used for MiSeq deep sequencing. Primers used for PCR amplification of the eight genes containing clonal and ubiquitous cancer cell signature mutations:

gene	primer	sequence	variant [mm9 position]	amplicon size
Trp53 (ubiquitous)	forward reverse	5'- GAAAGGGAGGAAGAAGGAAAG-3' 5'- CTTCCAGATACTCGGGATACA-3'	chr11:69402014 G>A	492 bp
Kras (ubiquitous)	forward reverse	5'-TGGACTTTCTTGCACCTATGG-3' 5'-AGTGTTGATGAGAAAGTTGTAAGTG-3'	chr6:145195291 C>T	481 bp
Olfr1157 (C8)	forward reverse	5'- TCTTAGATTTGGGAAGACCTTACA-3' 5'- CCCACCTCACAGTCATCATT-3'	chr2:87802181 G>C	494 bp
Nox4 (D10)	forward reverse	5'- GAGCACTTGGCAATGTAAGAATAG-3' 5'- CCCAGAATAACCCACTCACTAAA-3'	chr7:94462586 C>T	493 bp
Matn4 (F2)	forward reverse	5'- GCACATACACACCACCATCT-3' 5'- GCTACACTCAGAAGTGACATCC-3'	chr2:164222680 C>T	481 bp
Baiap3 (C5)	forward reverse	5'- GTAGGAGCCTTACAACAGGAAG-3' 5'- GCTAGTTGACTGGCAACAGTA-3'	chr17:25387359 G>T	500 bp
Arhgap25 (G8)	forward reverse	5'- GCTCCTTGTTCTCCTGAATCC-3' 5'- CATACACGTGATACCCAGACATAC-3'	chr6:87426299 T>C	497 bp
Pla2g4d (G9)	forward reverse	5'- AAGTTCCAGGATAGCGACAAG-3' 5'- GATCCTTGGATTCCCTTGGAG-3'	chr2:120094626 G>T	502 bp

Amplicons were pooled according to their sample type after quantitation as above. Pooled amplicons were normalized to a concentration of 10 ng/µL, and then diluted further to 0.2 ng/µL in nuclease free water. Library construction: Each amplicon pool was constructed into a library using the Nextera XT DNA library preparation kit (Illumina). Briefly, 1 ng of each amplicon pool was enzymatically sheared and simultaneously tagged with an adapter. A unique index sequence was added to each library sample through a 12-cycle PCR amplification. Each sample was purified and size selected to capture greater than 500 bp amplicons using AMPure XP beads. Quality of the indexed libraries was assessed using the High Sensitivity DNA kit on the 2100 Bioanalyzer system (Agilent Technologies). The libraries were normalized and pooled together by following the Nextera XT DNA user guide (Illumina).

MiSeq sequencing and data analysis

Before sequencing, an aliquot of the library pool was denatured at 96°C for 2 minutes and then kept on ice. One percent of 12.5 pM PhiX Control V3 (Illumina) was spiked into the denatured library pool. Paired end 2x150 bp sequencing was performed on the MiSeq using the MiSeq Reagent Nano kit v2 (300 cycles) according to the manufacturer's protocol (Illumina). All primary- and run-quality analyses were performed automatically on the MiSeq. Alignment to the mus musculus genome 9, NCBI 37 assembly (mm9) and quality trimming were executed by the Burrows-Wheeler Aligner tool on the MiSeq. All point mutations specific to each sample were reviewed by manual visualization of the reads in the Integrated Genomics Viewer (Broad Institute) and variant allele frequencies (VAF) were quantified. Clonal abundance in the tumors was normalized to the VAF of *Trp53*[R172H], to account for

wildtype stroma in the tumors. The minimum VAF for clone specific genes was set to 0.01%, in case the clonal mutations were below detection.

qRT-PCR analysis

RNA from allograft tumors was isolated using the RNeasy Mini Kit (Qiagen) following the manufacturer's protocol. 500 ng of RNA was used for complementary DNA synthesis with the iScript cDNA synthesis Kit (BioRad), with 4 µL reaction mix, 1 µL reverse transcriptase in a 20 µL reaction. The Epgradient Mastercycler (Eppendorf) cycling consisted of 5 min at 25 °C, 30 min at 42 °C, 5 min at 85 °C, hold at 4 °C. Next we performed qRT-PCR in a 20 µL reaction using the iQ SYBR Green Supermix (BioRad), containing 10 µL of SYBR Green mix, 1 µL of cDNA and 200 nM primers for the following mouse genes: (β-Actin forward primer GGCGCTTTTGACTCAGGATTTAA, β-Actin reverse primer CCTCAGC-CACATTTGTAGAACTTT; α-SMA forward primer GTCCCAGACATCAGGGAGTAA; α-SMA reverse primer TCGGATACTTCAGCGTCAGGA. The Realplex2 Mastercycler Epgradient S (Eppendorf) cycling consisted of 3 min at 95 °C, and 40 repeats of 15 sec at 95 °C, 30 sec at 60 °C, 20 sec at 68 °C. Data analysis was performed with Prism 5.01.

Flow Cytometry analysis of leukocytes in allograft tumors

The mixture of 6 clonal PDAC cell lines (1 million total) or individual clonal cell lines were injected subcutaneously into immune competent wildtype mice, and allograft tumors were allowed to grow for 10 days before tumor tissue collection. Single cell suspensions were generated by mechanic and enzymatic digestion of tumor tissues. Cell suspensions were washed and 1-2 million cells were stained as follows. Cells were labeled for Live/Dead (Invitrogen, Thermofisher, Ref: l-23105) followed by blockade of Fc receptors with CD16/CD32 (clone 2.4G2; BD Biosciences, 553141). After 10 minutes incubation, cells were stained with a cocktail of mAbs: anti-mouse-CD45 (clone 30-F11; 564590), NK-1.1 (clone PK136; 562864), B220 (clone RA3-6B2; 563103), CD3e (clone 145-2C11; 564661), CD4 (clone RM4-5, 563151), CD8a (clone 53-6.7, 564920), PD-1 (clone J43; 744549), CD25 (clone PC61; 565134), all from BD Biosciences. Cells were acquired with FACS Symphony, BD Biosciences and analyzed with FlowJo and Prism Graphpad 5.01.

Mouse caecal patch T-lymphocyte isolation

The mixture of 6 clonal PDAC cell lines (1 million total) was injected into the peritoneal cavities and subcutis of immune competent wildtype mice, and pancreatic tumors were allowed to grow for 2 weeks. After euthanasia, ceacal lymphoid patches were harvested resected in a sterile hood, then cut and shredded in 4 mL of sterile PBS containing 2% FBS and 1 mM EDTA. The cell suspensions were collected in gentle Macs C tube (cat. # 130-093-237) and further dissociated with the gentleMACS (Miltenyi Biotec) for 15 minutes as following: Loop, Spin 150 rpm 2 min, Ramp 400 rpm 30 sec, End loop. In a sterile hood,

remaining aggregates were removed by passing cell suspension through a 70 μm mesh nylon cell strainer cap (BD Falcon) into a 5 mL Polystyrene round bottom tube. The cells were centrifuged for 5 min at 200 x g, supernatant was aspirated and cells resuspended in 1.5 mL fresh PBS containing 2% FBS and 1 mM EDTA. T-lymphocytes were isolated using the EasySep Mouse T Cell Isolation Kit (Stemcell Technologies), according to the manufacturer's protocol. In brief, per 1.5 mL sample, 75 μL Rat Serum was added, in addition to 75 μL Isolation Cocktail. The samples were inverted 15 times and left at room temperature for 10 minutes. RapidSpheres were vortexed and 112 μL was added per sample. The samples were inverted 15 times and left at room temperature for 2.5 minutes. The samples were gently mixed by pipetting and placed inside the EasySep Violet Magnet (StemCell Technologies) for 2.5 minutes at room temperature. The T-lymphocyte suspensions were poured into sterile 15 mL Falcon tubes. Live T-lymphocytes were quantitated using Countess cell counting chamber slides (Invitrogen), and Trypan Blue stain (Invitrogen) with the Countess.

T-lymphocyte culture in vitro

The T-lymphocytes were centrifuged at 100 x g for 5 minutes, and after aspiration of the supernatant, the T-cells were suspended in RPMI (Gibco Life) with 10% fetal bovine serum, 100 units/mL penicillin and 100 μg/mL streptomycin, and 30 units/mL mouse recombinant Interleukin-2 (StemCell Technologies). The cells were plated in 96-well plates (~20,000 live T-cells per well) and placed in a humidified 37°C, 5% CO_2 incubator. As pilot experiment, 100 cancer cells of the equal mixture of the 6 PDAC clonal cell lines were added and incubated for 72 hours. In the following experiment, 1500 clonal cancer cells per well were added to the T-cells, together with 20 μg/mL rat monoclonal anti-mouse-PD-1 (clone BE0146, BioXCell) or 20 μg/mL isotype igG2a (BioXCell).

As the control condition of activated T-lymphocytes, the wells were incubated with 5 μg/mL hamster anti-mouse-CD3e (eBioscience) in sterile PBS overnight before T-cell isolation, whereafter T-lymphocytes were incubated with 30 units/mL mouse recombinant Interleukin-2 and 2 μg/mL hamster anti-mouse-CD28 (eBioscience). After 72 or 48 hours of T-cell incubation in vitro, images were taken with using an Olympus IX71 inverted microscope. The conditioned media was collected in 1.5 mL microcentrifuge tubes and spun down for 5 min at 300 x g. The supernatant was stored at -80 º Celsius in 100 μL aliquots until further analysis.

ELISA for mouse IFN-γ in the supernatant of T-lymphocytes

Supernatant from the T-cells was thawed on ice. IFN-γ was measured in 100 μL supernatant per condition using the Mouse IFN-γ ELISA Ready-SET-Go! Kit (Invitrogen), following the manufacturers' protocol. In brief, a Corning Costar 9018 ELISA 96-well plate was coated with 100 μL/well of capture antibody in 1X Coating Buffer. The plate was sealed and incu-

bated overnight at 4° Celsius. Wells were washed with 250 μL 0.05% PBS-T (wash buffer) 3 times. Wells were blocked with 200 μL 1X ELISA Diluent for 1 hour at room temperature. After washing once with wash buffer, 100 μL of the T-cell supernatant was added to the wells, or RPMI-10% or 1X Diluent as controls. The mouse IFN-γ standard was serial diluted in 1X Diluent from 4,000 to 4 pg/μL. After 2 hours incubation at room temperature, the wells were washed with wash buffer 5 times. Detection antibody in 1X Diluent was added to the wells in 100 μL incubated at room temperature for 1 hour. After 4 washes, 100 μL/well of Avidin-HRP* diluted in 1X ELISA/ELISPOT was added to the wells and incubated at room temperature for 30 minutes. Wells were washed 7 times before adding 100 μL/well of 1X TMB Solution. The plate was incubated at room temperature protected from light for 15 minutes. The reaction was stopped with 50 μL 1 M H_2SO_4 per well. Luminescence was measured at 450 nm using the Victor2 Wallac reader (Perkin Elmer).

RESULTS

Isolation of clonal cell lines from a mouse PDAC model

Genetically engineered mouse models (GEMM) can recapitulate human pancreatic ductal adenocarcinoma (PDAC) pathology. In particular, the LSL-*Kras*[G12D/+]; LSL-*Trp53*[R172H/+]; *P48-Cre*, (KPC) model [31], mimics the genomic instability and disease progression, including metastases, of human PDAC. In addition to the heterogeneity of primary pancreatic tumors in the KPC model, diaphragmatic and peritoneal metastases are polyclonal [35]. However, clonal variants within a single pancreatic tumor derived from this model have not been characterized in depth.

To model intratumoral clonal heterogeneity, we established clonal cell lines from a primary PDAC lesion of a KPC mouse (Fig. 1a). The primary tumor showed the characteristic ductal adenocarcinoma and desmoplastic histopathology (Fig. S1a), and the liver and lungs of the KPC mouse contained metastatic lesions (Fig. S1b). After a brief expansion of the primary PDAC cells from multiple tumor regions in 2D cell culture, we generated eleven clonal cell lines by single cell cloning (Fig. 1a). Genotyping of the clonal PDAC cell lines confirmed heterozygosity for the *Kras* locus (wildtype and recombined *Kras*) and a loss of the wildtype *Trp53* allele (Fig. S1c), similar to previous assessments of PDAC cells from KPC mice [31].

The clonal PDAC cell lines are polymorphic and genetically heterogeneous

From the initial cell line panel we selected six cell lines with distinct cell morphology and 3D growth phenotypes: The clones D10 and F2 are spindle-shaped, whereas C5, G8 and G9 display cuboidal morphology (Fig. S1d).

To evaluate signal transduction downstream of mutated KRAS, we assessed ERK1/2 phosphorylation in the individual clones by Western Blot analysis. Different levels of phospho ERK1/2 in the clonal cell lines grown in vitro (Fig. 1b) indicate distinct stimuli in addition to the presence of the *Kras*^{G12D} oncogenic driver mutation. Differences in the *Kras*^{G12D} variant allele frequency (VAF) of 1:1 to 4:1 (Fig. S1e) did not match with the different levels of ERK phosphorylation. This corroborates previous studies showing that *KRAS* mutation status is only poorly related to ERK activation [36-38], and suggests additional, distinct regulators of ERK1/2 activity amongst the clones derived from the same *Kras*^{G12D} driven tumor.

Collagen can reveal invasive behavior of pancreatic epithelial cells [39-41] and we assessed whether the clonal PDAC cell lines show different formation of ductal structures during 3D growth in type 1 collagen. The ability to develop ducts was poor for clones G8 and G9, whereas clone C5 formed wide ducts with blunt terminal buds, and C8 and F2 generated meshes of thin tubules (Fig. 1c).

Distinct gene expression patterns were found for the clonal cell lines grown in vitro by RNA sequencing. When comparing the clonal gene expression values to the average expression of all six clones, we found that clone G9 had the highest number of differentially expressed genes with 90 genes being upregulated more than 2-fold and 179 genes being down regulated. The lists of genes can be found in Data file S1. Gene set enrichment analysis was performed and the Hallmark Pathway families that were distinct for the clonal cell lines are shown in Figure 1d.

Next we assessed the genomic heterogeneity using whole exome sequencing of DNA from the parental tumor tissue and from the six individual clonal cell lines. To avoid contamination by circulating or metastatic cancer cells, genomic DNA from a tumor-free pancreas of a healthy female littermate mouse was used as a control. In the parental tumor tissue 174 non-synonymous that lead to amino acid substitutions were detected. The lists of mutations in the clonal cell lines and the tumor are shown in Data file S2. The clonal cell lines contained 146-247 mutations (Fig. 1e). Based on the multicellular oncogenic activation, the KPC model gives rise to multifocal cancer [35]. We found 64 ubiquitous mutations that are shared among all clonal cells and the parental tumor (Table S1), supporting the notion that the clonal cells were derived from a common ancestor that was selected for at an earlier stage of tumor progression. Approximately half (45% to 67%) of the mutations found in the clonal cell lines were detectable in the tumor tissue at the sequencing depth applied to the genomic DNA. The different abundance of the clonal subpopulation in the tumor tissue as well as the dilution of the tissue DNA by stromal cell DNA explains that not all of the mutations found in the cell lines were also detectable in the original tumor tissue. The number of unique mutations range from 18 in C5 and G8 to 89 in clone C8 (Fig. 1f). The list
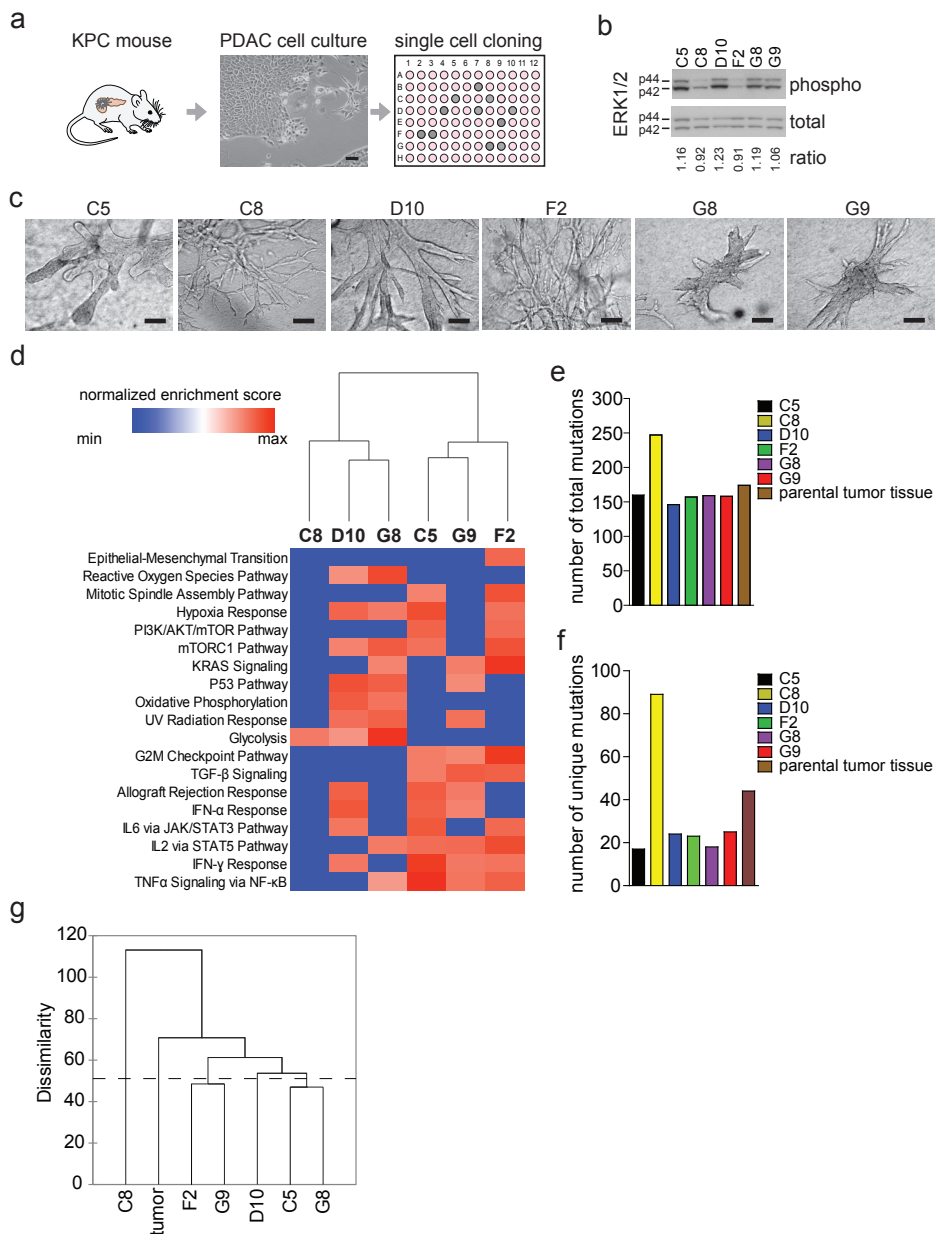
Figure 1. Characterization of clonal cell lines from a KPC mouse pancreatic tumor.

a. Workflow for the generation of clonal cell lines. A pancreatic tumor from an LSL-*Kras*[G12D/+]; LSL-*Trp53*[R172H/+]; P48Cre/- (KPC) mouse was harvested and cultured for one week. An image of the primary cancer cell growth is shown (scale bar = 100 µm). When the culture reached confluence, cells were transferred to a 96-well culture plate for single cell cloning. After 3 weeks of incubation eleven wells contained clonal cell lines (grey circles).

b. Western blot for phospho ERK1/2 (Thr202/Tyr204) and total ERK1/2 protein in clonal cell lines.

c. 3D tubular structures of clonal cell lines grown in collagen-1 for 10 days. Scale bar = 100 μm. Equal numbers of the clonal cells were grown as 2D monolayers in DMEM 10%FBS for 3 days.

d. Heatmap of the Hallmark Pathway Families of the clonal cell lines in vitro, based on Gene Set Enrichment Analysis (GSEA) of RNA-sequencing gene expression data.

e. Number of non-synonymous single nucleotide variations in the clonal cell lines and the parental tumor tissue detected by exome sequencing.

f. Number of unique signature mutations in the clonal cells and the parental tumor tissue.

g. Cluster analysis of the gene mutations in the clonal cells and the parental tumor tissue. The dashed line indicates significant differences (Euclidian distance).

of unique signature mutations is shown in Table S2. Cluster analysis of the mutations show the relationship between the tumor tissue and the clonal cells and Indicates that clone C8 is most distinct (Fig. 1g).

In summary, we found that the KPC tumor harbors genetically distinct cancer subpopulations, that matches with previous studies in both murine and human PDAC [11,35,42,43]. In the experiments described below we took advantage of the unique mutations in individual clones, to track and quantitate their abundance in clonal mixtures in cell culture as well as tumor growth in vivo.

In vitro drug responses of the clonal PDAC cell lines are distinct

To uncover potential differences in growth pathway activity of the clonal cell lines we evaluated their sensitivity to different drugs. Monolayer growth of the clonal cell lines shows some differences in the growth rates as well as at the maximum level of confluence, as indicated by the impedance measurement (Fig. 2a). Clone G8 has the highest growth rate compared to the other clones (Fig. 2b). We next assessed the sensitivity of the clonal cell lines to gemcitabine that is the approved for the treatment of PDAC, and evaluated the response of the clonal cell lines to a series of pathway-targeted drugs. Initially, 196 kinase inhibitors that target >34 kinases were tested for their growth inhibitory effect at a fixed concentration of 500 nM (data not shown). From this screen, we found that drugs targeting MEK, a RAS-effector known to be activated in human *KRAS* mutant PDAC [44] distinguished best between the clones. We also included the anti-metabolite gemcitabine in the analysis since it is approved for the treatment of PDAC. Dose response curves of treatment with gemcitabine and the clinically used MEK inhibitor trametinib (Fig. S2a) showed IC50 values ranging from 15 to 205 nM between the clonal cell lines in vitro (Fig. 2c). Gemcitabine was not as selective, with IC50 values ranging from 5 to 19 nM (Fig. 2c). These distinct sensitivities to anti-cancer drugs with different mechanisms of action amongst cell subpopulations from the same tumor indicate the functional heterogeneity of growth pathway activity in the clonal cell lines. There was no correlation between gemcitabine or trametinib sensitivity and the proliferation rates or the levels of ERK1/2 phosphorylation of the individual clones.
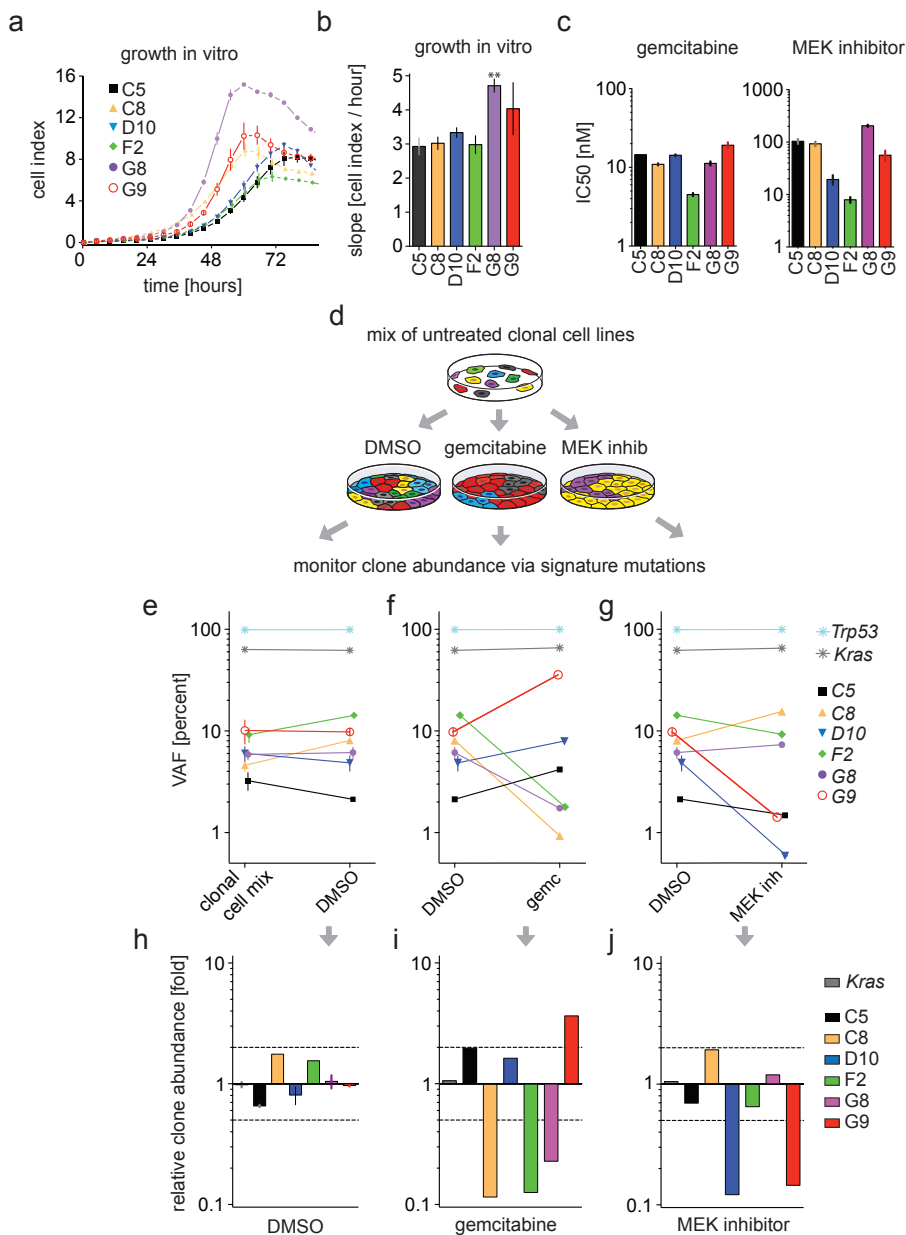
Figure 2. Clonal drug sensitivity in the context of the mixed population in vitro.

a. Cell growth of the individual clonal cell lines in vitro. Error bars are SEM of 4 replicate wells.

b. Growth rates of individual clonal cell lines in vitro. Slopes of growth curves were calculated from the data in Fig. 2a, with error bars representing the SEM of 4 replicate wells. ** P =0.0024 by t-test relative to other clonal cell lines.

c. IC$_{50}$ values of individual clonal cell lines after a 72 hour treatment in vitro with gemcitabine or trametinib, calculated from the dose response curves shown in Suppl.Fig 2b. Error bars represent SEM of drug treated cell growth in triplicate wells. Note: log scale of the Y-axis

d. Schematic depiction of the growth assay of the clonal cell mixture in vitro in the presence of DMSO, 25 nM gemcitabine or 100 nM trametinib. When cells reached 90% confluency, genomic DNA was extracted to measure clone abundance by deep sequencing.

e - g. Variant allele frequencies (VAF) of *Kras, Trp53* and 6 genes containing clone-specific signature mutations, measured by amplicon deep-sequencing. DNA from the untreated cell mix and the clone mixture grown in presence of DMSO (e), the clone mixture grown in presence of DMSO or gemcitabine (f) or trametinib (g) until confluent. Note the log scale of the Y-axis. Three and two sequencing runs were carried out for the starting clone mixture and DMSO treated cells respectively.

h - j. Change in clone abundance after treatment with DMSO (h), gemcitabine (i) or trametinib (j) based on the VAFs of the clonal signature mutations, compared to those in the starting clone mix. Note the log scale of the Y-axis. The dashed lines indicate 2-fold increase or decrease in clone abundance.

In vitro drug responses of clonal cells are altered when growing in the heterogeneous cell mixture

As a step towards the analysis of a heterogeneous cancer cell population, we next assessed the drug sensitivity of individual clones in the mixed population (Fig. 2d). We hypothesized that resistant clones in the population would have a selective advantage though the crosstalk between different clones via secreted factors or cell-cell contact might impact the sensitivity to pathway inhibitors. Deep sequencing for the signature mutation of each clone (Table 1) was employed to identify and quantitate the abundance of clones in the mixture. The number of reads of mutant and wildtype DNA are shown in Table S3. Variant allele frequencies (VAF) measured in the starting mixture of the clones were compared to those in the clone mixture that had grown under control conditions (DMSO) or gemcitabine (25 nM) or trametinib (100 nM) until reaching confluence (Fig. 2d). The VAFs under control and drug treatment are shown in Fig. 2e-g and the impact of drug treatment on the clonal contribution to the cell population in Fig. 2h-j. It should be noted that each cell line retains only one copy of the *Trp53* allele, with the R172H mutant, that is reflected in the ~100% read of the VAF for *Trp53*, irrespective of the treatment.

Table 1. Genes with signature mutations used to identify clones by deep sequencing.

clone	gene	chrom	position (mm9)	heterozygous variant	AAS	transcript
C5	*Baiap3*	chr17	25387359	G>T	L170I	NM_001163270
C8	*Olfr1157*	chr2	87802181	G>C	I289M	NM_146849
D10	*Nox4*	chr7	94462586	C>T	T89M	NM_015760
F2	*Matn4*	chr2	164222680	C>T	R339Q	NM_013592
G8	*Arhgap25*	chr6	87426299	T>C	K171R	NM_001037727
G9	*Pla2g4d*	chr2	120094626	G>T	S710R *	NM_001024137
Each clone	*Trp53*	chr11	69402014	G>A	R172H ^	NM_001127233
Each clone	*Kras*	chr6	145195291	C>T	G12D	NM_021284

chr = chromosome; mm9 = mus musculus reference genome 9; AAS = amino acid substitution;
* = mutation also present in the parental tumor tissue; ^ = loss of wildtype allele

When the mixed cancer cell population was grown under control conditions, no significant enrichment of clones was found (Fig. 2h). This was surprising since clone G8 grows significantly faster than the others when grown individually. Paracrine signaling may harmonize the growth rate of clones in the mixture. Gemcitabine treatment, selected for clone G9 by ~4-fold and led to a ~5-10-fold decreased abundance of clones C8, F2 and G8 (Fig. 2i). The latter 3 clones were the most sensitive to gemcitabine (Fig. 2c) and their reduced abundance matches with their relative sensitivity to the drug. This indicates that cancer cell crosstalk had no major impact on the effect of gemcitabine, in line with the cell-autonomous mechanism of action of this anti-metabolite.

In contrast to gemcitabine, treatment with trametinib led to a ~10-fold reduction of clones D10 and G9 in the mixed population (Fig. 2j). Clone C8 made up the largest portion of the population (Fig. 2f) and therefore seems unresponsive to trametinib when grown in the presence of the other clones. To our surprise, the most MEK inhibitor-resistant clone G8 (Fig. 2c) did not dominate when growing in the presence of the other cell lines and trametinib (Fig. 2j). To assess whether secreted factors from the other clones played a role in sensitizing clone G8 to trametinib, we conducted an experiment with conditioned media. As a comparison we used clone C8, which appeared favored by 2-fold when the mixture was treated with trametinib. Clonal cell lines G8 and C8 were grown individually and treated with different concentrations of trametinib in the presence of conditioned media from the matching cell line, or with the conditioned media from the mixed population. We found that clone G8 is sensitized to trametinib when conditioned media from the mixed population was added (Fig. S2b) but did not observe this effect for clone C8 (Fig. S2c). We conclude from this that growth behavior and drug sensitivity of cancer cell subpopulations can be altered by the composition of the population due to paracrine crosstalk.

Tumorigenesis of clonal cell lines in immune competent mice

When placed in the intraperitoneal cavity of immune-competent compatible mice, each clonal cell line homes to the pancreas, invading and destroying the tissue architecture (Fig. S3a). To easily monitor the tumor growth rate, the individual clonal cell lines were also injected subcutaneously into the flanks of compatible mice. It is noteworthy that the histopathological features of the subcutaneous tumors were indistinguishable from those of orthotopic allograft tumors in the pancreas (Fig. S3b vs S3a). In vivo, clone D10 the most fibroblast-like clone (Fig. S1d), generates poorly differentiated tumors, whereas the other clones developed differentiated adenocarcinomas with glandular structures, either orthotopically or subcutaneously. Differentiation of the tumors was not predictable from the 3D growth phenotype of the clonal cell lines in collagen type 1, in which D10 forms tube-like structures, whereas G9 and G8 do not (see Fig. 1c). Growth rates of the subcutaneous clonal tumors from C5 and D10 were relatively low, whereas clone G8 grew at a significantly

higher rate than the other clones (Figs. 3a, S3c). Interestingly, gene analysis indicated an upregulation of the allograft rejection response pathway for clones C5 and D10 (Fig. 1d) and corroborates the tumor growth phenotype. All clones recruited cancer-associated fibroblasts and induced desmoplasia that is pathognomonic for PDAC. Staining of the tumors for α-smooth muscle actin (α-SMA) revealed equal proportions of myofibroblasts across the subcutaneous allograft tumors from the clonal cell lines (Fig. S3d). The homogeneous recruitment of myofibroblasts was confirmed by qRT-PCR analysis of the gene expression levels of α-SMA in the clonal allograft tumors (Fig. S3e).

Response of heterogeneous tumors to different types of drug therapy

Tumor tissue architecture has profound effects on malignant progression and resistance to drug therapy and is controlled by cell-cell and extracellular matrix interactions [19,20,43]. In addition, cytotoxic drugs and pathway inhibitors can stimulate or inhibit stromal cells that participate in the immune response to a malignant lesion [45-47]. To assess treatment responses of PDAC subpopulations in the context of tumor stroma and an intact immune system, we inoculated compatible, immune-competent syngeneic mice with an equal mixture of the above described six clonal cell lines and treated them with prototypic drugs that target different hallmarks of malignancy. We hypothesized that the relative drug sensitivity of clonal subpopulations would be distinct for drugs that act via different mechanisms. Also, we surmised that clonal responses in vitro might differ from the in vivo sensitivity due to host-tumor interactions. The heterogeneous subcutaneous tumors were allowed to establish for one week and mice were then treated for two weeks with intraperitoneal injections of the control (PBS containing DMSO or control IgG), gemcitabine, an anti-programmed death-1 (PD-1) antibody, or oral gavage with trametinib (Fig. 3b). The maximal inhibitory effect on tumor sizes after gemcitabine and trametinib was reached after 5 days of treatment, whereas the α-PD-1 was most effective in reducing tumor size after 10 days of treatment (Fig. S4a). At the end of the two-week treatment period tumors were harvested for evaluation.

Distinct impact of different drugs on the allograft tumor stroma

The impact of stroma is crucial in cancer growth and known to modulate drug responses. Thus we initially evaluated the impact of drug treatment on the tumor cell/host stroma ratio. For this, we took advantage of the fact that the wildtype $Trp53$ allele is lost from the cancer cell lines and used the $Trp53^{R172H}$ variant allele frequency (VAF) as the readout of cancer cell abundance in the tumor tissues (Fig. 3c). Given that stromal cells from the host carry two copies of the wildtype $Trp53$ allele and the cancer cells only one copy of mutant $Trp53^{R172H}$, an equal contribution of stromal and cancer cells to the tumor would result in a $Trp53^{R172H}$ VAF of 33.3%. We observed a ~50% VAF indicating that 2/3 of the tumor mass is contributed by cancer cells. Although histologically the stroma appears dominant, this is mostly due to desmoplasia and not the abundant presence of stromal cells. After gemcitabine
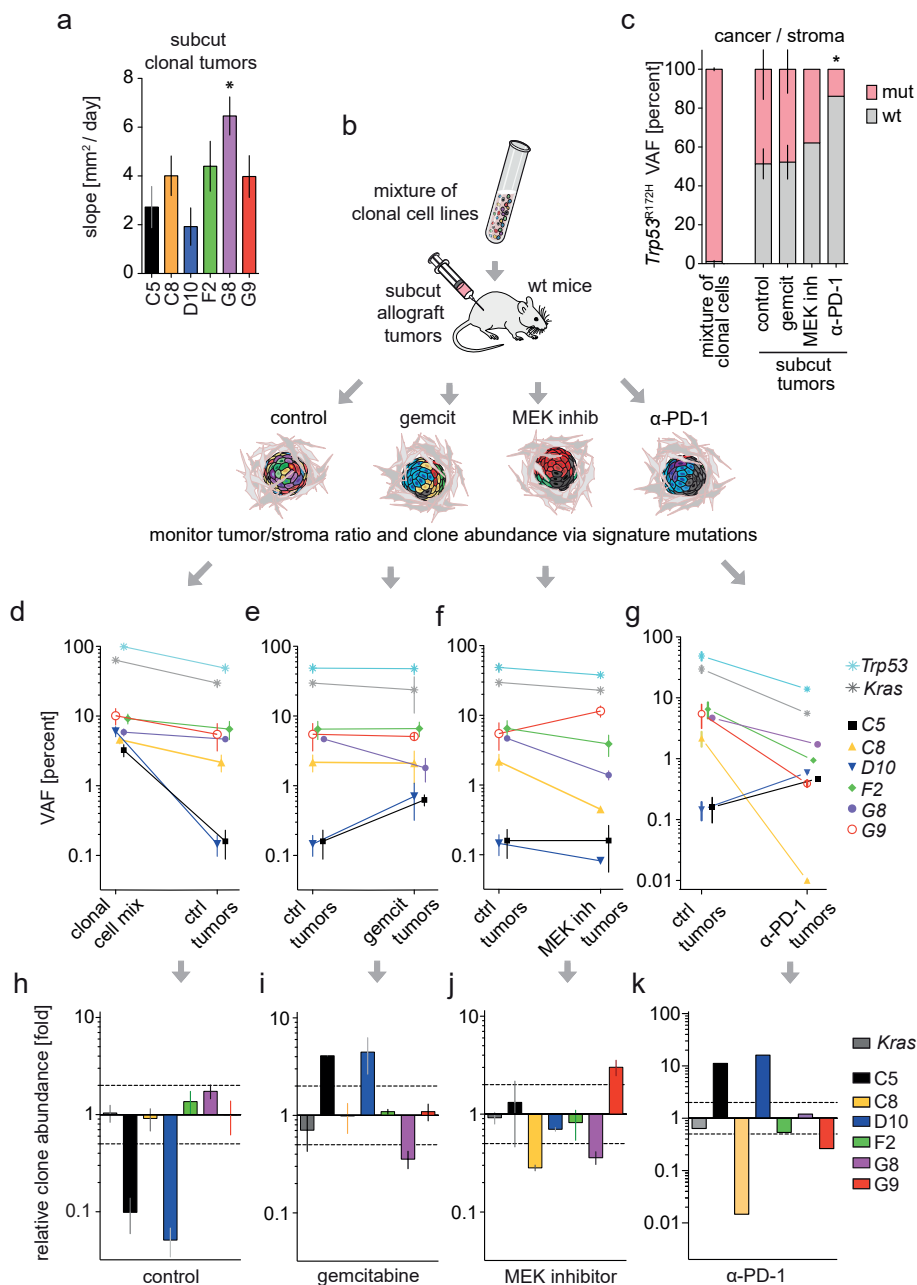
Figure 3. Clonal drug sensitivity in the context of heterogeneous tumors.

a. Growth rate of individual clonal allograft tumors. One million clonal cells were injected subcutaneously into the flanks of compatible immune competent mice. Error bars are SEM for n≥3 tumors, * *P* =0.0155 by t-test for the growth of G8 versus the median rate of the other clones.

b. Schematic depiction of allograft tumor generation using the pooled clonal mixture. One million mixed clonal cells were injected subcutaneously into the flanks of immune competent syngeneic mice.

When tumors had established, the animals were treated with control vehicle, gemcitabine, trametinib, or anti-PD-1 for 2 weeks. Tumors were collected for histology and genomic DNA was isolated.

c. $Trp53^{R172H}$ variant allele frequency (VAF) in DNA from ≥5 treated tumors, indicating cancer cell load in the tumors, measured by amplicon deep sequencing of signature mutations. * P =0.0206 t-test VAF in α-PD-1 tumors compared to control tumors. Error bars represent SEM from n=3 sequencing runs for the clonal cell mix, n=4 sequencing runs for control tumors, n=2 sequencing runs for gemcitabine tumors. DNA from ≥5 tumors was pooled per sequencing run.

d – g. VAFs of *Kras*, *Trp53* and 6 genes containing clonal signature mutations, measured by amplicon deep-sequencing, from DNA from (d) the untreated cell mixture and control treated tumors; (e) control and gemcitabine treated tumors; (f) control and trametinib treated tumors; (g) control and α-PD-1 treated tumors. Graphs have a log scale for the y-axes, error bars represent SEM, n=3 deep sequencing runs for the untreated cell mixture, n=5 for the control tumors, n=2 for the gemcitabine and trametinib tumors. DNA from ≥5 tumors was pooled per sequencing run.

h - k. Change in clone abundance in tumors treated with (h) control: (i) gemcitabine; (j) trametinib; or (k) α-PD-1. The graphs have a log scale for the Y-axis; the dashed lines indicate 2-fold increase or decrease in clone abundance. Clone abundance was normalized to total cancer cell load ($Trp53^{R172H}$ VAF) in the tumors. Error bars represent SEM, n=5 sequencing repeats for the control tumors, n=2 for the gemcitabine and trametinib tumors. DNA from ≥5 tumors was pooled per sequencing run.

treatment the contribution to tumors was not changed relative to control tumors, whereas a decrease in cancer cell-specific mutant $Trp53^{R172H}$ from ~49% to ~38% was observed in the MEK inhibitor treated tumors (Fig. 3c). Although this decrease was not statistically significant, this finding suggests that trametinib may have a greater inhibitory effect on the cancer cells than on the tumor stroma. Strikingly, the α-PD-1 treatment resulted in a significant decrease of mutant $Trp53^{R172H}$ DNA to ~14%, compared to ~49% in control tumors (Fig. 3c) due to immune cell recruitment as well as due to cancer cell death. The immune recruitment was validated in the tumor sections, in which showed increased leukocyte infiltration in the α-PD-1 treated tumors (Fig. S4b), whilst the different treatments did not impact the abundance of α-SMA positive fibroblasts (Fig. S4c).

Effects of gemcitabine and trametinib on the growth of clonal subpopulations in heterogeneous tumors are different from the effects in vitro

To monitor clonal drug responses we used deep sequencing of tumor DNA and quantitated the abundance of clonal signature mutations (Table 1). Variant allele frequencies (VAFs) of the clone-specific signature mutations and of mutant *Kras* and *Trp53* under the different treatment conditions are shown in Fig. 3d-g (for absolute read counts see Table S4). Changes in cancer cell subpopulation abundance in the tumors are shown in Fig. 3h-k and discussed in the next sections. Tumor growth of individual clonal tumors without drug treatment revealed the fastest rate for clone G8 and the slowest for C5 and D10 (Fig. 3a). These distinctions were maintained in the heterogeneous tumors (Fig. 3h), indicating that the growth conditions provided in the tumor microenvironment determine clone-specific growth rates.

Next, we compared the impact of gemcitabine and MEK inhibitor treatment on the growth of clonal subpopulations. Only the clone G8 showed a reduced contribution to the tumors after gemcitabine treatment whilst the slow growing clones C5 and D10 gained ~5-fold in abundance (Fig. 3i). Clones C8 and F2, which were inhibited by gemcitabine when grown in the mixed population in vitro (see Fig. 2h) were not impacted by gemcitabine in the heterogeneous tumors in vivo (Fig. 3i). This suggests that the stroma protects clones C8 and F2 from the inhibitory effects of gemcitabine.

The MEK inhibitor treatment of the reconstituted, heterogeneous tumors revealed that clones C8 and G8 are sensitive to trametinib treatment (Fig. 3j), whereas G9 gained in abundance and became the dominant subpopulation in the tumors (Fig. 3f & j). This contrasts with the in vitro findings where clone G9 was sensitive and C8 resistant to trametinib (see Fig. 2j), suggesting that the stroma provides stimuli that alter clonal sensitivity to the MEK inhibitor.

Distinct response of clonal subpopulations in heterogeneous tumors to PD-1 blockade

PDAC is notorious for its dense fibrosis, immune suppressive environment and low number of intratumoral effector T-lymphocytes [48,49]. It has been suggested that these factors drive the low PDAC responsiveness to immune checkpoint inhibition such as anti-programmed death-1 (PD-1) therapy. To assess whether cancer heterogeneity may also play a role in the resistance, we investigated the response of the different clones to anti-PD-1 monoclonal antibody therapy. Similar to the above drug sensitivity assessments, we injected the mixed population of PDAC clones subcutaneously in immune competent mice and treated the animals for 2 weeks. When measuring the clonal contribution to the allograft tumors (Fig. 3g), we found strikingly different responses between the clonal subpopulations. In particular, clone C8 was eliminated after α-PD-1 treatment and clone G9 by >70% (Fig. 3k). Interestingly, the contribution of clones C5 and D10 to the cancer lesions was increased by ~10-fold after the α-PD-1 treatment (Fig. 3k), suggesting that the growth disadvantage of these two clones under control conditions (see Fig. 3h) is not regulated by PD-1 dependent allograft rejection, but due to other microenvironmental factors. The differential clonal sensitivity to leukocyte-mediated killing of clone C8 and G9 initiated by PD-1 blockade suggests cancer cell-intrinsic selectivity and we evaluated the potential mechanism further.

Clonal PDAC cancer cell lines have different abilities to attract leukocytes

Based on the differences in allograft tumor formation and sensitivity to α-PD-1 treatment, we investigated the type of immune cells that infiltrate into the allograft tumors, using flow cytometry (Fig. S5). Analyses of lymphocytes revealed that the highest numbers of infiltrating CD4+ T cells are detected in tumors from clones D10 and G8, whereas the CD8+ T-lymphocytes in the tumors from clones C8, F2 and G9 are higher than in tumors

from the other clones (Fig. 4a). To further elucidate the activation of T-cells in the clonal tumors, we measured CD25 and PD-1 surface expression by flow cytometry. Programmed Cell Death protein-1 (PD-1) is expressed on T-cells upon continuous activation [50]. CD25, also known as Interleukin-2 Receptor α is expressed by regulatory T-cells after stimulation, resulting in CD8+ CD25+ memory T-cells, and CD4+ CD25+ suppressive T-cells [51]. Allograft tumors from clone C8 contain the highest number of CD4+ PD-1+ and CD8+/ PD-1+ that are stimulated via their T-cell receptors (Fig. 4b-c). This might explain the high sensitivity of clone C8 to the α-PD-1 treatment. The second most sensitivity clone to α-PD-1 treatment G9 also has the highest number of tumor infiltration CD8+ PD-1+ T-cells (Fig. 4c), supporting this hypothesis. The number of suppressive CD25+ CD4+ T-cells (mean 36.4% ± 9.1) in the clonal tumors is not associated to different growth phenotypes (Fig. 4b).

Gut associated lymphoid tissue in caecal patches contain cancer reactive T-cells

To investigate whether the differential α-PD-1 sensitivity is mediated by direct cell-cell contact between effector T-lymphocytes and cancer cells, we performed an in vitro co-culture experiment. First, we injected the mixture of the six PDAC clonal cell lines intraperitoneally in immune competent compatible mice to let allograft tumors develop for two weeks. We hypothesized that in tumor bearing mice naïve mouse T-lymphocytes get activated in the gut-associated lymphoid tissue (GALT) such as the Peyer's patches and the caecal patch (the murine equivalent of the human appendix vermiformis [52,53], via their T cell receptor (TCR), mediated by dendritic cells presenting tumor antigens from the cancer cells. Primed T-lymphocytes in the GALT differentiate into effector T-cells, which can migrate to the site of origin of the tumor antigens, and kill the malignant cells [54]. To test this hypothesis we initially studied the histology of the caecal patch lymphoid tissues and found a significant increase in the size of germinal centers in the ceacal patches of tumor bearing KPC mice (Figs. S6a-b), suggesting an increase in immune activation compared to healthy mice.

For functional studies, we subsequently isolated T-lymphocytes from caecal patches of tumor bearing mice for an in vitro activation assay. Figure 4d provides a schematic overview of the procedure. After allowing the mixed clonal allograft tumor growth for two weeks, we isolated T-lymphocytes from the caecal patches of the tumor bearing mice, yielding ~60,000-330,000 live T-cells per mouse. As controls, we isolated T-lymphocytes from the caecal patches of healthy wildtype mice, yielding 45,000-48,000 live T-cells per mouse. Growth media of the T-lymphocytes was supplemented with interleukin-2 (IL-2) and the PDAC clonal cells were added to the cell-cultures. Figure 4e provides a representative view of the PDAC clonal cell mixture growing together with the isolated T-cells after 48 hours. T-cells from healthy mice as well as from tumor bearing mice attach to the PDAC cells (Fig. 4e). Notably, the PDAC cells in co-culture with T-cells from tumor bearing mice de-attached from the plate at a higher rate and show signs of distress (Fig 4e).
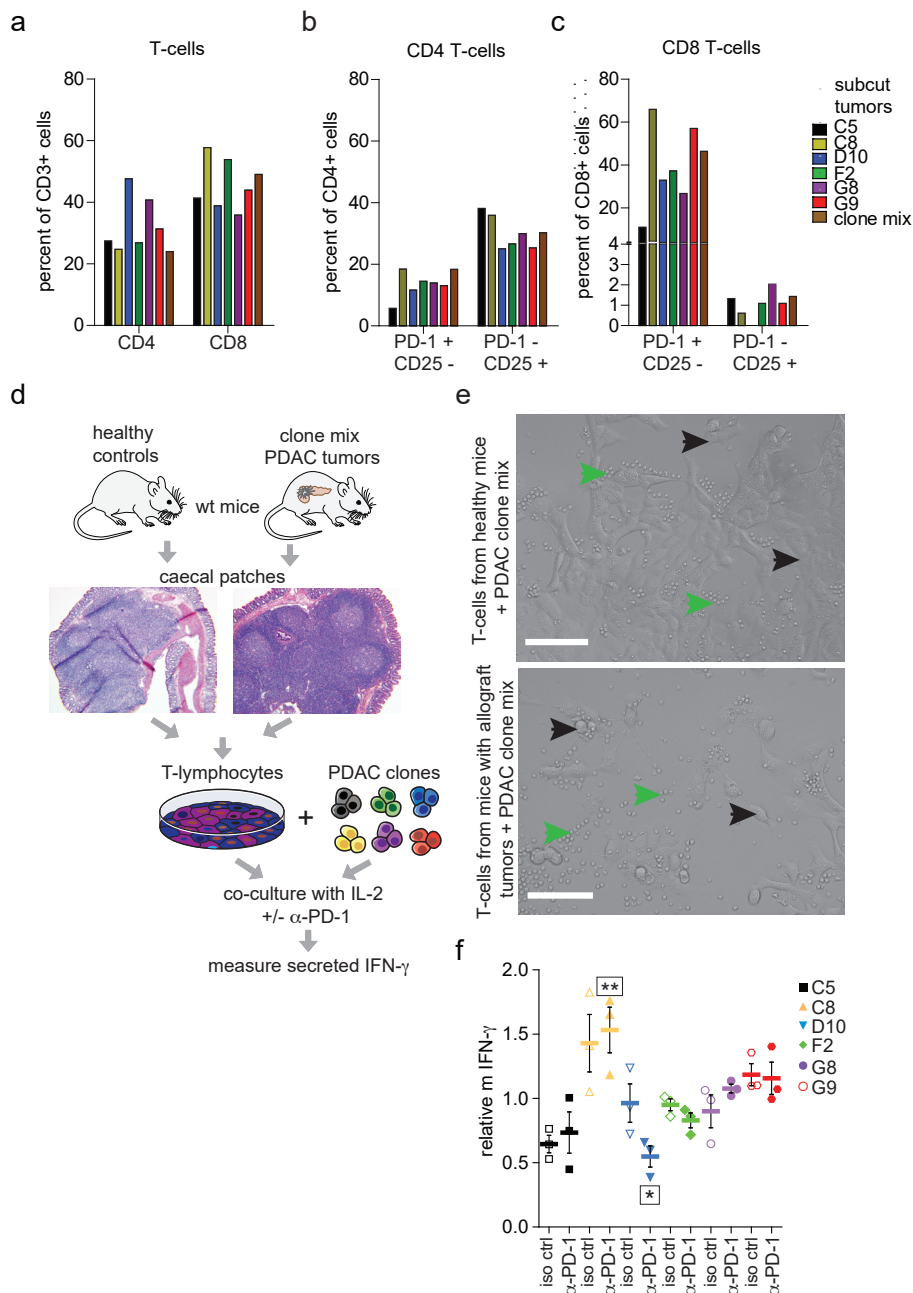
Figure 4. Differential activation of primed T-lymphocytes by clonal pancreatic cancer cells.
a. Flow cytometry results of tumor infiltrating lymphocytes. One million cells of the individual clones, or the clone mixture were injected subcutaneously into the flanks of immune competent syngeneic mice. When tumors had established after 10 days tumors were harvested and processed for flow cytometry analysis. Percentage of CD4 and CD8 T cells are graphed as frequency of total T cells (CD3+ T cells).

b. Flow cytometry results of PD-1 and CD25 expression on CD4 T cells in allograft tumors.

c. Flow cytometry results of PD-1 and CD25 expression on CD8 T cells in allograft tumors.

d. Schematic of workflow of T-lymphocytes isolation and culture. T-cells were isolated from the caecal patches of healthy control and PDAC allograft tumor bearing mice, and co-cultured together with the PDAC clonal cell lines supplemented with Internleukin-2. After 48 hours, interferon-γ was measured in the supernatants.

e. Images of the PDAC clone mixture and mouse caecal patch T-lymphocytes co-culture in vitro at 48 hours. Green arrows indicate T-lymphocytes, black arrows indicate PDAC cells. Scale bar = 100 μm.

f. Relative amount of IFN-γ in the supernatant of ceacal patch T-lymphocytes from mice that carried clone mix tumors, co-cultured with the individual PDAC clonal cell lines for 48 hours in presence of anti-PD-1 or the igG2a isotype control (iso control), measured by ELISA. Error bars are SEM, measurements from lymphocytes from n=3 mice. Levels of IFN-γ are normalized to the median level of IFN-γ secretion by lymphocytes per mouse. Clone C8 ** P=0.0017 and clone D10 * P = 0.0226, by t-test compared to average level of the other clones.

Clonal cancer cells activate caecal patch T-cells from tumor bearing mice to a different extent

One of the effector mechanisms of activated T-cells is production of Interferon-γ (IFN-γ). Indeed, T-lymphocytes harvested from caecal patches of healthy mice do not secrete IFN-γ when co-cultured with the clonal PDAC cells (Fig. S6b), whereas T-lymphocytes from tumor-bearing mice with intraperitoneal, mixed clone tumors initiated elevated IFN-γ secretion in co-cultures with the clonal PDAC cells (Fig. S6c). Although efficiency of the T-lymphocyte isolation varies between mice (see Fig. S6c), co-cultures of T-cells from tumor bearing mice with PDAC clone C8 elicited the highest level of IFN-γ secretion, and clone G9 the second highest, relative to the other PDAC clones (Fig. 4f). Oncogenic mutation burden and the abundance of tumor infiltrating CD8+ T-lymphocytes are potential predictors for response to anti-PD-1 therapy [55]. Both were found for α-PD-1 sensitive clone C8, which has the highest number of unique non-synonymous mutations (see Fig. 1e-f) and high numbers of tumor infiltration CD8+ T-cells (see Fig. 4a-b). Complementary to these observations, the IFN-γ production by T-cells from allograft tumor bearing mice that are co-cultured with PDAC clone D10 in the presence of α-PD-1 is significantly lower than the levels elicited by the other PDAC clones (Fig. 4d) and this corroborates the resistance of clone D10 to α-PD-1 treatment in vivo (see Fig. 3k). In conclusion, clonal PDAC cell lines originating from the same parental PDAC tumor have distinct intrinsic capacities to activate primed T-lymphocytes in vitro (Fig. 4f), matching with the distinct responses to α-PD-1 treatment in vivo.

We conclude from the above analyses that the crosstalk amongst cancer cell subpopulations and the host stroma impacts the sensitivity to different therapeutic approaches distinctly, allowing the emergence of discrete resistant subpopulations. Moreover, our results suggest that cancer cell-intrinsic factors impact the ab initio sensitivity of subpopulations to immune checkpoint inhibitors.

DISCUSSION

Heterogeneity of human cancers emerges during evolutionary selection of cell subpopulations with different genetic and epigenetic alterations that provide a survival advantage under pressure from the microenvironment [9,10,13,26] and continues during therapy [17]. Crosstalk between tumor subpopulations is one of the modulators that impact cell growth and was recognized in a mammary tumor model several decades ago [56]. A recent study systematically evaluated and modeled this crosstalk via secreted factors [28]. The authors used the established human breast cancer cell line MDA-MB-468 to generate a panel of eighteen derivative cell lines by lentiviral expression of single secreted factors and showed that paracrine stimuli from small, less fit clonal subpopulations can still drive malignant progression of xenograft tumors in immune-compromised mice. Also, the biologic significance of a highly dynamic but small subpopulation of cells was uncovered in human melanoma. It was shown that epigenetic regulation by an H3K4 demethylase maintains a slow growing, minor subpopulation in melanoma that can escape from treatments targeting fast growing populations, can repopulate the tumor and contribute to metastatic growth [57]. Patient derived xenografts (PDXs) can partially retain tumor heterogeneity [58]. However, PDXs need to be maintained in immune compromised animals and thus retain only a subset of the microenvironmental features. These examples illustrate the complex biology and challenges to generate appropriate experimental platforms that capture the dynamics of tumor evolution and allow for the assessment of therapeutic interventions.

In this study, we first deconvoluted a PDAC tumor from the classic KPC model into clonal cell lines and then reconstituted heterogeneous tumors to follow clonal dynamics during drug treatment in syngeneic, immune competent hosts. Based on the signature mutations identified for each clone and the shared *Trp53* variant allele amongst the clones, the relative abundance and stromal contribution can be quantitated in our model in the context of an intact immune environment. One of our findings was that clonal cell growth of the mixed population in vitro correlated only in part with growth in the presence of host stroma and immune cells. Under control conditions the growth in vivo of some clones was slower despite their indistinguishable growth rates in vitro. This suggests that the crosstalk with immune cells and tumor stroma is different for these clonal cancer cells, though they were derived from the same original tumor specimen.

Previous studies have shown the impact of stromal signals on cancer cell drug sensitivity [59,60] and more recent models have tried to capture some of the features of the environment in vitro [59-63]. In the current study, the MEK kinase inhibitor showed the most striking differences between the findings in vitro and in vivo and we attribute some of this to the impact of the inhibitor on crosstalk between cancer cells and stromal cells. Paracrine clonal

crosstalk amongs cancer cells can explain the sensitization of clone G8 that was resistant to trametinib on its own but sensitized in the mixed cancer cell culture in vitro. A comparison of clonal effects of trametinib in the mixed culture in vitro and in the tumors however, showed a discordant result for clone G9 that moved from sensitive in vitro to resistant in the tumors and clone C8 that moved in the opposite direction (see Fig. 2j vs Fig. 3j). Still, under the MEK inhibitor treatment stromal cell abundance increased (Fig. 3c) suggesting additional crosstalk of tumor cells and stroma that altered the clonal sensitivity in vivo.

The potential contribution of host immune cells to the differential growth we observed in vivo versus in vitro is suggested by earlier studies. One classic study showed distinct immunogenicity of clonal subpopulations of a mouse mammary adenocarcinoma [64]. Surprisingly, we found that immune checkpoint blockade, which leads to increased lymphocyte-mediated cancer cell killing [65,66], did not reduce the growth of slow growing clones any further. In contrast, these clones increased in abundance in the residual tumor after α-PD-1 treatment and thus appear resistant to checkpoint inhibition. Also, the slower clones C5 and D10 increased in abundance after treatment with the cytotoxic drug gemcitabine. This finding is reminiscent of a recent report that showed that minor dormant human colorectal cancer clones can become dominant and reinitiate tumor growth after chemotherapy [67].

The striking differences in immunotherapy efficacy towards clones present in heterogeneous tumor mix provides some interesting insights that may allow to overcome resistance. One of the clonal cell lines, clone C8, is particularly sensitive to α-PD-1 therapy. The co-culture experiment with primed mouse T-lymphocytes and the clonal PDAC cell lines corroborated the finding. Antigens specific to clone C8 activated primed T-lymphocytes significantly better than those of the other clonal lines generated from the same tumor. TILs are often exhausted and thus difficult to use in cell culture experiments [68]. We conducted this experiment with T-lymphocytes from the caecal patches of allograft tumor bearing mice. We are the first to show that caecal patches of in PDAC bearing mice contain cancer-specific effector T-cells, providing a new approach to assess immunotherapy efficacy.

In conclusion, the composition of heterogeneous cancers is affected by crosstalk amongst the cancer subpopulations as well as the host environment that includes the immune system as a major player. We developed an in vivo model that allows for the quantitation of clonal cancer subpopulations in heterogeneous tumors, growing in immune competent animals. Our model is suited for the assessment of stromal and immune modulators and their impact on growth of heterogeneous cancer cells. Our study shows that prediction of drug efficacy from in vitro analysis of heterogeneous cancer cell populations is dependent on the mechanism of action of the studies drugs. Immune response and sensitivity to checkpoint

blockade is cancer clone specific and predictable using co-cultures with appropriately primed effector T-cells.

Data availability statement

The RNA and exome sequencing datasets generated during the current study are available from the corresponding author on reasonable request.

Acknowledgements

Author contributions

EEV, AW and ATR conceived the project and generated the manuscript. IP and EEV generated the clonal cell lines. EBB performed the 3D matrix cell cultures, and edits to the manuscript. EBB and EEV performed the analysis of the exome sequencing data. MDP and MOS performed the RNA seq analysis. EEV, SMR, AJ, MDP, IP and MHBCS performed animal studies and tumor analyses. JKS designed the in vitro drug assays and clonal drug sensitivity. EEV, JKS and MHBCS performed the in vitro drug screens. EEV, AJ and SMR performed the ddPCR, qPCR and amplicon experiments. JNM and EEV performed amplicon deep sequencing and analysis. SMR, MM and MC performed the flow cytometry analyses. BAM and ATR contributed to advancements of the project and edits of the manuscript. All authors discussed and approved the manuscript.

Competing financial interests and Conflicts of interest

The authors have no competing financial interests or conflicts of interest to disclose.

Supplementary Table 1. List of ubiquitous non-synonymous single nucleotide variations in the clonal cancer cell lines and the corresponding parental tumor tissue measured by exome sequencing. AAS = amino acid substitution

Gene	AAS	Gene	AAS	Gene	AAS	Gene	AAS
AB124611	D73G	*Kri1*	K241E	*Rbm12b2*	T574P	*Tmem52*	T91P
Aloxe3	A667V	*Lzts2*	H327Q	*Rbpjl*	T368S	*Tonsl*	T1086M
Atp13a4	F568L	*Mbp*	G27R	*Sec16b*	R31C	*Trp53*	R172H
Car4	A97V	*Ncoa3*	A706V	*Shisa6*	L368I	*Trp53rkb*	A208E
Clec2g	N12S	*Nfam1*	R220S	*Slc15a5*	G452S	*Ttll8*	R702L
Cntn5	T966A	*Nrip2*	P158S	*Slc30a4*	G64R	*Ugt1a1*	K80M
Cox11	V62A	*Nup160*	L7R	*Slc45a1*	S433L	*Uimc1*	E709D
Cypt4	N152S	*Olfr311*	A210T	*Slfn14*	V301I	*Vmn1r12*	F61L
Dock6	W145R	*Olfr314*	T238A	*Smco2*	T163N	*Vmn1r15*	T38I
Ecsit	S75L	*Olfr743*	N84S	*Smco3*	K193R	*Vmn1r6*	L264V
Gjd4	V80L	*Pdcd11*	P1556L	*Spint3*	T86I	*Wbp11*	D360N
Gm14459	M80I	*Pitpnm3*	R21Q	*Srebf2*	R621H	*Wfdc12*	L70P
Gtse1	P399L	*Ppfibp1*	L371P	*Tas2r136*	G202D	*Xaf1*	C135S
Kcnk15	I195V	*Ppl*	G179R	*Tekt1*	A237V	*Yipf2*	L227F
Klrc2	A188P	*Rangap1*	E389D	*Timm9*	R89W	*Zc3h7b*	A681T
Kras	G12D	*Rbbp8*	K178R	*Tmem241*	A85S	*Zfp426*	S54T

Supplementary Table 2. Unique signature single nucleotide variations in the clonal cell lines and the parental tumor measured by exome sequencing. Mutations in bold are used as clone identifiers in the heterogeneous mixtures.

Clone C5	Clone C8	Clone D10	Clone F2	Clone G8	Clone G9	Parental tumor tissue
Baiap3,L170I	1700113H08Rik, I192S	4921524L21Rik,	AA792892, K124N	4933402J07Rik,K17M	Ctnna3,L211V	4933409G03Rik,
Btnl2,A244V	Abcc12,S895G	Q233H	Abca1,F1535V	Adad2,T459P	Ctsn,R109H	D188E
Ceacam1, V437G	Adrbk1,P679A	4930444G20Rik,	Bcor,T941P	*Arhgap25,*	Cybrd1,H188R	A830010M20Rik,P47T
Epn1,T347P	Apoc2,L68F	H69Q	Ccdc61,A5P	*K171R*	Frmpd3,M429V	C2cd4a,R284C
Flg2,Q1327P	Apol7b,L353P	Adh4,I374T	Ccr1,S191T	Bmper,T570P	Grin2d,A764G	Ceacam20,S470N
Ifit2,D207E	Atpaf1,K267N	Anapc5,A522V	Clh3,I286T	Creld2,A44G	Hnf4a,R177W	Cep290,M2352L
Ifna7,R60G	Bcorl1,A242G	Cgn,Q1077H	Haplh4,L67F	Demd1c,T495P	Hyou1,S527R	Cux1,L1583P
Jak3,D809A	Cdh11,R137K	Chd6,A1204G	Herc3,N424S	Depdc7,M103I	Ighmbp2,K866N	Dcpp3,T39A
L3mbtl1,A146V	Cdk4,D221H	Cldn4,V32G	Huwe1,T3219P	Gpr89,V336G	Ino80,A1457P	Defa34,K24N
Ocm,A41P	Cfh,L138P	Coa7,V41G	Llgl2,T247P	H2-T9,H167Q	Lrp12,V671G	Dpy19l1,L367V
Olfr1212,L65P	Clpsl2,D92A	Coro6,I50V	Lrp2,I3348M	Mafk,K141T	Mmrn1,T389M	Duox1,H129R
Olfr1214, A118S	Crb2,L655F	Elf4,S496I	*Matn4,R339Q*	Pcdhga12,	Mnda,S205L	Dyrk1b,D668A
Slc24a3,T291P	Csf2rb,K195N	Gtf2a2,A33V	Olfr368,C183Y	A696P	Nlrp1a,S827T	Ear10,T30P
Snx14,G7R	Cyp2c54,K399T	Klhl13,Q416H	Pcdhgb8,	Ppp1r10,C463R	Nudt12,H251P	Fhad1,T1129M
Snx33,H140P	Dagla,A777P	Lactb1l,S317A	S170R	Rnf121,T119P	*Pla2g4d,S710R*	Gm14085,V338F
Spata31d1c, T688A	Dctn1,R1236K	Manea,V216G	Psg18,L259I	Siglech,H79P	Plp2,F78L	Gm4303,Q253H
Tacc2,T2575P	Dlgap4,A962P	Mark4,L469F	Psg27,F151I	Tcf25,E512D	Prg4,T441P	Hic1,S23P
Vmn1r193,	Dmd,G3185E	Mcm9,K38N	Ptgis,P489A	Thk2,D471A	Pydc4,E91V	Itgad,P1119L
I156V	Fat4,T3878P	*Nox4,T163M*	Rapgef1,	Usp49,A13P	Rapgef4,N213S	Kank3,R165G
	Fbh5,Y66D	Nup155,V280F	A429G	Vmn2r84,R571T	Rars2,T466P	Kazn,G48R
	Fbxw19,L212S	Pmaip1,L94F	Rrs1,L218M		Ret,R960P	Lactb1l,S539A
	Fcgr2b,T66I	Rgl2,D216A	Slc22a20,		Sparcl1,D199E	Macrod2,K6N
	Fgfr3,G650D	Tle3,S407C	L472F		Tas2r134,C50F	Mrps35,T11S
	Fmo2,H154P	Tyk2,T865P	Slc6a3,R614C		Ubr4,Q3355K	Naf1,L1187P

Supplementary Table 2. Unique signature single nucleotide variations in the clonal cell lines and the parental tumor measured by exome sequencing. Mutations in bold are used as clone identifiers in the heterogeneous mixtures. (continued)

Clone C5	Clone C8	Clone D10	Clone F2	Clone G8	Clone G9	Parental tumor tissue
	Gm12171,H57R	Vmn1r20,S94T	Sulf1,L607F		Zfp663,E35D	Olfr221,R303K
	Gm13083,A18V	Zfp458,E469G	Tert,F550L			Olfr311,M101I
	Gm13271, S176Y					Olfr311,V96A
	Gnas,D962Y					Pdzd3,T10K
	H2-M10.1, P234L					Phyh,Y46F
	H2-M10.5, N245I					Pira6,G199S
	Hydin,T4349P					Pkd1,L3P
	Ifna9,S81T					Prkag2,V229A
	Kcna5,G127A					Prr3,G27V
	Kcnc2,T366P					Rsf1,A4T
	Klhl36,D369A					Samd8,S15Y
	Laptm5,L121V					Sap130,T992N
	Map2,A831G					Sbpl,S135N
	Masp2,G528D					Smyd1,V114G
	Megf8,C612W					Tgds,G133R
	Mier3,R311W					Tgs1,V323L
	Mmp16,D400H					Tmc1,A372G
	Myh2,I1032T					Ube2ql1,S48G
	Myh7,E981K					Vmn1r124,T289P
	Nlrc3,V1100L					Zcchc3,T63A
	Olfml3,A195S					Zkscan4,T109A
	Olfr113,A95G					
	Olfr1157,I289M					
	Olfr1511,A165T					

Supplementary Table 2. Unique signature single nucleotide variations in the clonal cell lines and the parental tumor measured by exome sequencing. Mutations in bold are used as clone identifiers in the heterogeneous mixtures. (continued)

Clone C5	Clone C8	Clone D10	Clone F2	Clone G8	Clone G9	Parental tumor tissue
	Olfr175-ps1, N89D					
	Olfr312,Q136H					
	Olfr661,S10N					
	Olfr742,I37V					
	Osgep,E330D					
	Pcdhb4,R624H					
	Pde3b,R223K					
	Pdf,P171R					
	Phf8,C327W					
	Sec24c,S26W					
	Serpina3i,S81G					
	Sfi1,E1110K					
	Sidt1,H24R					
	Slc15a4,E433G					
	Slc25a3,V5I					
	Slc26a10,S279T					
	Sorbs3,P678L					
	Sp140,S461G					
	Spsb2,A72G					
	Tbc1d16,A325P					
	Tcf7l1,E62K					
	Tmem132e, V176A					
	Tmem232, A273T					
	Tnc,Q149H					

Supplementary Table 2. Unique signature single nucleotide variations in the clonal cell lines and the parental tumor measured by exome sequencing. Mutations in bold are used as clone identifiers in the heterogeneous mixtures. (continued)

Clone C5	Clone C8	Clone D10	Clone F2	Clone G8	Clone G9	Parental tumor tissue
	Tubb4b,G140V					
	Ubap2,Y941H					
	Usp19,L805V					
	Vmn1r171,I30V					
	Vmn1r205, I188M					
	Vmn1r9,S108N					
	Vmn2r104, N611H					
	Vmn2r115, D500G					
	Vmn2r28,C756F					
	Vmn2r49,E40G					
	Vmn2r52,R690K					
	Vmn2r60,F777L					
	Vmn2r78,T257I					
	Vps13c,T2230A					
	Wbscr27,R88P					
	Zfp874b,R297M					
	Zfp982,V100I					

Supplementary Table 3. Deep sequencing read counts of the clone-specific signature mutations and ubiquitous *Kras* and *Trp53* mutations in DNA from the heterogeneous clone mixtures in vitro. chrom = chromosome; mm9 = mus musculus reference genome 9; VAF = variant allele frequency

clone	gene	chrom	position (mm9)	variant	read depth	wildtype reads	variant reads	VAF
EQUAL MIX OF UNTREATED CLONAL CELLS – DEEP-SEQ RUN 1								
all	*Trp53*	chr11	69402014	G>A	NA	NA	NA	NA
all	*Kras*	chr6	145195291	C>T	725	264	461	63.59%
C5	*Baiap3*	chr17	25387359	G>T	1235	1203	32	2.59%
C8	*Olfr1157*	chr2	87802181	G>C	501	475	26	5.19%
D10	*Nox4*	chr7	94462586	C>T	651	625	26	3.99%
F2	*Matn4*	chr2	164222680	C>T	508	475	33	6.50%
G8	*Arhgap25*	chr6	87426299	T>C	1207	1136	71	5.88%
G9	*Pla2g4d*	chr2	120094626	G>T	656	583	73	11.13%

clone	gene	chrom	position (mm9)	variant	read depth	wildtype reads	variant reads	VAF
EQUAL MIX OF UNTREATED CLONAL CELLS – DEEP-SEQ RUN 2								
all	*Trp53*	chr11	69402014	G>A	860	0	855	99.42%
all	*Kras*	chr6	145195291	C>T	533	184	349	65.48%
C5	*Baiap3*	chr17	25387359	G>T	1298	1264	34	2.62%
C8	*Olfr1157*	chr2	87802181	G>C	825	797	28	3.39%
D10	*Nox4*	chr7	94462586	C>T	955	883	72	7.54%
F2	*Matn4*	chr2	164222680	C>T	1050	925	125	11.90%
G8	*Arhgap25*	chr6	87426299	T>C	1230	1141	87	7.07%
G9	*Pla2g4d*	chr2	120094626	G>T	742	704	38	5.12%

clone	gene	chrom	position (mm9)	variant	read depth	wildtype reads	variant reads	VAF
EQUAL MIX OF UNTREATED CLONAL CELLS – DEEP-SEQ RUN 3								
all	*Trp53*	chr11	69402014	G>A	2371	20	2331	98.31%
all	*Kras*	chr6	145195291	C>T	2575	1012	1562	60.66%
C5	*Baiap3*	chr17	25387359	G>T	2651	2531	120	4.53%
C8	*Olfr1157*	chr2	87802181	G>C	2663	2522	140	5.26%
D10	*Nox4*	chr7	94462586	C>T	2823	2643	180	6.38%
F2	*Matn4*	chr2	164222680	C>T	2614	2381	232	8.88%
G8	*Arhgap25*	chr6	87426299	T>C	3340	3177	157	4.70%
G9	*Pla2g4d*	chr2	120094626	G>T	2370	2027	336	14.18%

MIX OF CELLS GROWN IN VITRO WITH DMSO – DEEP-SEQ RUN 1

clone	gene	chrom	position (mm9)	variant	read depth	wildtype reads	variant reads	VAF
all	*Trp53*	chr11	69402014	G>A	1415	0	1407	99.43%
all	*Kras*	chr6	145195291	C>T	1247	434	813	65.20%
C5	*Baiap3*	chr17	25387359	G>T	1492	1461	31	2.08%
C8	*Olfr1157*	chr2	87802181	G>C	0	-	-	-
D10	*Nox4*	chr7	94462586	C>T	2011	1930	81	4.03%
F2	*Matn4*	chr2	164222680	C>T	0	-	-	-
G8	*Arhgap25*	chr6	87426299	T>C	2551	2413	137	5.37%
G9	*Pla2g4d*	chr2	120094626	G>T	1658	1499	159	9.59%

MIX OF CELLS GROWN IN VITRO WITH DMSO – DEEP-SEQ RUN 2

clone	gene	chrom	position (mm9)	variant	read depth	wildtype reads	variant reads	VAF
all	*Trp53*	chr11	69402014	G>A	2054	6	2027	98.69%
all	*Kras*	chr6	145195291	C>T	2578	1056	1522	59.04%
C5	*Baiap3*	chr17	25387359	G>T	2439	2385	53	2.17%
C8	*Olfr1157*	chr2	87802181	G>C	3013	2770	243	8.07%
D10	*Nox4*	chr7	94462586	C>T	2868	2705	163	5.68%
F2	*Matn4*	chr2	164222680	C>T	2795	2393	398	14.24%
G8	*Arhgap25*	chr6	87426299	T>C	3566	3319	246	6.90%
G9	*Pla2g4d*	chr2	120094626	G>T	2448	2199	244	9.97%

MIX OF CELLS GROWN IN VITRO WITH GEMCITABINE – DEEP-SEQ RUN 1

clone	gene	chrom	position (mm9)	variant	read depth	wildtype reads	variant reads	VAF
all	*Trp53*	chr11	69402014	G>A	1227	0	1221	99.51%
all	*Kras*	chr6	145195291	C>T	858	294	564	65.73%
C5	*Baiap3*	chr17	25387359	G>T	1891	1812	79	4.18%
C8	*Olfr1157*	chr2	87802181	G>C	1405	1392	13	0.93%
D10	*Nox4*	chr7	94462586	C>T	924	851	73	7.90%
F2	*Matn4*	chr2	164222680	C>T	1620	1591	29	1.79%
G8	*Arhgap25*	chr6	87426299	T>C	1663	1634	29	1.74%
G9	*Pla2g4d*	chr2	120094626	G>T	1316	845	469	35.64%

				MIX OF CELLS GROWN IN VITRO WITH TRAMETINIB– DEEP-SEQ RUN 1				
clone	gene	chrom	position (mm9)	variant	read depth	wildtype reads	variant reads	VAF
all	*Trp53*	chr11	69402014	G>A	869	1	866	99.65%
all	*Kras*	chr6	145195291	C>T	740	256	484	65.41%
C5	*Baiap3*	chr17	25387359	G>T	948	933	14	1.48%
C8	*Olfr1157*	chr2	87802181	G>C	805	680	125	15.53%
D10	*Nox4*	chr7	94462586	C>T	1022	1016	6	0.59%
F2	*Matn4*	chr2	164222680	C>T	940	853	87	9.26%
G8	*Arhgap25*	chr6	87426299	T>C	1555	1439	114	7.33%
G9	*Pla2g4d*	chr2	120094626	G>T	843	831	12	1.42%

Supplementary Table 4. Deep sequencing read counts of the clone-specific mutations and ubiquitous *Kras* and *Trp53* mutations in DNA from the heterogeneous allograft tumors after 2 weeks treatment. chrom = chromosome; mm9 = mus musculus reference genome 9; VAF = variant allele frequency; * = Arbitrary number, set as minimum sequencing detection threshold (in the case of 0 mutant reads).

clone	gene	chrom	position (mm9)	variant	read depth	wildtype reads	variant reads	VAF
all	*Trp53*	chr11	69402014	G>A	0	-	-	-
all	*Kras*	chr6	145195291	C>T	474	387	87	18.35%
C5	*Baiap3*	chr17	25387359	G>T	1519	1519	0	0.01% *
C8	*Olfr1157*	chr2	87802181	G>C	430	418	12	2.79%
D10	*Nox4*	chr7	94462586	C>T	567	567	0	0.01% *
F2	*Matn4*	chr2	164222680	C>T	1038	1009	29	2.79%
G8	*Arhgap25*	chr6	87426299	T>C	1120	1073	47	4.19%
G9	*Pla2g4d*	chr2	120094626	G>T	782	755	27	3.45%

SUBCUT TUMORS AFTER CONTROL TREATMENT – DEEP-SEQ RUN 1

clone	gene	chrom	position (mm9)	variant	read depth	wildtype reads	variant reads	VAF
all	*Trp53*	chr11	69402014	G>A	854	471	379	44.38%
all	*Kras*	chr6	145195291	C>T	760	502	258	33.95%
C5	*Baiap3*	chr17	25387359	G>T	948	948	0	0.01% *
C8	*Olfr1157*	chr2	87802181	G>C	829	806	23	2.77%
D10	*Nox4*	chr7	94462586	C>T	1060	1057	3	0.28%
F2	*Matn4*	chr2	164222680	C>T	1981	1782	196	9.89%
G8	*Arhgap25*	chr6	87426299	T>C	1236	1192	44	3.56%
G9	*Pla2g4d*	chr2	120094626	G>T	943	890	52	5.51%

SUBCUT TUMORS AFTER CONTROL TREATMENT – DEEP-SEQ RUN 2

clone	gene	chrom	position (mm9)	variant	read depth	wildtype reads	variant reads	VAF
all	*Trp53*	chr11	69402014	G>A	588	419	168	28.57%
all	*Kras*	chr6	145195291	C>T	953	658	294	30.85%
C5	*Baiap3*	chr17	25387359	G>T	1303	1300	2	0.15%
C8	*Olfr1157*	chr2	87802181	G>C	923	921	2	0.22%
D10	*Nox4*	chr7	94462586	C>T	1138	1135	1	0.09%
F2	*Matn4*	chr2	164222680	C>T	1120	1106	13	1.16%
G8	*Arhgap25*	chr6	87426299	T>C	1202	1145	57	4.74%
G9	*Pla2g4d*	chr2	120094626	G>T	1196	1194	2	0.17%

SUBCUT TUMORS AFTER CONTROL TREATMENT – DEEP-SEQ RUN 3

				SUBCUT TUMORS AFTER CONTROL TREATMENT – DEEP-SEQ RUN 4					
clone	**gene**	**chrom**	**position (mm9)**	**variant**	**read depth**	**wildtype reads**	**variant reads**	**VAF**	
all	*Trp53*	chr11	69402014	G>A	4074	1614	2431	59.67%	
all	*Kras*	chr6	145195291	C>T	5669	4354	1314	23.18%	
C5	*Baiap3*	chr17	25387359	G>T	5280	5256	20	0.38%	
C8	*Olfr1157*	chr2	87802181	G>C	5823	5732	87	1.49%	
D10	*Nox4*	chr7	94462586	C>T	5705	5691	13	0.23%	
F2	*Matn4*	chr2	164222680	C>T	3889	3551	336	8.64%	
G8	*Arhgap25*	chr6	87426299	T>C	6124	5833	284	4.64%	
G9	*Pla2g4d*	chr2	120094626	G>T	5286	4538	742	14.04%	

				SUBCUT TUMORS AFTER CONTROL TREATMENT – DEEP-SEQ RUN 5					
clone	**gene**	**chrom**	**position (mm9)**	**variant**	**read depth**	**wildtype reads**	**variant reads**	**VAF**	
all	*Trp53*	chr11	69402014	G>A	2638	985	1635	61.98%	
all	*Kras*	chr6	145195291	C>T	4076	2355	1721	42.22%	
C5	*Baiap3*	chr17	25387359	G>T	4422	4411	11	0.25%	
C8	*Olfr1157*	chr2	87802181	G>C	5481	5282	197	3.59%	
D10	*Nox4*	chr7	94462586	C>T	4177	4172	5	0.12%	
F2	*Matn4*	chr2	164222680	C>T	4668	4194	470	10.07%	
G8	*Arhgap25*	chr6	87426299	T>C	5218	4891	326	6.25%	
G9	*Pla2g4d*	chr2	120094626	G>T	4372	4193	170	3.89%	

				SUBCUT TUMORS AFTER GEMCITABINE TREATMENT – DEEP-SEQ RUN 1					
clone	**gene**	**chrom**	**position (mm9)**	**variant**	**read depth**	**wildtype reads**	**variant reads**	**VAF**	
all	*Trp53*	chr11	69402014	G>A	1142	487	645	56.48%	
all	*Kras*	chr6	145195291	C>T	1329	844	485	36.49%	
C5	*Baiap3*	chr17	25387359	G>T	1625	1613	12	0.74%	
C8	*Olfr1157*	chr2	87802181	G>C	1241	1200	39	3.14%	
D10	*Nox4*	chr7	94462586	C>T	1467	1451	16	1.09%	
F2	*Matn4*	chr2	164222680	C>T	1644	1510	134	8.15%	
G8	*Arhgap25*	chr6	87426299	T>C	1784	1740	44	2.47%	
G9	*Pla2g4d*	chr2	120094626	G>T	1453	1380	73	5.02%	

SUBCUT TUMORS AFTER GEMCITABINE TREATMENT – DEEP-SEQ RUN 2

clone	gene	chrom	position (mm9)	variant	read depth	wildtype reads	variant reads	VAF
all	Trp53	chr11	69402014	G>A	1923	1159	751	39.05%
all	Kras	chr6	145195291	C>T	3141	2795	345	10.98%
C5	Baiap3	chr17	25387359	G>T	2539	2525	13	0.51%
C8	Olfr1157	chr2	87802181	G>C	3644	3601	39	1.07%
D10	Nox4	chr7	94462586	C>T	3444	3432	11	0.32%
F2	Matn4	chr2	164222680	C>T	3050	2895	154	5.05%
G8	Arhgap25	chr6	87426299	T>C	3536	3494	40	1.13%
G9	Pla2g4d	chr2	120094626	G>T	2951	2796	152	5.15%

SUBCUT TUMORS AFTER TRAMETINIB TREATMENT – DEEP-SEQ RUN 1

clone	gene	chrom	position (mm9)	variant	read depth	wildtype reads	variant reads	VAF
all	Trp53	chr11	69402014	G>A	-	-	-	-
all	Kras	chr6	145195291	C>T	1195	955	240	20.08%
C5	Baiap3	chr17	25387359	G>T	1883	1882	1	0.05%
C8	Olfr1157	chr2	87802181	G>C	884	880	4	0.45%
D10	Nox4	chr7	94462586	C>T	1105	1104	1	0.09%
F2	Matn4	chr2	164222680	C>T	1293	1259	34	2.63%
G8	Arhgap25	chr6	87426299	T>C	2013	1982	31	1.54%
G9	Pla2g4d	chr2	120094626	G>T	1147	1037	110	9.59%

SUBCUT TUMORS AFTER TRAMETINIB TREATMENT – DEEP-SEQ RUN 2

clone	gene	chrom	position (mm9)	variant	read depth	wildtype reads	variant reads	VAF
all	Trp53	chr11	69402014	G>A	2199	1361	833	37.88%
all	Kras	chr6	145195291	C>T	3242	2397	845	26.06%
C5	Baiap3	chr17	25387359	G>T	2275	2269	6	0.26%
C8	Olfr1157	chr2	87802181	G>C	3813	3795	16	0.42%
D10	Nox4	chr7	94462586	C>T	2563	2559	2	0.08%
F2	Matn4	chr2	164222680	C>T	2634	2494	137	5.20%
G8	Arhgap25	chr6	87426299	T>C	3467	3425	41	1.18%
G9	Pla2g4d	chr2	120094626	G>T	3068	2647	417	13.59%

SUBCUT TUMORS AFTER α-PD-1 TREATMENT – DEEP-SEQ RUN 1								
clone	**gene**	**chrom**	**position (mm9)**	**variant**	**read depth**	**wildtype reads**	**variant reads**	**VAF**
all	*Trp53*	chr11	69402014	G>A	497	428	69	13.88%
all	*Kras*	chr6	145195291	C>T	594	561	33	5.56%
C5	*Baiap3*	chr17	25387359	G>T	639	636	3	0.47%
C8	*Olfr1157*	chr2	87802181	G>C	455	455	0	0.01% *
D10	*Nox4*	chr7	94462586	C>T	682	678	4	0.59%
F2	*Matn4*	chr2	164222680	C>T	638	632	6	0.94%
G8	*Arhgap25*	chr6	87426299	T>C	754	740	13	1.72%
G9	*Pla2g4d*	chr2	120094626	G>T	519	517	2	0.39%
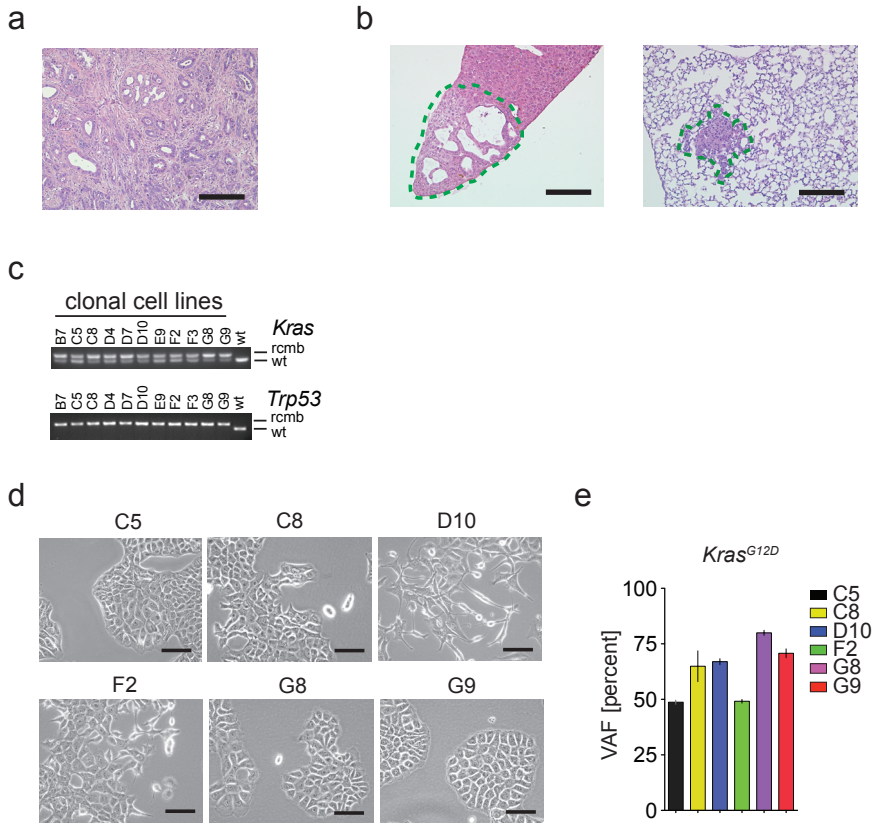
Supplementary Figure 1. Characterization of heterogeneous clonal cell lines from a KPC mouse pancreatic tumor (Related to Figure 1)

a, b. Images of H&E stained, formalin fixed paraffin embedded (FFPE) primary KPC mouse pancreatic tumor (a) as well as liver and lung metastases (b). Scale bar = 100 μm.

c. Allele specific PCR products of *Kras* and *Trp53* DNA from eleven clonal KPC PDAC cell lines that underwent Cre recombination. Lower bands indicate wildtype (wt) alleles; upper bands are the recombined alleles containing the 34 basepair LoxP.

d. Images taken from the 2D monolayers of the individual clonal cell lines in vitro. Scale bar = 30 μm.

e. *Kras*[G12D] variant allele frequency (VAF) in six clonal cell lines. Droplet Digital PCR was performed using a HEX labeled probe for wildtype *Kras* and a FAM labeled probe for mutant *Kras*[G12D]. Data is presented as ratio of positive *Kras*[G12D] droplets over total *Kras* positive droplets is shown. Error bars are SEM of 2 replicate PCR reactions from 2 clonal cell DNA preparations.
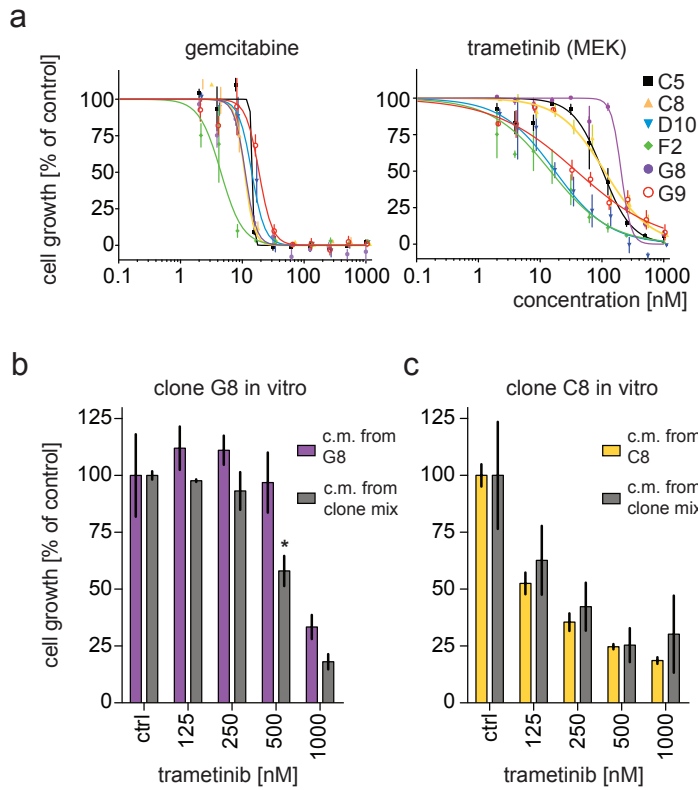
Supplementary Figure 2. Distinct clonal growth rates and drug sensitivity (Related to Figure 2)

a. Dose response curves of gemcitabine or trametinib after 72 hours. Drugs were added to the clonal PDAC cell lines one day after plating. Error bars are SEM from triplicate wells.

b, c. Dose-response of trametinib for clone G8 (b) and C8 (c) in the presence of conditioned media (c.m.) harvested from the clone mixture or from G8 or C8 only. A 1:1 ratio of c.m. and DMEM/10%FBS was used. Error bars are SEM of 2 replicate experiments, * p< 0.05 t-test for c.m. from the clone mix vs c.m. from G8.
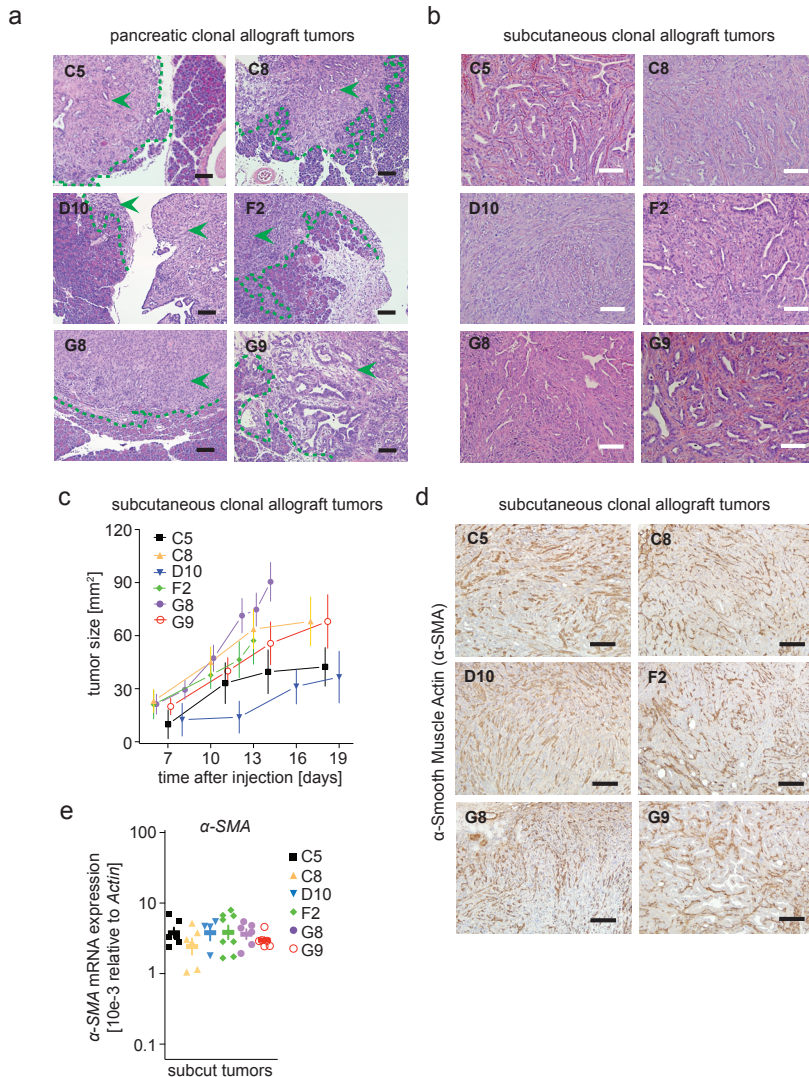
Supplementary Figure 3. Growth of clonal allograft tumors

a. Images of H&E stained FFPE pancreatic clonal allograft tumors. One million clonal cells were injected intraperitoneally into compatible immune competent mice and allowed to form tumors. Green dashed lines indicate the invasive cancer margins into healthy pancreas tissue. Green arrows indicate cancer. Scale bar =100 μm.

b. Images of H&E stained FFPE subcutaneous clonal allograft tumors. One million clonal cells were injected subcutaneously into the flanks of compatible immune competent mice. Scale bar =100 μm.

c. Growth curves of the clonal subcutaneous allograft tumors.

d. Immunohistochemical staining for α-Smooth Muscle Actin protein in FFPE subcutaneous clonal allograft tumors. Scale bar =100 μm.

e. Expression of α-Smooth Muscle Actin mRNA in subcutaneous clonal allograft tumors by qRT-PCR. The expression is normalized to beta-Actin. Note the log scale for the Y-axis. Error bars are SEM of 2 replicate measurements in ≥2 tumors per clonal cell line.
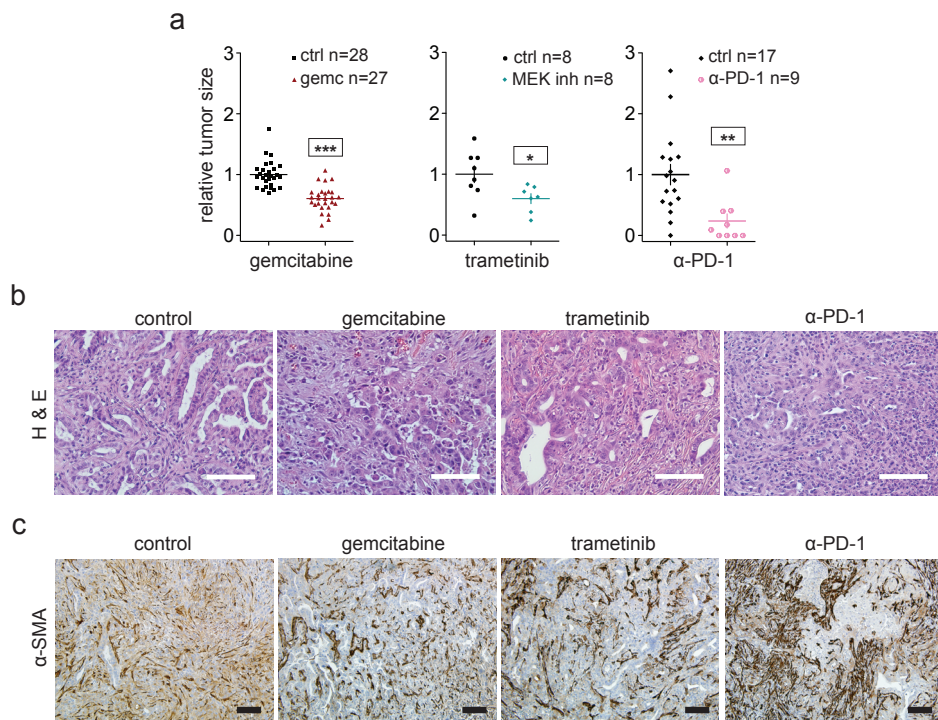
Supplementary Figure 4. Drug effects on growth of heterogeneous tumors.

a. Relative size of the subcutaneous clone mix allograft tumors. One million cells of the PDAC clone mixture were injected subcutaneously into the flanks of compatible immune competent mice. When tumors had established, mice were treated for 2 weeks with either vehicle control, 4 injections of 250 μg rat anti-mouse-PD-1 mAb, 7 injections of 40 mg/kg gemcitabine, or daily oral gavage with 0.5 mg/kg trametinib. The relative tumor size is shown per treatment group. Maximal growth inhibition was reached at day 5 for gemcitabine and trametinib. and at day 10 of α-PD-1. Error bars are SEM, ***p<0.0001; *p=0.032 **p=0.0054; versus the respective control group.

b, c. Representative , H&E (b), or α-Smooth Muscle Actin stained (c) subcutaneous allograft tumors at the end of different treatments indicated. Scale bar =100 μm.

Gating strategy Tumor infiltrating cells
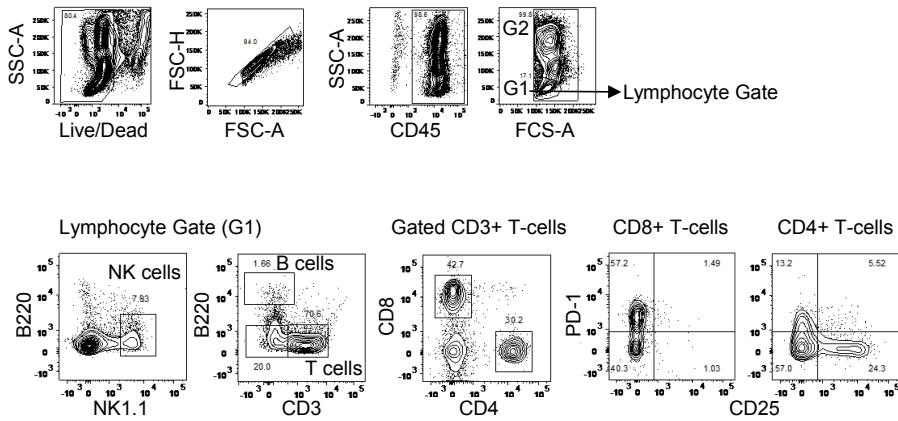
Supplementary Figure 5. Gating strategy in the flow cytometry analysis of tumor infiltrating lympho-cytes. Tumor infiltrating cells were gated on time, FCS-SSC and live cells. Hematopoietic cells were selected by CD45 expression. Lymphocytes subsets were gated based on expression of: NK cells (NK1.1+), B cells (B220+), T cells (CD3+). CD4 T cells (CD3+CD4+) and CD8 T cells (CD3+CD8+) were further analyzed by surface expression of PD-1 and CD25.
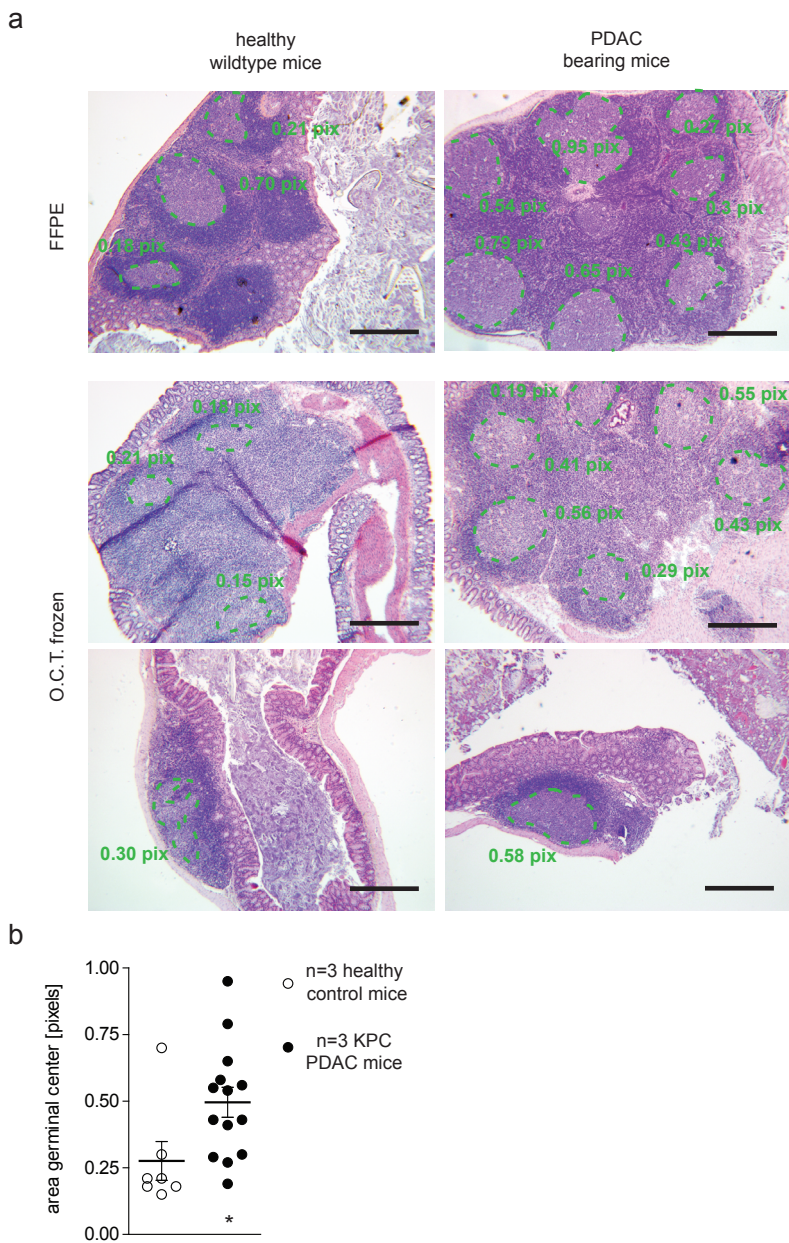
Supplementary Figure 6. Mouse ceacal patch derived T-lymphocytes

a. Images of mouse ceacal patches (equivalent to human vermiform appendix) stained with H&E. Ceacal patches from n=3 healthy immune competent mice and from n=3 KPC mice were either formalin fixed or frozen in O.C.T cryo embedding media, and sectioned. Green dashed lines encircle the germinal centers of the lymphoid tissues. Scale bar = 500 μm.

b. Areas of the germinal centers in the lymphoid tissue of the caecal patches from n=3 healthy mice and n=3 PDAC bearing KPC mice. * p=0.0316 by t-test.

b

Caecal patch derived T-lymphocytes
from n=2 healthy mice

PDAC cancer cells	-	-	-	C5	C8	D10	F2	G8	G9
IL-2 (30 U/mL)	-	+	+	+	+	+	+	+	+
α-CD3e (5 µg/mL)	-	-	+	-	-	-	-	-	-
α-CD28 (2 µg/mL)	-	-	+	-	-	-	-	-	-

c

Caecal patch derived T-lymphocytes
from n=3 allograft PDAC bearing mice

PDAC cancer cells	C5	C5	C8	C8	D10	D10	F2	F2	G8	G8	G9	G9	
ctrl IgG2a (20 µg/mL)	+	-	+	-	+	-	+	-	+	-	+	-	
α-PD-1(20 µg/mL)	-	+	-	+	-	+	-	+	-	+	-	+	
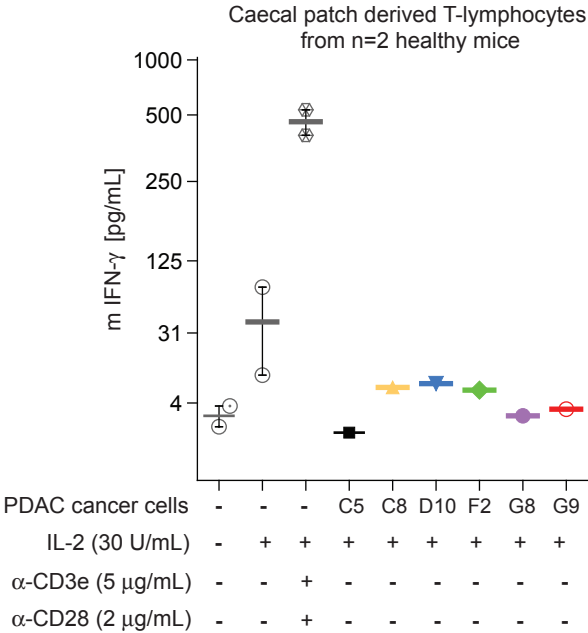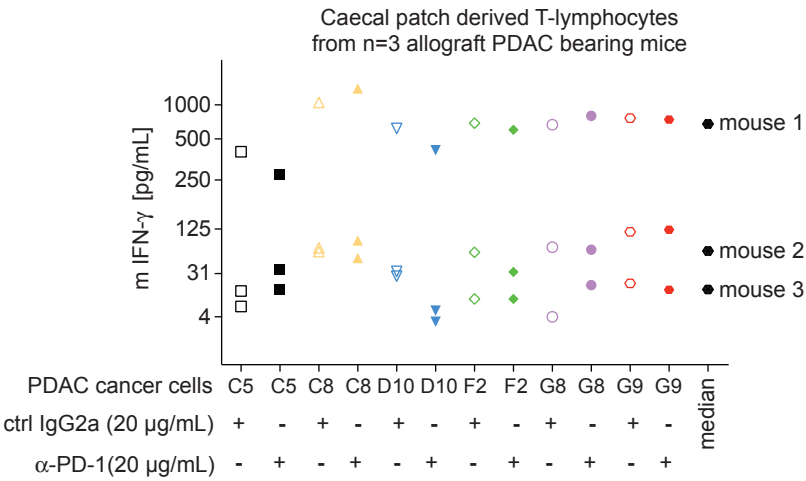
Supplementary Figure 6. Mouse ceacal patch derived T-lymphocytes
c. IFN-γ levels in the supernatant of T-lymphocytes isolated from ceacal patches of n=2 healthy mice, co-cultured with clonal PDAC cell lines, measured after 48 hours by ELISA. Note the log2 –scale for the Y-axis. Error bars are SEM of n=2 mice.
d. IFN-γ levels in the supernatant of primed appendix T-lymphocytes isolated from n=3 mice bearing mixed allograft PDAC tumors, co-cultured with the clonal PDAC cell lines in vitro, measured after 48 hours by ELISA. Note the log2 scale for the y-axis.

REFERENCES

1. Vincent, A., Herman, J., Schulick, R. et al. (2011) Pancreatic cancer. *Lancet* 378, 607-620
2. Oettle, H., Post, S., Neuhaus, P. et al. (2007) Adjuvant chemotherapy with gemcitabine vs observation in patients undergoing curative-intent resection of pancreatic cancer: a randomized controlled trial. *Jama* 297, 267-277
3. Bailey, P., Chang, D. K., Nones, K. et al. (2016) Genomic analyses identify molecular subtypes of pancreatic cancer. *Nature* 531, 47-52
4. Witkiewicz, A. K., McMillan, E. A., Balaji, U. et al. (2015) Whole-exome sequencing of pancreatic cancer defines genetic diversity and therapeutic targets. *Nat Commun* 6, 6744
5. Gilmartin, A. G., Bleam, M. R., Groy, A. et al. (2011) GSK1120212 (JTP-74057) is an inhibitor of MEK activity and activation with favorable pharmacokinetic properties for sustained in vivo pathway inhibition. *Clin Cancer Res* 17, 989-1000
6. Infante, J. R., Somer, B. G., Park, J. O. et al. (2014) A randomised, double-blind, placebo-controlled trial of trametinib, an oral MEK inhibitor, in combination with gemcitabine for patients with untreated metastatic adenocarcinoma of the pancreas. *Eur J Cancer* 50, 2072-2081
7. Greten, F. R. (2014) YAP1 takes over when oncogenic K-Ras slumbers. *Cell* 158, 11-12
8. Zhang, W., Nandakumar, N., Shi, Y. et al. (2014) Downstream of mutant KRAS, the transcription regulator YAP is essential for neoplastic progression to pancreatic ductal adenocarcinoma. *Sci Signal* 7, ra42
9. Aparicio, S. & Caldas, C. (2013) The implications of clonal genome evolution for cancer medicine. *N Engl J Med* 368, 842-851
10. Burrell, R. A., McGranahan, N., Bartek, J. et al. (2013) The causes and consequences of genetic heterogeneity in cancer evolution. *Nature* 501, 338-345
11. Kim, M. S., Zhong, Y., Yachida, S. et al. (2014) Heterogeneity of pancreatic cancer metastases in a single patient revealed by quantitative proteomics. *Mol Cell Proteomics* 13, 2803-2811
12. Bozic, I., Reiter, J. G., Allen, B. et al. (2013) Evolutionary dynamics of cancer in response to targeted combination therapy. *Elife* 2, e00747
13. Saunders, N. A., Simpson, F., Thompson, E. W. et al. (2012) Role of intratumoural heterogeneity in cancer drug resistance: molecular and clinical perspectives. *EMBO Mol Med* 4, 675-684
14. Bhang, H. E., Ruddy, D. A., Krishnamurthy Radhakrishna, V. et al. (2015) Studying clonal dynamics in response to cancer therapy using high-complexity barcoding. *Nat Med* 21, 440-448
15. Jamal-Hanjani, M., Quezada, S. A., Larkin, J. et al. (2015) Translational implications of tumor heterogeneity. *Clin Cancer Res* 21, 1258-1266
16. Kleppe, M. & Levine, R. L. (2014) Tumor heterogeneity confounds and illuminates: assessing the implications. *Nat Med* 20, 342-344
17. Beckman, R. A., Schemmann, G. S. & Yeang, C. H. (2012) Impact of genetic dynamics and single-cell heterogeneity on development of nonstandard personalized medicine strategies for cancer. *Proc Natl Acad Sci U S A* 109, 14586-14591
18. Neesse, A., Algul, H., Tuveson, D. A. et al. (2015) Stromal biology and therapy in pancreatic cancer: a changing paradigm. *Gut* 64, 1476-1484
19. Ozdemir, B. C., Pentcheva-Hoang, T., Carstens, J. L. et al. (2014) Depletion of carcinoma-associated fibroblasts and fibrosis induces immunosuppression and accelerates pancreas cancer with reduced survival. *Cancer Cell* 25, 719-734
20. Rhim, A. D., Oberstein, P. E., Thomas, D. H. et al. (2014) Stromal elements act to restrain, rather than support, pancreatic ductal adenocarcinoma. *Cancer Cell* 25, 735-747

21. Muerkoster, S., Wegehenkel, K., Arlt, A. et al. (2004) Tumor stroma interactions induce chemoresistance in pancreatic ductal carcinoma cells involving increased secretion and paracrine effects of nitric oxide and interleukin-1beta. *Cancer Res* 64, 1331-1337

22. Binenbaum, Y., Na'ara, S. & Gil, Z. (2015) Gemcitabine resistance in pancreatic ductal adenocarcinoma. *Drug Resist Updat* 23, 55-68

23. Sainz, B., Jr., Alcala, S., Garcia, E. et al. (2015) Microenvironmental hCAP-18/LL-37 promotes pancreatic ductal adenocarcinoma by activating its cancer stem cell compartment. *Gut* 64, 1921-1935

24. Nielsen, M. F., Mortensen, M. B. & Detlefsen, S. (2016) Key players in pancreatic cancer-stroma interaction: Cancer-associated fibroblasts, endothelial and inflammatory cells. *World J Gastroenterol* 22, 2678-2700

25. Feig, C., Jones, J. O., Kraman, M. et al. (2013) Targeting CXCL12 from FAP-expressing carcinoma-associated fibroblasts synergizes with anti-PD-L1 immunotherapy in pancreatic cancer. *Proc Natl Acad Sci U S A* 110, 20212-20217

26. Heppner, G. H. (1984) Tumor heterogeneity. *Cancer Res* 44, 2259-2265

27. Heppner, G. H. (1991) Cell-to-cell interaction in regulating diversity of neoplasms. *Semin Cancer Biol* 2, 97-103

28. Marusyk, A., Tabassum, D. P., Altrock, P. M. et al. (2014) Non-cell-autonomous driving of tumour growth supports sub-clonal heterogeneity. *Nature* 514, 54-58

29. Miller, B. E., Miller, F. R. & Heppner, G. H. (1981) Interactions between tumor subpopulations affecting their sensitivity to the antineoplastic agents cyclophosphamide and methotrexate. *Cancer Res* 41, 4378-4381

30. Zhao, B., Hemann, M. T. & Lauffenburger, D. A. (2014) Intratumor heterogeneity alters most effective drugs in designed combinations. *Proc Natl Acad Sci U S A* 111, 10773-10778

31. Hingorani, S. R., Wang, L., Multani, A. S. et al. (2005) Trp53R172H and KrasG12D cooperate to promote chromosomal instability and widely metastatic pancreatic ductal adenocarcinoma in mice. *Cancer Cell* 7, 469-483

32. Li, H. & Durbin, R. (2009) Fast and accurate short read alignment with Burrows-Wheeler transform. *Bioinformatics* 25, 1754-1760

33. McKenna, A., Hanna, M., Banks, E. et al. (2010) The Genome Analysis Toolkit: a MapReduce framework for analyzing next-generation DNA sequencing data. *Genome Res* 20, 1297-1303

34. Sharif, G. M., Schmidt, M. O., Yi, C. et al. (2015) Cell growth density modulates cancer cell vascular invasion via Hippo pathway activity and CXCR2 signaling. *Oncogene* 34, 5879-5889

35. Maddipati, R. & Stanger, B. Z. (2015) Pancreatic Cancer Metastases Harbor Evidence of Polyclonality. *Cancer Discov* 5, 1086-1097

36. Yip-Schneider, M. T., Lin, A., Barnard, D. et al. (1999) Lack of elevated MAP kinase (Erk) activity in pancreatic carcinomas despite oncogenic K-ras expression. *Int J Oncol* 15, 271-279

37. Yeh, J. J., Routh, E. D., Rubinas, T. et al. (2009) KRAS/BRAF mutation status and ERK1/2 activation as biomarkers for MEK1/2 inhibitor therapy in colorectal cancer. *Mol Cancer Ther* 8, 834-843

38. Sakakura, C., Hagiwara, A., Shirahama, T. et al. (1999) Infrequent activation of mitogen-activated protein kinase in human colon cancers. *Hepatogastroenterology* 46, 2831-2834

39. Drifka, C. R., Loeffler, A. G., Mathewson, K. et al. (2016) Highly aligned stromal collagen is a negative prognostic factor following pancreatic ductal adenocarcinoma resection. *Oncotarget* 7, 76197-76213

40. Egeblad, M., Rasch, M. G. & Weaver, V. M. (2010) Dynamic interplay between the collagen scaffold and tumor evolution. *Curr Opin Cell Biol* 22, 697-706

41. Whatcott, C. J., Diep, C. H., Jiang, P. et al. (2015) Desmoplasia in Primary Tumors and Metastatic Lesions of Pancreatic Cancer. *Clin Cancer Res* 21, 3561-3568

42. Campbell, P. J., Yachida, S., Mudie, L. J. et al. (2010) The patterns and dynamics of genomic instability in metastatic pancreatic cancer. *Nature* 467, 1109-1113

43. Yachida, S., Jones, S., Bozic, I. et al. (2010) Distant metastasis occurs late during the genetic evolution of pancreatic cancer. *Nature* 467, 1114-1117

44. Collisson, E. A., Trejo, C. L., Silva, J. M. et al. (2012) A central role for RAF-->MEK-->ERK signaling in the genesis of pancreatic ductal adenocarcinoma. *Cancer Discov* 2, 685-693

45. Galluzzi, L., Senovilla, L., Zitvogel, L. et al. (2012) The secret ally: immunostimulation by anticancer drugs. *Nat Rev Drug Discov* 11, 215-233

46. Kidd, B. A., Wroblewska, A., Boland, M. R. et al. (2016) Mapping the effects of drugs on the immune system. *Nat Biotechnol* 34, 47-54

47. Ott, P. A. & Adams, S. (2011) Small-molecule protein kinase inhibitors and their effects on the immune system: implications for cancer treatment. *Immunotherapy* 3, 213-227

48. Sideras, K., Braat, H., Kwekkeboom, J. et al. (2014) Role of the immune system in pancreatic cancer progression and immune modulating treatment strategies. *Cancer Treat Rev* 40, 513-522

49. Clark, C. E., Hingorani, S. R., Mick, R. et al. (2007) Dynamics of the immune reaction to pancreatic cancer from inception to invasion. *Cancer Res* 67, 9518-9527

50. Chikuma, S., Terawaki, S., Hayashi, T. et al. (2009) PD-1-mediated suppression of IL-2 production induces CD8+ T cell anergy in vivo. *J Immunol* 182, 6682-6689

51. Shevach, E. M. (2001) Certified professionals: CD4(+)CD25(+) suppressor T cells. *J Exp Med* 193, F41-46

52. Alkadhi, S., Kunde, D., Cheluvappa, R. et al. (2014) The murine appendiceal microbiome is altered in spontaneous colitis and its pathological progression. *Gut Pathog* 6, 25

53. Watson Ng, W. S., Hampartzoumian, T., Lloyd, A. R. et al. (2007) A murine model of appendicitis and the impact of inflammation on appendiceal lymphocyte constituents. *Clin Exp Immunol* 150, 169-178

54. Halle, S., Halle, O. & Forster, R. (2017) Mechanisms and Dynamics of T Cell-Mediated Cytotoxicity In Vivo. *Trends Immunol* 6,432-443

55. Topalian, S. L., Taube, J. M., Anders, R. A. et al. (2016) Mechanism-driven biomarkers to guide immune checkpoint blockade in cancer therapy. *Nat Rev Cancer* 16, 275-287

56. Miller, B. E., Miller, F. R., Leith, J. et al. (1980) Growth interaction in vivo between tumor subpopulations derived from a single mouse mammary tumor. *Cancer Res* 40, 3977-3981

57. Roesch, A., Fukunaga-Kalabis, M., Schmidt, E. C. et al. (2010) A temporarily distinct subpopulation of slow-cycling melanoma cells is required for continuous tumor growth. *Cell* 141, 583-594

58. Cassidy, J. W., Caldas, C. & Bruna, A. (2015) Maintaining Tumor Heterogeneity in Patient-Derived Tumor Xenografts. *Cancer Res* 75, 2963-2968

59. Nakasone, E. S., Askautrud, H. A., Kees, T. et al. (2012) Imaging tumor-stroma interactions during chemotherapy reveals contributions of the microenvironment to resistance. *Cancer Cell* 21, 488-503

60. Straussman, R., Morikawa, T., Shee, K. et al. (2012) Tumour micro-environment elicits innate resistance to RAF inhibitors through HGF secretion. *Nature* 487, 500-504

61. Majumder, B., Baraneedharan, U., Thiyagarajan, S. et al. (2015) Predicting clinical response to anticancer drugs using an ex vivo platform that captures tumour heterogeneity. *Nat Commun* 6, 6169

62. McMillin, D. W., Delmore, J., Weisberg, E. et al. (2010) Tumor cell-specific bioluminescence platform to identify stroma-induced changes to anticancer drug activity. *Nat Med* 16, 483-489

63. Bartlett, R., Everett, W., Lim, S. et al. (2014) Personalized in vitro cancer modeling - fantasy or reality? *Transl Oncol* 7, 657-664

64. Miller, F. R. & Heppner, G. H. (1979) Immunologic heterogeneity of tumor cell subpopulations from a single mouse mammary tumor. *J Natl Cancer Inst* 63, 1457-1463

65. Topalian, S. L., Hodi, F. S., Brahmer, J. R. et al. (2012) Safety, activity, and immune correlates of anti-PD-1 antibody in cancer. *N Engl J Med* 366, 2443-2454

66. Borghaei, H., Paz-Ares, L., Horn, L. et al. (2015) Nivolumab versus Docetaxel in Advanced Nonsquamous Non-Small-Cell Lung Cancer. *N Engl J Med* 373, 1627-1639

67. Kreso, A., O'Brien, C. A., van Galen, P. et al. (2013) Variable clonal repopulation dynamics influence chemotherapy response in colorectal cancer. *Science* 339, 543-548

68. Jiang, Y., Li, Y. & Zhu, B. (2015) T-cell exhaustion in the tumor microenvironment. *Cell Death Dis* 6, e1792

CHAPTER 3

Circulating cell-free DNA mutation patterns in early and late stage colon and pancreatic cancer

Eveline E. Vietsch[1]
Garrett T. Graham[1]
Justine N. McCutcheon[1]
Aamir Javaid[1]
Giuseppe Giaccone[1]
John L. Marshall[1,2]
Anton Wellstein[1,2].

1 Department of Oncology, Georgetown University, Washington, DC, USA.
2 Otto J. Ruesch Center for the Cure of Gastrointestinal Cancer, Lombardi Comprehensive Cancer Center, Georgetown University, Washington, DC, USA.

ABSTRACT

Cancer is a heterogeneous disease harboring diverse subclonal populations that can be discriminated by their DNA mutations. Environmental pressure selects subclones that ultimately drive disease progression and tumor relapse. Circulating cell-free DNA (ccfDNA) can be used to approximate the mutational makeup of cancer lesions and can serve as a marker for monitoring disease progression at the molecular level without the need for invasively acquired samples from primary or metastatic lesions. This potential for molecular analysis makes ccfDNA attractive for the study of clonal evolution and for uncovering emerging therapeutic resistance or sensitivity. We assessed ccfDNA from colon and pancreatic adenocarcinoma patients using next generation sequencing of 56 cancer-associated genes at the time of primary resectable disease and metastatic progression and compared this to the mutational patterns of the primary tumor. 28%-47% of non-synonymous mutations in the primary tumors were also detected in the ccfDNA while 71%-78% mutations found in ccfDNA were not detected in the primary tumors. ccfDNA collected at the time of progression harbored 3-5 new mutations not detected in ccfDNA at the earlier collection time points. We conclude that incorporation of ccfDNA analysis provides crucial insights into the changing molecular makeup of progressive colon and pancreatic cancer.

INTRODUCTION

Genomic mutations are one of the hallmarks of cancer [1]. The molecular characterization of a given cancer relies on the analysis of tissue specimen from a primary or metastatic lesion typically obtained at a single time point. However, due to intratumoral heterogeneity, the selection of cell subpopulations during cancer evolution and metastasis, the analysis of a single tissue specimen will provide only a limited characterization of the molecular makeup of the disease [2,3]. Monitoring the molecular characteristics of cancer by serial analyses of circulating cell-free DNA (ccfDNA) enables capture of emerging heterogeneity of the disease and may support treatment decisions [4,5]. CcfDNA analysis has evolved since its inception with improvements in the technologies and detection limits [6,7] and represents a set of research tools that appear poised to enter routine clinical care [8,9]. The recent FDA approval of a ccfDNA assay for the *EGFR* T790M mutation in lung cancer supports this notion [10]. Whether ccfDNA should complement tissue analyses in all cancer types remains to be studied, especially in early stage diseases [9,11]. However, ccfDNA may be superior to tumor tissue DNA in the assessment of cancer heterogeneity and evolution during disease progression [12,13]. Here we study the mutational landscape of ccfDNA at diagnosis and disease recurrence and compare it to that of DNA from the primary tumor tissues in ten patients with colon and pancreatic cancer.

MATERIALS AND METHODS

Patient Samples
Patients with newly diagnosed colon adenocarcinoma (colon AC) or pancreatic ductal adenocarcinoma (PDAC) were recruited for blood and tissue collection under the IRB protocol 2007-345 "Establishment of the High Quality Tumor Biobank and Clinical Database" and the Non-Therapeutic Subject Registry (NTSR) Shared Resource protocol Pr000000007 at the Lombardi Comprehensive Cancer Center at Georgetown University after obtaining informed consent. Ten patients were retrospectively selected with the following inclusion criteria: initial diagnosis of treatment-naïve resectable primary adenocarcinoma (n=5 colon; n=5 pancreatic), surgical resection of the primary tumor, and development of progressive disease after surgery. None of the patients had a previous malignant disease. Peripheral venous blood samples were collected in EDTA plasma tubes before the surgical removal of the primary tumors as well as at time of metastatic disease progression (1-70 months after surgery). The blood samples were centrifuged at ≤1300 RCF for 10 min within 2 hours of blood collection, after which plasma was

separated and stored at -80 °C until further analysis. Surgical specimens of the primary tumors were frozen in O.C.T and cryo-sectioned into 20 μm scrolls and examined by a pathologist for the presence of cancer cells.

DNA isolation

The plasma samples were thawed on ice and circulating cell-free circulating DNA (ccfDNA) was isolated from 2 x 100 μL plasma per patient, using the DNA extractor SP Kit (Wako cat. # 296-60501) following the manufacturer's protocol. In brief, 200 μL Enzyme Reaction Solution and 5 μL Protein Digestion Solution was added to 100 μL plasma and mixed by vortexing. The samples were incubated at 56 °C for 10 min. Thereafter 300 μL of Sodium Iodide Solution and 600 μL Alcohol Solution were added and mixed by vortexing. After 10 min incubation at room temperature, the samples were centrifuged at 16,000 x g for 10 min at room temperature. The supernatant was discarded and ccfDNA pellets were washed with 1 mL Washing Solution A by vortexing. After 5 min centrifugation at 16,000 x g the supernatant was discarded. The ccfDNA pellets were washed with 1 mL Washing Solution B and centrifuged once more for 5 min. The supernatant was discarded again and DNA pellets were allowed to dry. The ccfDNA was diluted in 15 μL of ultra pure water and quantitated with the NanoDrop 2000c (Thermo Scientific) and the Promega Quantifluor ONE dsDNA Fluorescence Assay (Promega).

Two frozen tumor tissue scrolls of 20 μm thickness per patient with an average weight of 75 μg and surface of 1.15 cm2 were used for genomic DNA isolation. DNA was isolated using the PrepEase Genomic DNA Isolation Kit (USB), following the manufacturer's protocol. In brief, the tissue was homogenized in 240 μL Homogenization Buffer in MagNA Lyser Green Beads (Roche) in the MagNA Lyser (Roche). A mixture of 200 μL Chloroform/Isoamyl Alcohol (24:1), as well as 800 μL Protein Precipitation Buffer were added to the lysates. Samples were mixed by vortexing and centrifuged at 13,000 x g for 4 min at room temperature. 880 μL of the upper aqueous phase of the sample was transferred to a new microcentrifuge tube containing 620 μL isopropanol. The samples were mixed by inverting the tubes and centrifuged at 13,000 x g for 4 min. The supernatant was discarded and DNA pellets were washed with 1 mL of 70% ethanol by vortexing. The samples were centrifuged for 2 min and DNA pellets were allowed to dry. The tumor DNA was diluted in 15 μL of ultra pure water and quantitated with the NanoDrop 2000c (Thermo Scientific) and the Promega Quantifluor ONE dsDNA Fluorescence Assay (Promega).

56G Oncology Panel Sequencing Library preparation

DNA mutation analysis was conducted using a Targeted Next Generation Sequencing Library Preparation Kit that is compatible with circulating cell-free DNA and the Illumina MiSeq Platform: the 56G Oncology Panel v2 from Swift Biosciences (Cat. # AL-56248). This

panel contains 263 amplicons sized 92-184 bp that covers hotspots, exonic SNPs and contiguous regions of 56 human genes. The list of genes and number of amplicons is provided in Table 1. The kit contains a DNA standard with a set of 11 defined allelic frequencies for major oncology targets to be used as a sequencing control and DNA from HCT116, RKO and SW48 colon cancer cell lines. The 56G Oncology library was prepared according to the manufacturer's protocol. In brief, 10 ng DNA per sample was used for the Multiplex PCR Step using the Reaction Mix, and the following Thermocycler Program: 30 sec at 98 °C, 4 cycles of 10 sec at 98 °C, 5 min at 63 °C, 1 min at 65 °C, followed by 21 cycles of 10 sec at 98 °C, 1 min at 64 °C, followed by 1 min at 65 °C and hold at 4 °C. The resulting amplicons were purified using SPRIselect beads (Beckman Coulter, Cat. #B23318) and a DynaMag magnetic rack (Invitrogen). Next, a unique combination of Index D50X + Index D7XX was added to each sample bead pellet, together with the Indexing Reaction Mix (Swift Biosciences). The samples were incubated at 37 °C for 20 min with the lid heating turned off. The libraries were purified once more with SPRIselect beads and quantitated in triplicates by qRT-PCR in a 20 μL reaction using the iQ SYBR Green Supermix (BioRad), containing 10 μL of SYBR Green mix, 10 μL of diluted library (1:1000), and 500 nM of the following primers: 5' AATGATACGGCGACCACCGAGAT 3'; and 5' CAAGCAGAAGACGGCATACGA 3'. Serial dilutions of the PhiX Sequencing Control v3, (Illumina Cat. # FC- 110-3001) was used as standard. After quantitation, the libraries were normalized to a concentration of 2 nM and pooled together.

MiSeq Loading

The library pool was sequenced using the MiSeq v2 300 cycle Reagent Kit (Illumina). Five μL of the pooled amplicon library was denatured with 5 μL 0.2N NAOH for 5 min at room temperature. The library pool was then diluted to 8 pM with chilled HT1 buffer and 10% PhiX v3 control (Illumina) was spiked into the diluted library pool. Six hundred μL of the diluted pooled library with PhiX spike-in was loaded into the MiSeq reagent cartridge.

Sequencing data analysis

Adapter trimming was conducted per Swift Biosciences recommendation, using *cutadapt*[14]. Paired-end FASTQ samples were aligned to GRCh38 with BWA-MEM. Sorting and indexing was done using *samtools*. Base quality score recalibration followed by local realignment was done using the GATK Java package in conjunction with dbSNP annotation (b149) [15]. Variant calling was conducted using the LoFreqV2 (LoFreq*) mutation caller [16]. Visualizations were created in R using custom scripts (available on request) employing Bioconductor package VariantAnnotation [17]. as well as the plotting framework *ggplot2* and further adapted in Excel 2010 and Illustrator CS3 (Adobe). After mutations were called, percent representation was established as (number of variant reads)/(number of reference reads + number of variant reads). Variants leading to amino acid changes, with a minimum

read count of 5 reads and a frequency above 1% in at least one of the DNA samples are shown. The variant frequencies of the expected mutations that were detected in the DNA standard are shown in the Supplementary Figure 1. Three variants detected in amplicons from patient samples and the DNA standard were discarded as false positives (*FGFR1* D166del; *MSH6* F1088frameshift and *TP53* P72R).

Table 1. Genes included in the analysis. The amplicon panel is from Swift Biosciences 'Accel-Amplicon 56G Oncology Panel v2'. The number of amplicons (#) for each gene is shown.

Gene name	# amplicons	Gene name	# amplicons
ABL1	5	*IDH2*	2
AKT1	2	*JAK2*	2
ALK	2	*JAK3*	3
APC	9	*KDR*	9
ATM	19	*KIT*	14
BRAF	2	*KRAS*	3
CDH1	3	*MAP2K1*	5
CDKN2A	2	*MET*	6
CSF1R	2	*MLH1*	1
CTNNB1	1	*MPL*	1
DDR2	1	*MSH6*	4
DNMT3A	1	*NOTCH1*	3
EGFR (HER1)	9	*NPM1*	1
ERBB2 (HER2)	4	*NRAS*	3
ERBB4 (HER4)	8	*PDGFRA*	4
EZH2	1	*PIK3CA*	11
FBXW7	6	*PTEN*	14
FGFR1	2	*PTPN11*	2
FGFR2	4	*RB1*	12
FGFR3	6	*RET*	6
FLT3	4	*STK11*	5
FOXL2	1	*SMAD4*	10
GNA11	2	*SMARCB1*	4
GNAQ	2	*SMO*	5
GNAS	2	*SRC*	1
HNF1A	4	*TP53 (P53)*	21
HRAS	2	*TSC1*	1
IDH1	1	*VHL*	3

RESULTS

Patient characteristics and analysis approach

Patients with treatment-naïve adenocarcinomas of the colon (n=5) or the pancreas (n=5) that were considered resectable at the time of initial diagnosis were included in this study (Table 2). Plasma samples were collected before surgical removal of the primary tumors and at the time of disease progression. Resected tumor tissues were cryo-sectioned and evaluated by a pathologist to assess cancer cell and stroma abundance. After surgery, patients received different adjuvant therapies that are listed in Table 2. To assess the mutation patterns in early and late stage colon and pancreatic cancer we compared plasma DNA at the time of initial diagnosis to that of the primary tumor, as well as to the plasma DNA at the time of metastatic disease (Figure 1). For DNA mutation analysis, we sequenced 30 DNA samples from 10 patients in a single, next generation deep-sequencing run of 263 mutation hotspots in a set of 56 cancer-related genes. The same platform was used for the analysis of tissue and circulating cell-free DNA (ccfDNA) to avoid discrepancies in mutation findings due to variability in sequencing methods or reagents.

DNA mutations detected

Next generation deep-sequencing of amplicons showed a median depth of 754,000 reads per sample. In all pre-surgery plasma samples genomic alterations with a 1% frequency were detected, despite a relatively low read coverage in one of the ccfDNA samples (patient 9 pre-surgery). One out of 10 late stage plasma samples (ccfDNA patient 4 at metastasis) did not contain genomic alterations above 1% frequency due to hemolysis and wildtype cellular DNA contamination that diluted the ccfDNA mutations. We focused on non-synonymous DNA alterations with a variant frequency of at least 1% in one of the samples per patient. In the 56 genes assessed we found an average of 10 mutations (range 4-15) in 17 genes in the ccfDNA of five colon cancer patients before surgery (Figure 2). The ccfDNA of the five patients with resectable PDAC contained fewer mutations, i.e. an average of 8 (range 5-12) mutations in 14 of the 56 genes assessed.

Surprisingly, the number of mutations detected in the primary tumors was much lower than that in the plasma: In the colon cancer tissues an average of 3 mutations (range 1-4) were found in 7 genes (*APC, BRAF, CDKN2A, KIT, KRAS, PTEN, TP53*; Figure 3). In the pancreatic cancer tissues 4 mutations (range 3-6) were found in 7 genes (*CDNKN2A, JAK3, KDR, KIT, KRAS, SMAD4, TP53*; Figure 3). Although our analysis detected mutations in only 7 genes, it is striking that each patient still had a unique combination of genomic alterations.

At the time of disease progression, the ccfDNA of five patients with metastasized colon cancer contains an average of 7 mutations (range 2-11) in 16 genes. The plasma of the patients

with metastatic PDAC contained an average of 9 mutations (range 3-12) in 20 genes (Figure 4). This number is close to the number of ccfDNA mutations before surgery. However, some of the ccfDNA mutations detected at the time of primary disease were lost at the time of metastatic disease, i.e. *ABL1, ATM, DNMT3A, FLT3, HNF1A, NRAS* and *SMAD4.* Possible explanations are that these mutations occurred in cancer cell subpopulations in the primary cancers that were resected, or that the clones carrying the mutations were selected against during disease progression.

a. / b. / c. : NGS mutation analysis of 263 amplicons in 56 cancer genes
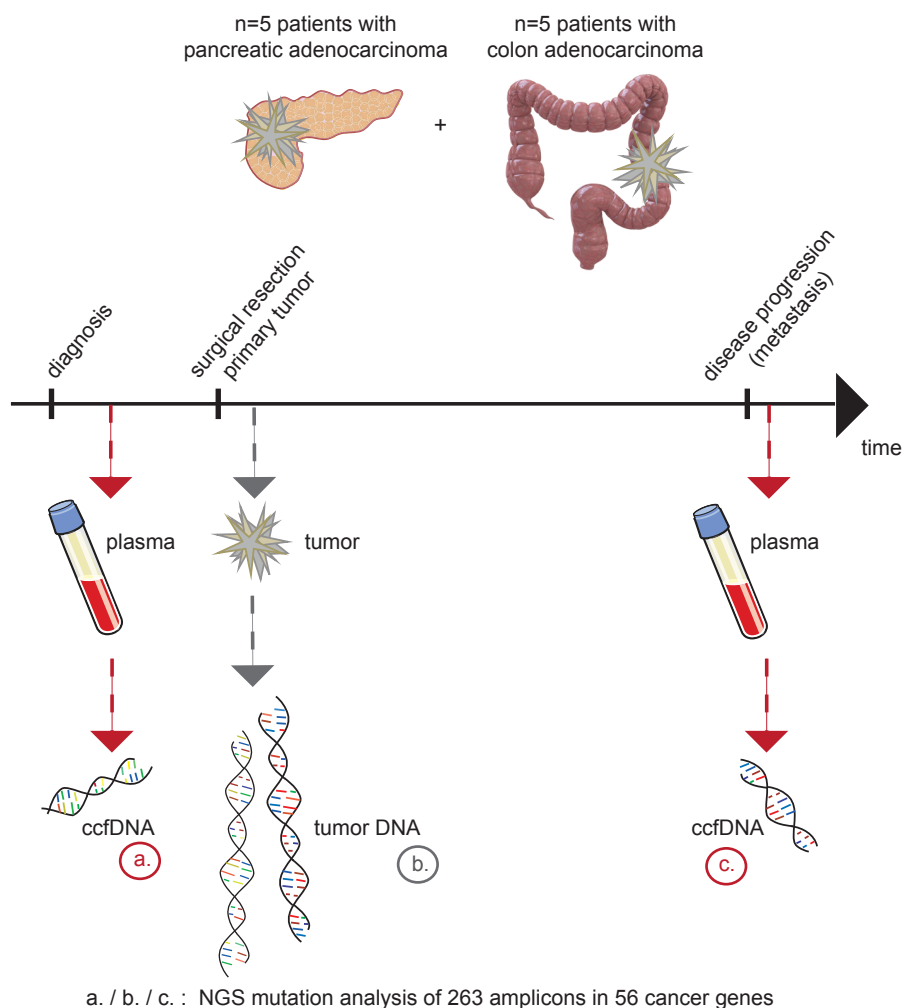
Figure 1. Overview of the study. Ten patients were included in the analysis of circulating cell-free DNA (ccfDNA) at diagnosis of primary cancer and at the time of progressive disease. DNA from frozen primary tumors that were collected during surgery was for comparison. All 30 DNA samples were subjected to next generation sequencing (NGS) of 56 genes with cancer-associated mutations.

Table 2. Patient characteristics.

Disease	Colon adenocarcinoma					Pancreatic adenocarcinoma				
Patient #	1 (1A0383)	2 (1A0390)	3 (1A0690)	4 (1A0816)	5 (1A1118)	6 (1A0431)	7 (1A0522)	8 (1A0551)	9 (1A0843)	10 (1A1128)
Pathological stage	3c T3N2M0	4a T3N1M1	3b T3N2(4/17) M0	2 pT4pN0M0	4a TxNxM1a	2b pT3N1M0	2b pT3pN2	2b pT3N1M0	2a pT3N0M0	2b T3N1M0
Age [years]	67	62	50	66	51	54	69	66	45	57
Gender	Male	Female	Female	Male	Male	Male	Female	Male	Female	Female
Surgery	Hemi-colectomy	Colon tumor resection	Colon resection	Right colectomy	Hemi-colectomy	Total pancreatectomy, splenectomy	Whipple	Whipple	Distal pancreatectomy, splenectomy	Distal pancreatectomy, splenectomy
Histology tumor scroll	50% tumor, 50% fibrosis	70% tumor, 30% fibrosis	90% tumor, 10% fibrosis	70% tumor, 30% necrosis	90% tumor, 10% fibrosis	30% tumor, 70% fibrosis	40% tumor, 60% fibrosis	50% tumor, 50% fibrosis	50% tumor, 50% fibrosis	40% tumor, 60% fibrosis
Time to metastasis after surgery [months]	70	20	12	5	1	16	9	18	15	7
Metastatic site	Mesentery, Anastomosis	Liver, Lung	Peritoneum, Liver	Liver	Peritoneum, Liver	Peritoneum, Liver	Liver	Lung	Ovary	Liver

Table 2. Patient characteristics. (continued)

Disease	Colon adenocarcinoma		Pancreatic adenocarcinoma
Adjuvant therapy before 2nd plasma sample	1. FOLFOX 2. FOLFIRI + GI4000 + Bevacizumab	1. FOLFOX 1. Capecitabine + Oxaliplatin 2. Capecitabine + Oxaliplatin + Bevacizumab 3. Capecitabine + Bevacizumab 4. 5-FU + Bevacizumab 5. 5-FU /	1. Capecitabine + Radiotherapy 2. Gemcitabine 1. Veliparib+ FOLFOX 2. Gemcitabine 3. MEDI-565 1. Gemcitabine 2. Capecitabine 1. FOLFOX 2. Capecitabine 3. PF05082566 1. Gemcitabine 2. Capecitabine

FOLFOX (Folinic acid + Fluorouracil + Oxaliplatin); FOLFIRI (Folinic acid, Fluorouracil and Irinotecan); GI4000 (vaccine against mutated Ras); Bevacizumab (anti-VEGF-A antibody); 5-FU (Fluorouracil); Veliparib (poly(ADP-ribose) polymerase (PARP) -1 and -2 inhibitor); MEDI-565 (anti-CEA/CD_3 antibody); PF05082566 (anti-CD_{137} stimulating antibody).
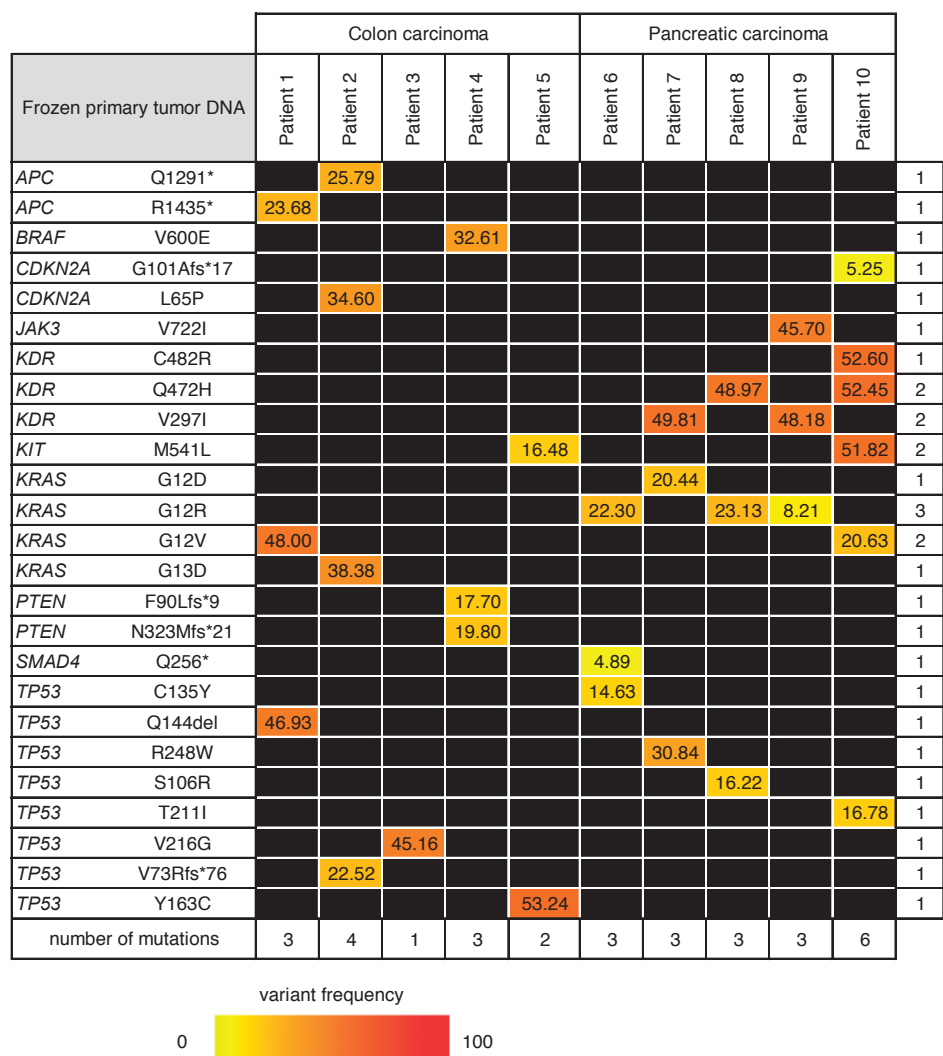
Plasma ccfDNA before surgery		Colon carcinoma					Pancreatic carcinoma					
		Patient 1	Patient 2	Patient 3	Patient 4	Patient 5	Patient 6	Patient 7	Patient 8	Patient 9	Patient 10	
APC	E1560V	5.74					5.54					2
APC	K1308*	1.84										1
APC	P1458H			12.06			15.83	6.35		28.13		4
BRAF	S465P							1.14				1
BRAF	S467P			1.20								1
BRAF	V600E	1.91	6.23	3.39	8.28		2.55					5
CDKN2A	G136Afs*10	1.27									0.70	2
EGFR	V96A	7.38										1
ERBB2	C315R			1.50								1
ERBB4	C326F	5.37	3.96	7.26			12.73		8.28	22.83		6
ERBB4	M953K	3.22										1
EZH2	X649_splice				1.28							1
GNA11	R166H						4.64					1
KDR	C482R										52.25	1
KDR	Q472H								61.00		52.32	2
KDR	V297I							42.00				1
KIT	M541L					46.66					53.84	2
KIT	Y568C				1.52							1
MAP2K1	R47*	6.39		9.62			20.18	12.56	7.61			5
MET	Q155H	7.38	3.25	10.13	1.41		16.21	7.85	5.97	93.84		8
NOTCH1	V1578del	1.69			0.78	0.61						3
PIK3CA	L94P				1.64						1.18	2
PTEN	L112P				1.49							1
PTEN	N323Mfs*21				5.81							1
PTEN	X85_splice	23.76	3.16	41.14	1.98		14.07	12.20	7.84	6.88		8
SMARCB1	P383Rfs*100					0.21	1.90					2
SMO	M525V	1.52										1
TP53	D281G				2.04							1
TP53	I251M			9.63			14.24	7.63		20.29		4
TP53	N268Tfs*77			2.93								1
TP53	P152Rfs*18				4.76							1
TP53	Q144del	1.10										1
TP53	R175G									100.00		1
TP53	R273C				5.87							1
TP53	S9N			2.29								1
TP53	X331_splice			1.97	1.43							2
TP53	Y163C					3.24						1
TP53	Y234H				1.29							1
VHL	A149P	8.72	7.02	9.45			18.97	6.86	7.59	100.00		7
VHL	R107L	3.80					7.74			82.45		3
number of mutations		15	5	13	14	4	12	8	6	8 ˉ	5	

ˉ = low coverage

variant frequency

0   100

Figure 2. Circulating cell-free DNA mutation frequency before surgery. Non-synonymous mutations at ≥1% variant frequency in at least one of the ccfDNA samples. * = premature stop codon; fs=frameshift; del=deletion; ˉ = low coverage.

Frozen primary tumor DNA		Colon carcinoma					Pancreatic carcinoma					
		Patient 1	Patient 2	Patient 3	Patient 4	Patient 5	Patient 6	Patient 7	Patient 8	Patient 9	Patient 10	
APC	Q1291*		25.79									1
APC	R1435*	23.68										1
BRAF	V600E				32.61							1
CDKN2A	G101Afs*17										5.25	1
CDKN2A	L65P		34.60									1
JAK3	V722I									45.70		1
KDR	C482R										52.60	1
KDR	Q472H								48.97		52.45	2
KDR	V297I							49.81		48.18		2
KIT	M541L					16.48					51.82	2
KRAS	G12D							20.44				1
KRAS	G12R						22.30		23.13	8.21		3
KRAS	G12V	48.00									20.63	2
KRAS	G13D		38.38									1
PTEN	F90Lfs*9				17.70							1
PTEN	N323Mfs*21				19.80							1
SMAD4	Q256*						4.89					1
TP53	C135Y						14.63					1
TP53	Q144del	46.93										1
TP53	R248W							30.84				1
TP53	S106R								16.22			1
TP53	T211I									16.78		1
TP53	V216G			45.16								1
TP53	V73Rfs*76		22.52									1
TP53	Y163C					53.24						1
number of mutations		3	4	1	3	2	3	3	3	3	6	

variant frequency

0 ▮▮▮▮▮ 100

Figure 3. DNA mutation frequency in primary tumors. Non-synonymous mutations at ≥1% variant frequency in at least one of the primary tumors. * = premature stop codon; fs=frameshift; del=deletion.

Comparison of mutations in primary tumors and the circulation at early and late stage disease

We evaluated the concordance between DNA mutations in the primary tumors and the circulation. For each patient, the mutations above a 1% variant frequency threshold in at least one of the DNA samples are shown in Fig. 5. First we compared the similarity between primary tumor DNA and ccfDNA before surgery (Table 3). In the patients with colon cancer about half (47%) of tumor tissue mutations are also detected in the circulation though there is a wide variation between patients. In patients with primary PDAC this concordance
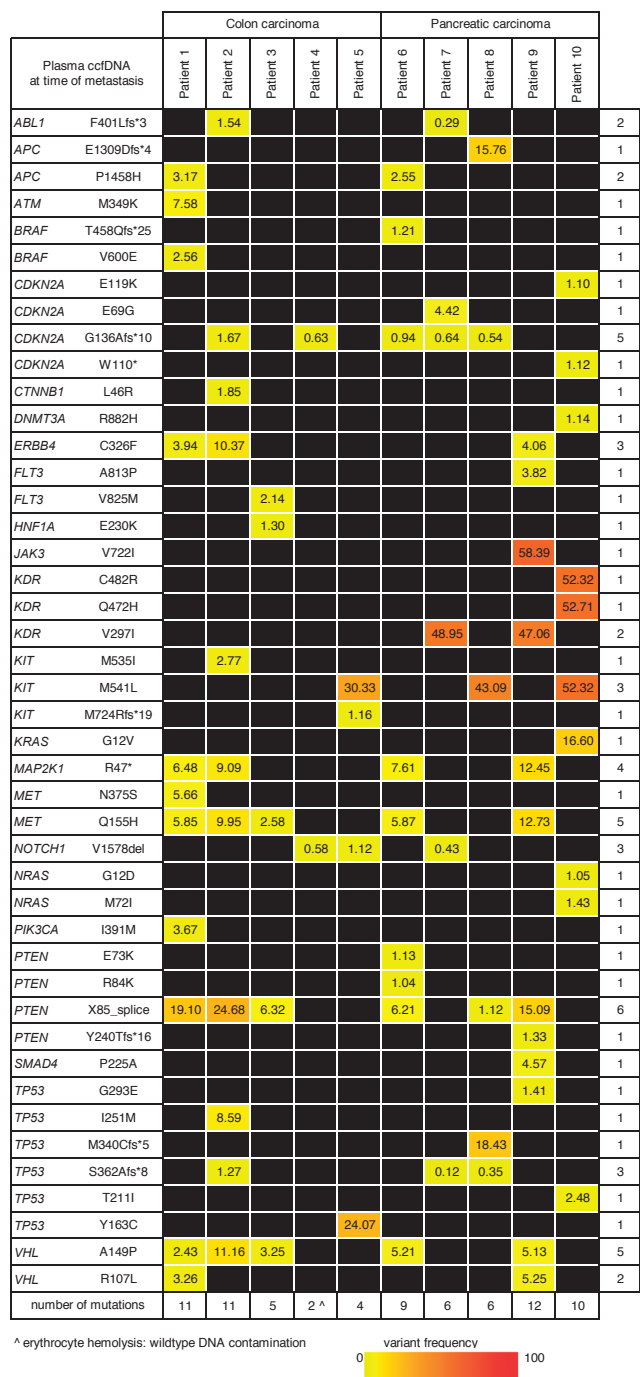
is below one third (28%). On the other hand, it is notable that cancer heterogeneity within each patient was much more evident in the mutational landscape of the ccfDNA than in tumor tissue DNA. The majority of mutations in the ccfDNA were not detected in the primary tumor tissues: 71% in colon cancer and 78% of the mutations in PDAC (Table 3). This finding illustrates that a tissue section of a given tumor can fail to represent the molecular makeup of the entire cancer.

Table 3. Concordance and discordance between the number of mutations detected in plasma and primary tumor DNA at the time of initial diagnosis.

Primary tumor versus plasma at the time of diagnosis				
Patient	Disease	Tumor tissue DNA mutations detected in plasma samples	Plasma DNA mutations <u>not</u> detected in tumor tissues	Cancer cells in tumor
1	colon AC	60% (3/5)	79% (11/14)	50%
2	colon AC	0% (0/5)	100% (5/5)	70%
3	colon AC	0% (0/1)	100% (13/13)	90%
4	colon AC	75% (3/4)	77% (10/13)	70%
5	colon AC	100% (3/3)	0% (0/3)	90%
average		**47%**	**71.2%**	**74%**
6	PDAC	25% (1/4)	92% (11/12)	30%
7	PDAC	33% (1/3)	89% (8/9)	40%
8	PDAC	33% (1/3)	86% (6/7)	50%
9 ⁻	PDAC	0% (0/3) ⁻	100% (8/8)	50%
10	PDAC	50% (3/6)	25% (1/4)	40%
average		**28.2%**	**78.4%**	**42%**

AC= adenocarcinoma; PDAC= pancreatic ductal adenocarcinoma; ⁻ = low sequencing coverage in plasma DNA

For the current study we had selected a set of patients that developed metastatic disease after removal of the primary tumors. We evaluated the genomic evolution during this progression by comparing the ccfDNA at the time of surgery and metastasis. Table 4 summarizes the differences in the ccfDNA mutational landscape at the time of primary and metastatic cancer. In five patients with metastatic colon cancer, 34% of the ccfDNA mutations were not detected in the circulation at the time of primary disease. These emerging mutations indicate clonal evolution of the disease during malignant progression. In PDAC, the proportion of these metastasis-associated ccfDNA mutations is higher; 63% of the mutations were not detected during primary disease. Interestingly, the fraction of new mutations at the time of metastatic disease is not correlated with the length of time to progression, (Table 4) or the type of adjuvant therapy (Table 2). Although this is a small number of patients, it is noteworthy that approximately half of ccfDNA mutations detected at the time of primary disease were not detected after progression to metastatic disease (45% in colon AC, 59% in

Plasma ccfDNA at time of metastasis		Colon carcinoma					Pancreatic carcinoma					
		Patient 1	Patient 2	Patient 3	Patient 4	Patient 5	Patient 6	Patient 7	Patient 8	Patient 9	Patient 10	
ABL1	F401Lfs*3		1.54					0.29				2
APC	E1309Dfs*4								15.76			1
APC	P1458H	3.17					2.55					2
ATM	M349K	7.58										1
BRAF	T458Qfs*25						1.21					1
BRAF	V600E	2.56										1
CDKN2A	E119K										1.10	1
CDKN2A	E69G							4.42				1
CDKN2A	G136Afs*10		1.67		0.63		0.94	0.64	0.54			5
CDKN2A	W110*										1.12	1
CTNNB1	L46R		1.85									1
DNMT3A	R882H										1.14	1
ERBB4	C326F	3.94	10.37							4.06		3
FLT3	A813P								3.82			1
FLT3	V825M			2.14								1
HNF1A	E230K			1.30								1
JAK3	V722I								58.39			1
KDR	C482R									52.32		1
KDR	Q472H									52.71		1
KDR	V297I							48.95		47.06		2
KIT	M535I		2.77									1
KIT	M541L					30.33			43.09	52.32		3
KIT	M724Rfs*19					1.16						1
KRAS	G12V										16.60	1
MAP2K1	R47*	6.48	9.09				7.61			12.45		4
MET	N375S	5.66										1
MET	Q155H	5.85	9.95	2.58			5.87			12.73		5
NOTCH1	V1578del				0.58	1.12		0.43				3
NRAS	G12D										1.05	1
NRAS	M72I										1.43	1
PIK3CA	I391M	3.67										1
PTEN	E73K						1.13					1
PTEN	R84K						1.04					1
PTEN	X85_splice	19.10	24.68	6.32			6.21		1.12	15.09		6
PTEN	Y240Tfs*16									1.33		1
SMAD4	P225A									4.57		1
TP53	G293E									1.41		1
TP53	I251M		8.59									1
TP53	M340Cfs*5							18.43				1
TP53	S362Afs*8		1.27					0.12	0.35			3
TP53	T211I										2.48	1
TP53	Y163C					24.07						1
VHL	A149P	2.43	11.16	3.25			5.21			5.13		5
VHL	R107L	3.26								5.25		2
number of mutations		11	11	5	2 ^	4	9	6	6	12	10	

^ erythrocyte hemolysis: wildtype DNA contamination

variant frequency 0 — 100

Figure 4. Circulating cell-free DNA mutation frequency at the time of metastasis. Non-synonymous mutations at ≥1% variant frequency in at least one of the ccfDNA samples. * = premature stop codon; fs=frameshift; del=deletion; ^ = hemolysis, increase of wildtype DNA.

Table 4. Concordance between the number of mutations detected in plasma at the time of initial diagnosis and detection of metastasis.

ccfDNA mutations at the time of primary versus metastatic disease			
Patient	Disease	Gain of mutations after metastasis	Loss of mutations after metastasis	Time to metastasis [months]
1	colon AC	40% (4/10)	38% (5/14)	70
2	colon AC	64% (7/11)	20% (1/5)	20
3	colon AC	40% (2/5)	77% (10/13)	12
4 ^	colon AC	0% (0/1)	92% (12/13)	5
5	colon AC	25% (1/4)	0% (0/3)	1
average		33.8%	45.4%	21.6
6	PDAC	38% (3/8)	58% (7/12)	16
7	PDAC	67% (2/3)	89% (8/9)	9
8	PDAC	80% (4/5)	86% (6/7)	18
9	PDAC	58% (7/12)	38% (3/8)	15
10	PDAC	70% (7/10)	25% (1/4)	7
average		62.6%	59.2%	13

AC, adenocarcinoma; PDAC, pancreatic ductal adenocarcinoma; ^, hemolysis and wildtype cellular DNA contamination

PDAC, Table 4). This would indicate that cancer cell subpopulations carrying these mutations were likely dominant in the primary tumor that was removed surgically. Also, these subpopulations did not play a significant role in the metastatic lesions.

In conclusion, we found that ccfDNA analysis complements the molecular insight into the genetic make-up of colon and pancreatic cancer and can be particularly helpful in monitoring molecular changes over time.

DISCUSSION

The majority of molecular profiling of human tumors has relied on the analysis of aliquots of cancer tissues obtained from surgical resection specimen. Biopsies of cancerous lesions at disease progression are used rarely due to obvious disadvantages: They are potentially risky invasive procedures, time consuming and expensive. Also, cancer cells in tissue biopsies may be sparse due to the limited size of tissue recovered and against the background of wildtype stromal cells. Most importantly, subpopulations of a heterogeneous tumor may be poorly represented in biopsies. In the current study we sought to assess the changes in the mutational makeup of colon and pancreatic adenocarcinoma between the time of primary tumor surgery and detection of metastatic disease using ccfDNA. In this study we provide a direct comparison of mutation detection in primary tumor DNA and plasma ccfDNA

Patient 1 Colon Carcinoma		pre surgery ccfDNA	primary tumor DNA	metastasis ccfDNA	
APC	E1560V	5.74			1
APC	K1308*	1.84			1
APC	P1458H			3.17	1
APC	R1435*		23.68		1
ATM	M349K			7.58	1
BRAF	V600E	1.91		2.56	2
CDKN2A	G136Afs*10	1.27	0.88		2
EGFR	V96A	7.38			1
ERBB4	C326F	5.37		3.94	2
ERBB4	M953K	3.22			1
KRAS	G12V		48.00		1
MAP2K1	R47*	6.39		6.48	2
MET	N375S			5.66	1
MET	Q155H	7.38		5.85	2
NOTCH1	V1578del	1.69	0.58		1
PIK3CA	I391M			3.67	1
SMO	M525V	1.52			1
TP53	Q144del	1.10	46.93		2
VHL	A149P	8.72		2.43	2
VHL	R107L	3.80		3.26	2
number of mutations		14	5	10	

Patient 2 Colon Carcinoma		pre surgery ccfDNA	primary tumor DNA	metastasis ccfDNA	
ABL1	F401Lfs*3			1.54	1
APC	Q1291*		25.79		1
BRAF	V600E	6.23			2
CDKN2A	G136Afs*10		0.73	1.67	2
CDKN2A	L65P		34.60		1
CTNNB1	L46R			1.85	1
ERBB4	C326F	3.96		10.37	2
KIT	M535I			2.77	1
KRAS	G13D		38.38		1
MAP2K1	R47*			9.09	1
MET	Q155H	3.25		9.95	2
PTEN	X85_splice	3.16		24.68	2
TP53	I251M			8.59	1
TP53	S362Afs*8			1.27	1
TP53	V73Rfs*76		22.52		1
VHL	A149P	7.02		11.16	2
number of mutations		5	5	11	

Patient 6 Pancreatic Carcinoma		pre surgery ccfDNA	primary tumor DNA	metastasis ccfDNA	
APC	E1560V	5.54			1
APC	P1458H	15.83		2.55	2
BRAF	T458Qfs*25			1.21	1
BRAF	V600E	2.55			1
ERBB4	C326F	12.73			1
GNA11	R166H	4.64			1
KRAS	G12R		22.30		1
MAP2K1	R47*	20.18		7.61	2
MET	Q155H	16.21		5.87	2
PTEN	E73K			1.13	1
PTEN	R84K			1.04	1
PTEN	X85_splice	14.07		6.21	2
SMAD4	Q256*		4.89		1
SMARCB1	P383Rfs*100	1.90	0.18		2
TP53	C135Y		14.63		1
TP53	I251M	14.24			1
VHL	A149P	18.97		5.21	2
VHL	p.R107L	7.74			1
number of mutations		12	4	8	

Patient 7 Pancreatic Carcinoma		pre surgery ccfDNA	primary tumor DNA	metastasis ccfDNA	
APC	P1458H	6.35			1
BRAF	K473*	1.49			1
BRAF	S465P	1.14			1
CDKN2A	E69G			4.42	1
KDR	V297I	42.00	49.81	48.95	3
KRAS	G12D		20.44	0.47	2
MAP2K1	R47*	12.56			1
MET	Q155H	7.85			1
PTEN	X85_splice	12.20			1
TP53	I251M	7.63			1
TP53	R248W		30.84		1
VHL	A149P	6.86			1
number of mutations		9	3	3	

Figure 5. Mutation frequency in ccfDNA and tumors. The results from individual patients are shown (n=10). Non-synonymous mutations with ≥1% variant frequency in at least one of the ccfDNA samples. * = premature stop codon; fs=frameshift; del=deletion; ^ = hemolysis; ‾ = low coverage.

Patient 3 Colon Carcinoma

Gene	Mutation	pre surgery ccfDNA	primary tumor DNA	metastasis ccfDNA	
APC	P1458H	12.06			1
BRAF	S467P	1.20			1
BRAF	V600E	3.39			1
ERBB2	C315R	1.50			1
ERBB4	C326F	7.26			1
FLT3	V825M			2.14	1
HNF1A	E230K			1.30	1
MAP2K1	R47*	9.62			1
MET	Q155H	10.13		2.58	2
PTEN	X85_splice	41.14		6.32	2
TP53	I251M	9.63			1
TP53	N268Tfs*77	2.93			1
TP53	S9N	2.29			1
TP53	V216G		45.16		1
TP53	X331_splice	1.97			1
VHL	A149P	9.45		3.25	2
number of mutations		13	1	5	

Patient 4 Colon Carcinoma

Gene	Mutation	pre surgery ccfDNA	primary tumor DNA	metastasis ccfDNA	
BRAF	V600E	8.28	32.61		2
EZH2	X649_splice	1.28			1
KIT	Y568C	1.52			1
MET	Q155H	1.41			1
PIK3CA	L94P	1.64	0.73	0.67	3
PTEN	F90Lfs*9		17.70		1
PTEN	L112P	1.49			1
PTEN	N323Mfs*21	5.81	19.80		2
PTEN	X85_splice	1.98			1
TP53	D281G	2.04			1
TP53	P152Rfs*18	4.76			1
TP53	R273C	5.87			1
TP53	X331_splice	1.43			1
TP53	Y234H	1.29			1
number of mutations		13	4	1 ^	

^ erythrocyte hemolysis: wildtype DNA contamination

Patient 5 Colon Carcinoma

Gene	Mutation	pre surgery ccfDNA	primary tumor DNA	metastasis ccfDNA	
KIT	M541L	46.66	16.48	30.33	3
KIT	M724Rfs*19			1.163	1
NOTCH1	V1578del	0.611	0.276	1.119	3
TP53	Y163C	3.236	53.24	24.07	3
number of mutations		3	3	4	

Patient 8 Pancreatic Carcinoma

Gene	Mutation	pre surgery ccfDNA	primary tumor DNA	metastasis ccfDNA	
APC	E1309Dfs*4			15.76	1
ERBB4	C326F	8.28			1
KDR	Q472H	61.00	48.97		2
KIT	M541L			43.09	1
KRAS	G12R		23.13		1
MAP2K1	R47*	7.61			1
MET	Q155H	5.97			1
PIK3CA	E545A			1.02	1
PTEN	X85_splice	7.84		1.12	2
TP53	L206Wfs*41	1.13			1
TP53	M340Cfs*5			18.43	1
TP53	S106R		16.22		1
VHL	A149P	7.59			1
number of mutations		7	3	5	

Patient 9 Pancreatic Carcinoma

Gene	Mutation	pre surgery ccfDNA	primary tumor DNA	metastasis ccfDNA	
APC	P1458H	28.13			1
ERBB4	C326F	22.83		4.06	1
FLT3	A813P			3.82	1
JAK3	V722I		45.70	58.39	2
KDR	V297I		48.18	47.06	2
KRAS	G12R		8.21		1
MAP2K1	R47*			12.45	1
MET	Q155H	93.84		12.73	2
PTEN	X85_splice	40.75		12.54	2
PTEN	Y240Tfs*16			1.33	1
SMAD4	P225A			4.57	1
TP53	G293E			1.41	1
TP53	I251M	20.29			1
TP53	R175G	100.00			1
VHL	A149P	100.00		5.13	2
VHL	R107L	82.45		5.25	2
number of mutations		8 ⁻	3	12	

Patient 10 Pancreatic Carcinoma

Gene	Mutation	pre surgery ccfDNA	primary tumor DNA	metastasis ccfDNA	
CDKN2A	E119K			1.10	1
CDKN2A	G101Afs*17		5.25		1
CDKN2A	W110*			1.12	1
DNMT3A	R882H			1.14	1
KDR	C482R	52.25	52.60	52.32	3
KDR	Q472H	52.32	52.45	52.71	3
KIT	M541L	53.84	51.82	52.32	3
KRAS	G12V		20.63	16.60	2
NRAS	G12D			1.05	1
NRAS	M72I			1.43	1
PIK3CA	L94P	1.18			1
TP53	T211I		16.78	2.48	2
number of mutations		4	6	10	

⁻ = low coverage

Figure 5. Mutation frequency in ccfDNA and tumors. The results from individual patients are shown (n=10). Non-synonymous mutations with ≥1% variant frequency in at least one of the ccfDNA samples. * = premature stop codon; fs=frameshift; del=deletion; ^ = hemolysis; ⁻ = low coverage.

at diagnosis and at disease recurrence. For this, amplicons covering 263 mutations in 56 cancer-associated genes were analyzed by deep-sequencing.

It is thought that ccfDNA can provide a better representation of the molecular makeup of a malignant disease than a single section from a surgical tumor specimen or a tissue biopsy. Also, blood samples can be drawn at deliberate intervals because they only require a minimally invasive procedure. In the present study the notion of a broader molecular representation is supported by the fact that the ccfDNA revealed approximately twice as many mutations as tumor tissue DNA. Very likely the tissue sections analyzed missed portions of the primary tumor that carried subpopulations with these additional mutations. It is also conceivable that patients had already developed occult metastatic disease at the time of the initial diagnosis and the additional ccfDNA mutations found represented the cancer cell subpopulations in the metastatic lesions. It appears that the ccfDNA provides a more complex picture of the disease.

Most studies focus on the presence of ccfDNA mutations in one or two genes to compare their presence to clinical outcome [18,19]. In our study, we sought to assess the mutation patterns in a broad set of genes to highlight tumor heterogeneity and demonstrate clonal evolution over the course of disease progression. In colon cancer, for example, ccfDNA has been used to track clonal evolution during treatment with the epidermal growth factor receptor (EGFR)-specific antibodies. Alterations in *KRAS, NRAS, MET, ERBB2, FLT3, EGFR* and *MAP2K1* were detected in ccfDNA of patients with primary or acquired resistance to EGFR blockade [20]. Using a broad panel of cancer-associated genes rather than frequently altered candidate oncogenes such as *KRAS* overcame one of the potential pitfalls encountered. None of the *KRAS* mutations from the seven patients with *KRAS* mutant primary tumors were detected in the ccfDNA at the time of diagnosis, while mutations in other genes were detected. Mutant *KRAS* ccfDNA was, however, found by others in 10 of 34 pancreatic patients (29%) [21] or in 136 of 188 (72.3%) of patients with metastatic PDAC [22]. Another study showed that mutant *KRAS* ccfDNA was detected in 14.8%, 45.5%, 30.8%, and 57.9% of age-matched controls, localized, locally advanced, and metastatic PDAC patients, respectively [19]. In circulating exosomal DNA the percentages of mutant *KRAS* in these groups were even higher, i.e. 7.4%, 66.7%, 80%, and 85% respectively [19].

At the time of surgical removal of the primary tumors between 28% and 47% of tumor mutations were also detected in ccfDNA. Others have found that in formalin-fixed paraffin-embedded cancer tissues and plasma from patients with different types of cancer an overall concordance of 60% in mutations of 19 genes analyzed [23]. Thus, the concordance found here is relatively low. In contrast, over 70% of mutations detected in ccfDNA were not found in the tumor samples. This could be due to metastatic disease at the time of diagnosis or

poor representation of the primary tumor composition by the histological section obtained for the DNA analysis.

Shed DNA in the circulation is fragmented into relatively short size fragments with tumor-derived DNA exhibiting even higher fragmentation than normal cellular DNA [24]. This was also found for specific examples such as the *BRAF* V600E mutant allele with a fragment size <145 base pairs. Indeed detection of *EGFR* T790M mutant DNA in the circulation of cancer patients was improved by selecting for shorter DNA fragment lengths [25]. Comparisons of tumor tissue somatic DNA and ccfDNA mutation rate can be impacted by the application of different sequencing technologies and amplicon sizes [26,27] as well as read depths and these technical issues may bias the data interpretation [21]. To avoid this pitfall we used a platform that is adapted to the detection of short DNA fragments found as circulating cell-free DNA. Thus, we sought to avoid differences in amplicon generation, library preparation or sequencing depth and all samples were subjected to the same amplicon and library generation protocol and analyzed in parallel.

We also compared the clonal evolution of cancer in the ccfDNA mutations over the course of disease progression. After metastasis, new ccfDNA mutations are gained both in colon (33.8%) and pancreatic cancer (62.6%) and were not detected at the time of diagnosis of the primary cancer. This indicates clonal selection due to treatment, malignant progression or metastatic spread to different tissues with different microenvironmental selection pressure. Complementary to the gain of mutations after metastasis, we also observed a loss of approximately half of the ccfDNA mutations. This loss of cancer subpopulations will be due to surgical removal of the primary tumor as well as patient treatment.

One final caveat in ccfDNA mutation analysis is the assignment of mutant DNA to cancer lesions under study rather than spontaneous mutations that occurred in other tissues and have no disease relevance. Recently reported analysis of mutation accumulation in human adult stem cells in different tissues showed that on average 40 new mutations arise per year during the life time of an individual [28]. In a study focused on the analysis of human skin, biopsies of physiologically normal skin showed 2 to 6 mutations per million bases per cell and matched to a large extent with cancer-associated mutations [29]. Notably, the frequency of mutations seen in normal skin is within the median range of 1 - 10 somatic mutations observed for human cancers [1]. We did not find detailed reports on ccfDNA mutation frequencies in healthy individuals but the occurrence of spontaneous mutations in healthy tissues provide a caveat on interpreting mutant ccfDNA as evidence of the presence of a cancerous lesion.

In conclusion, we found that ccfDNA appears to represent the heterogeneity of colon and pancreatic cancer more extensively than tumor tissue DNA. The analysis of a relatively broad panel of cancer-related genes is feasible for ccfDNA and would allow monitoring of changes in the molecular makeup over time and under therapy. A challenge will be to what extent altered mutation patterns in ccfDNA could also prompt a change in treatment.

Acknowledgements

Conflicts of interest

None of the authors have conflicts to disclose.

library control DNA		
gene	variant	VAF
BRAF	p.V600E	8.56
EGFR	p.E746_A750del	1.30
EGFR	p.L858R	2.21
EGFR	p.G719S	28.50
KIT	p.D816V	9.33
KRAS	p.G12D	5.95
KRAS	p.G13D	16.69
NRAS	p.Q61K	12.78
PIK3CA	p.E545K	8.46
PIK3CA	p.H1047R	16.36

VAF: variant allele frequency

Supplementary Figure 1. Non-synonymous mutations in the DNA standard provided as a control.

REFERENCES

1 Alexandrov, L. B. et al. (2013) Signatures of mutational processes in human cancer. *Nature* 500, 415-421

2 Gerlinger, M. et al. (2012) Intratumor heterogeneity and branched evolution revealed by multiregion sequencing. *N Engl J Med* 366, 883-892

3 Marusyk, A., Almendro, V. & Polyak, K. (2012) Intra-tumour heterogeneity: a looking glass for cancer? *Nat Rev Cancer* 12, 323-334

4 Schiavon, G. et al. (2015) Analysis of ESR1 mutation in circulating tumor DNA demonstrates evolution during therapy for metastatic breast cancer. *Sci Transl Med* 7, 313ra182

5 Garcia-Murillas, I. et al. (2015) Mutation tracking in circulating tumor DNA predicts relapse in early breast cancer. *Sci Transl Med* 7, 302ra133

6 Diehl, F. et al. (2005) Detection and quantification of mutations in the plasma of patients with colorectal tumors. *Proc Natl Acad Sci U S A* 102, 16368-16373

7 Diehl, F. et al. (2008) Circulating mutant DNA to assess tumor dynamics. Nat Med 14, 985-990

8 Crowley, E., Di Nicolantonio, F., Loupakis, F. & Bardelli, A. (2013) Liquid biopsy: monitoring cancer-genetics in the blood. *Nat Rev Clin Oncol* 10, 472-484

9 Haber, D. A. & Velculescu, V. E. (2014) Blood-based analyses of cancer: circulating tumor cells and circulating tumor DNA. Cancer Discov 4, 650-661

10 Rosell, R. & Karachaliou, N. (2016) Lung cancer: Using ctDNA to track EGFR and KRAS mutations in advanced-stage disease. *Nat Rev Clin Oncol* 13, 401-402

11 Alix-Panabieres, C. & Pantel, K. (2016) Clinical Applications of Circulating Tumor Cells and Circulating Tumor DNA as Liquid Biopsy. *Cancer Discov* 6, 479-491

12 Rapisuwon, S., Vietsch, E. E. & Wellstein, A. (2016) Circulating biomarkers to monitor cancer progression and treatment. *Comput Struct Biotechnol J* 14, 211-222

13 Vietsch, E. E., van Eijck, C. H. & Wellstein, A. (2015) Circulating DNA and Micro-RNA in Patients with Pancreatic Cancer. *Pancreat Disord Ther.* 2015 Jun;5(2). pii: 156.

14 Martin, M. (2011) Cutadapt removes adapter sequences from high-throughput sequencing reads. 2011 17, 3, doi:10.14806/ej.17.1.200

15 McKenna, A. et al. (2010) The Genome Analysis Toolkit: a MapReduce framework for analyzing next-generation DNA sequencing data. *Genome Res* 20, 1297-1303

16 Wilm, A. et al. (2012) LoFreq: a sequence-quality aware, ultra-sensitive variant caller for uncovering cell-population heterogeneity from high-throughput sequencing datasets. *Nucleic Acids Res* 40, 11189-11201

17 Obenchain, V. et al. (2014) VariantAnnotation : a Bioconductor package for exploration and annotation of genetic variants. *Bioinformatics* 30, 2076-2078

18 Scholer, L. V. et al. (2017) Clinical implications of monitoring circulating tumor DNA in patients with colorectal cancer. *Clin Cancer Res* 15;23(18):5437-5445.

19 Allenson, K. et al. (2017) High prevalence of mutant KRAS in circulating exosome-derived DNA from early-stage pancreatic cancer patients. *Ann Oncol* 28, 741-747

20 Siravegna, G. et al. (2015) Clonal evolution and resistance to EGFR blockade in the blood of colorectal cancer patients. *Nat Med* 21, 795-801

21 Pishvaian, M. J. et al. (2016) A pilot study evaluating concordance between blood-based and patient-matched tumor molecular testing within pancreatic cancer patients participating in the Know Your Tumor (KYT) initiative. *Oncotarget* 8;8(48):83446-83456

22   Cheng, H. et al. (2017) Analysis of ctDNA to predict prognosis and monitor treatment responses in metastatic pancreatic cancer patients. *Int J Cancer* 140, 2344-2350

23   Perkins, G. et al. (2012) Multi-purpose utility of circulating plasma DNA testing in patients with advanced cancers. *PLoS One* 7, e47020

24   Mouliere, F. et al. (2011) High fragmentation characterizes tumour-derived circulating DNA. *PLoS One* 6, e23418

25   Underhill, H. R. et al. (2016) Fragment Length of Circulating Tumor DNA. PLoS Genet 12, e1006162

26   Jiang, P. et al. (2015) Lengthening and shortening of plasma DNA in hepatocellular carcinoma patients. *Proc Natl Acad Sci U S A* 112, E1317-1325

27   Mouliere, F. & Rosenfeld, N. (2015) Circulating tumor-derived DNA is shorter than somatic DNA in plasma. *Proc Natl Acad Sci U S A* 112, 3178-3179

28   Blokzijl, F. et al. (2016) Tissue-specific mutation accumulation in human adult stem cells during life. *Nature* 538, 260-264

29   Martincorena, I. et al. (2015) Tumor evolution. High burden and pervasive positive selection of somatic mutations in normal human skin. *Science* 348, 880-886

CHAPTER 4

Circulating miR-125b-5p and miR-99a-5p are associated with disease progression in pancreatic cancer patients after resection

Eveline E. Vietsch[1,2]
Ivana Peran[1]
Mustafa Suker[2]
Thierry P.P. van den Bosch[3]
Johan M. Kros[3]
Anton Wellstein[1]
Casper H.J. van Eijck[2]

1 Department of Oncology, Lombardi Comprehensive Cancer Center, Georgetown University, Washington DC, USA
2 Department of Surgery, Erasmus Medical Center, Rotterdam, The Netherlands
3 Department of Pathology, Erasmus Medical Center, Rotterdam, The Netherlands

ABSTRACT

Objectives: Monitoring responses to therapy using changes in the expression of circulating microRNAs (miRs) could be useful in prognostication of pancreatic cancer (PDAC) patients.

Methods: Changes in circulating miRs due to cancer progression in the transgenic *Kras*[G12D/+]; *Trp53*[R172H/+]; *P48-Cre* (KPC) animal model of PDAC were analyzed for serum miRs that are altered in metastatic disease. An analysis of serum miR expression profiles of human patients with resectable PDAC was performed using the novel RT-qPCR based IDEAL Assay which allows for highly sensitive and miR-specific quantitation. Up to 250 serum miRs from 28 patients with PDAC were analyzed for changes indicative of PDAC recurrence after resection.

Results: Consistent with the results in the KPC mice, we found that high serum miR-125b-5p and miR-99a-5p expression could distinguish PDAC patients with short progression free survival (PFS) after surgery. In situ hybridization of miR-125b-5p and miR-99a-5p in the resected PDAC tissues showed that the miRs are highly expressed in inflammatory cells, mostly consisting of CD79A expressing cells of the B-lymphocyte lineage.

Conclusions: Circulating miR-125b-5p and miR-99a-5p are potential prognostic biomarkers after surgery in patients with PDAC, that reflect an altered immune landscape in response to cancer recurrence.

INTRODUCTION

Pancreatic ductal adenocarcinoma (PDAC) is expected to become the second most frequent cause of cancer death by 2030 [1]. Approximately 15% of patients have resectable disease (stage I or II), whereas more than half of patients have unresectable PDAC [2] . Although PDAC can be removed surgically in early stage disease, the 5-year survival rate of patients that undergo surgical resection is still only 10% [3-5] . After surgery, adjuvant chemotherapy such as gemcitabine treatment is indicated. However, approximately half of the patients are not able to receive adjuvant chemotherapy due to health deterioration [6]. Also, rapid development of metastases shortly after removal of the primary tumor occurs in a subset of PDAC patients. Clinical follow up uses CT imaging, whereas molecular markers of PDAC progression during follow up remain underexplored. Since collection of tissue biopsies from the pancreas is risky, minimally invasive biomarkers attainable as 'liquid biopsies' from blood draws are sorely needed to aid in prognostic stratification of patients and possible adjustment of the treatment regimen. Here we describe circulating, cell free nucleic acids as potential biomarkers.

Mature microRNAs (miRs) are highly conserved short strands of non-coding RNA that regulate gene expression. To date, more than 2600 human mature miRs have been identified and annotated [7], with more than half of human protein-coding genes likely regulated by at least one miR [8]. MiRs are dysregulated in cancer and play crucial roles in immune function, cell proliferation, apoptosis, metastasis, angiogenesis and tumor-stroma interactions [9-11]. It is noteworthy that miRs released from cells can induce miR-mediated gene expression alterations in neighboring as well as in distant cells when entering the circulation [12,13]. In the circulation, miRs are relatively stable and easy to measure, which has inspired a vast amount of biomarker research. The majority of research on circulating miR signatures in oncology is focused on diagnostics [14-18], however miRs can provide crucial insights into cancer progression and the effects of therapeutic interventions [19-22]. In the present study, we profiled serum miRs in patients with PDAC who underwent tumor resection, and in a transgenic mouse model of PDAC progression, to identify novel circulating biomarkers of pancreatic cancer progression.

MATERIAL AND METHODS

Serum miR analysis in KPC mice

The animal experiment with the genetically engineered *LSL-Kras*$^{G12D/+}$; *LSL-Trp53*$^{R172H/+}$; *P48-Cre* or KPC mice [23] in this study was approved by the Georgetown University Institutional Animal Care and Use Committee (IACUC). Twelve KPC mice were euthanized at the age of 5 months before ~ 1 mL blood was collected via intracardial puncture in Serum

Z-Gel tubes with clotting activator (Sarstedt). The serum tubes were inverted 5 times and centrifuged at 10,000 x g for 15 minutes. Afterwards the serum was stored in aliquots at -80 °C until further analyses. In addition, pancreas, liver and lungs were collected and processed by formalin fixation and paraffin embedding (FFPE). Tissues were stained with hematoxylin and eosin (H&E) and the slides were examined by a pathologist to evaluate pancreatic neoplasia and to determine the tumor stages. The animals were then divided into two groups based on disease progression: one group with PanIN-3 lesions as the worst disease stage, and a second group with mice that had invasive pancreatic cancer as well as lymph nodes, liver and lung metastases.

Equal volumes of serum samples from the mice belonging to the same group were pooled together, followed by miR isolation using the miRCURY RNA Isolation Kit for Biofluids (Exiqon). The murine miRs were reverse transcribed to cDNA using the miRCURY LNA™ Universal RT microRNA PCR, Polyadenylation and cDNA synthesis kit II (Exiqon). Expression of 179 miRs was analyzed with the qPCR-based Serum/Plasma Focus microRNA PCR Panel (Exiqon) using the ExiLENT SYBR® Green master mix (Exiqon). MiRs with Ct values higher than 30 cycles were excluded, resulting in 154 miRs that were evaluated. The median miR expression value in each pooled serum sample was used to normalize for miR expression. The fold differential expression for each miR was calculated ($2^{-\Delta\Delta Ct}$) and plotted using Prism Graphpad 5.01.

Patient blood collection

All patients provided written informed consent for participation and the protocols associated with this research were approved by the Erasmus Medical Center Medical Ethical Committee (MEC2017-1203). Peripheral venous blood samples were obtained from patients with treatment-naïve resectable PDAC 1 day before pancreaticoduodenectomy and ~4 weeks (range 2-6) after resection. Patients who had prior gastro-intestinal malignancies were excluded. For each serum sample, a total of 8.5 mL of venous blood was collected in SST II Advance serum tubes (BD) with clot activator of silica particles to induce coagulation. After inverting the tubes 6 times, the samples were spun within 4 hours after blood draw at 1258 g for 10 min at 4 °C in a swing-bucket centrifuge (Eppendorf 5810R). The serum was divided in 1 mL aliquots and stored at -80°C until further analyses.

Patients serum miR quantitation

Cell-free circulating miRs from the patients were isolated from 200 μL serum using the miRNeasy serum/plasma miRNA Isolation Kit (Qiagen). Two proprietary pre-mixed spike-in ~20 nt control RNAs (MiRXES) with sequences distinct from annotated mature human miRNAs (miRbase version21) were added into the lysis buffer prior to sample miR isolation, in order to evaluate RNA isolation efficiency. Serum miRs were isolated per manufacturer's

recommendation (Qiagen) and eluted in 15 μL nuclease free water. MiRs were reverse transcribed using IDEAL miR-specific oligos in a multiplex reaction per manufacturer's instruction (MiRXES). In brief, up to 2 μL sample RNA was mixed together with 1 μL RT Spike-in RNA, RT Buffer, nuclease free water, Reverse Transcriptase and a maximum of 10 different miR-specific RT oligos into 20 μL reactions and incubated at 42 °C for 30 min followed by heat inactivation at 95 °C for 5 min, in a SimpliAmp thermal cycler (Applied Biosystems). cDNA was stored at -20 °C (up to 4 weeks) and thawed only once. Before miR quantitation, the cDNA was diluted 1:10 in nuclease free water.

For the quantitative PCRs, 5 μL of sample cDNAs were mixed with the individual miRNA qPCR Assays (MiRXES), nuclease free water and the IDEAL miRNA qPCR Master Mix containing the passive reference dye ROX, into reactions of 20 μL volume. PCR amplifications in the 7500 Fast Real-Time PCR System (Applied Biosystems) were performed using the following protocol: 10 minutes at 95 °C, 5 minutes at 40 °C, followed by 40 cycles of: 10 seconds at 95 °C and 30 seconds at 60 °C with FAM fluorescence reading at the end of this step. The raw threshold cycle (Ct) values were determined using the 7500 Software (Applied Biosystems) with automatic baseline setting. Technical variations introduced during RNA isolation and the process of RT-qPCR were normalized using the measurements of the spike-in control RNAs.

In screen 1 two hundred fifty miRs were measured in n=3 patients before and after surgery. The Ct value cutoff was 33 cycles to ensure reliability of the measurements. MiR levels in screen 1 were normalized using the mean expression value of all measured miRs per sample. From miR screen 1, 44 miRs were selected for further analyses based on the following two criteria: 1.) differential expression before and after surgical tumor removal; 2.) differential regulation after resection in patients with different progression free survival.

Next, the selected 44 miRs plus an additional 12 miRs we identified from the literature were measured in a second cohort of n=10 patients. Two stably expressed reference genes from miR screens 1 and 2 were selected for normalization: miR-29c-5p and miR-421 expression was used because they represent the mean miR expression values in all our patient serum samples. This approach to miR normalization was described by Mestdagh et al. [24]. Potential prognostic miRs were selected according to the two criteria described above. In a third patient cohort (n=15) sixteen miRs were measured, including the two reference genes miR-29c-5p and miR-421.

Data analysis

Patient data were collected during the standard clinical follow up and included patient age, sex, treatment type and timing, resection information, pathological TNM-stage, time to

death, new co-morbidities, time to progression and type of progressive disease. The qPCR Ct values were processed in Excel and converted to fold expression using $2^{-\Delta Ct}$, normalized to the median miR expression (in the KPC mice and patient screen 1 analyses), or to the expression of reference miR-29c-5p and miR-421 (in the patient screens 2 and 3). The pre- and post-surgery serum miR expression values were presented and analyzed in Prism Graphpad 5.01 and compared between three patient groups: patients with short PFS (0-8 months); median PFS (8-16 months) and long PFS (>16 months). MiRs that were differentially expressed between the patients with short versus long PFS within all three patient cohorts were considered as potential prognostic miRs. The pre- and post-surgery expression values of the selected miRs in patients from all cohorts were analyzed by single factor ANOVA comparing the short (red) versus long (green) PFS patient groups. Kaplan-Meier graphs of PFS for patients with high versus low post-surgery serum miR-122-5p; 125b-5p or 99a-5p expression values compared were analyzed by Chi square (Logrank) test. The cutoff for high and low expression of each miR is based on the median post-surgery expression of the respective miR in all 28 patients.

In situ hybridization (ISH) of FFPE pancreatic cancer tissues

Pancreaticoduodenectomy tissue specimens were collected at the Erasmus Medical Center for clinical pathology evaluation. Stored FFPE tissue blocks were analyzed for clinical histopathological diagnosis. Residual material was used for biomarker analysis. Four µm thick tissue sections on extra adhesive glass slides (Leica, Biosystems) were processed in the Discovery Ultra instrument (Ventana, Roche). The following automated Discovery Universal protocol was used: tissues were preheated at 70 °C for 4 minutes then deparaffinized at 70 °C for 12 min. Pretreatment was performed with CC1 for 16 minutes (Cat. # 950-224, Ventana). One drop of DISC inhibitor (Cat. # 760-4840, Ventana) was applied and incubated for 12 min. The 3' and 5' - DIG labeled miRCURY LNA miRNA Detection probes (Qiagen, hsa-miR-125b-5p cat. # YD00611756-BCG; hsa-miR-99a-5p cat. # YD00619276-BCG; positive control hsa-U6 cat. # YD00699002-BCG and negative control Scramble-miR cat. # YD00699004-BCG) were diluted in formamide-free MiRCURY LNA miRNA ISH Buffer (Qiagen cat. # 339450) to a final 20 nM concentration, applied to the slides and incubated for 8 minutes. Denaturation was established at 90 °C for 8 min, followed by hybridization for 1 hour (at 55 °C for miR-125b-5p; 53 °C for miR-34a-5p; 52 °C for miR-99a-5p; 54 °C for U6 and at 57 °C for the Scramble-miR). Slides were washed twice with SCC (DISCOVERY Ribowash 1x cat. # 760-105, Ventana) and heated to 55 °C for 8 min. Slides were washed and heated again to 55 °C for 8 min. One drop of anti-DIG HRP enzyme conjugate (Cat. # 760-4822, Ventana) was applied and incubated for 16 min. Discovery amplification was performed using one drop of DISC AMP TSA BF and one drop of DISC AMP H2O2 BF (Cat. # 760-226, Ventana) for 32 min of incubation. One drop of DISC anti-BF HRP (cat#760-4828, Ventana) was incubated 16 min, followed by

one drop of DISC Ag C silver (Cat. # 760-227, Ventana) incubation for 16 min. The tissues were counterstained with Hematoxylin II (Cat. # 790-2208, Ventana) for 8 min, followed by incubation with Bluing Reagent Post Counterstain (Cat. # 760-2037, Ventana) incubation for 4 min. Adjacent tissue sections were stained with Hematoxylin and Eosin (H&E). The slides were scanned using the Nanozoomer 2.0-HT slide imager (Hamamatsu).

Immunohistochemistry for CD79A human pancreatic cancer tissues

Immunohistochemistry was performed with an automated immunohistochemistry staining system (Ventana BenchMark ULTRA, Ventana Medical Systems) using the 3,3'-diamino-benzidine method. In brief, following deparaffinization and heat-induced antigen retrieval for 64 min, the tissue sections were incubated with a rabbit monoclonal antibody raised against human CD79A (clone EP82, ready to use, Cell Marque) for 32 minutes at 36 °C. A subsequent amplification step was followed by incubation with hematoxylin II counter stain for 8 min and then a blue-colouring reagent for 8 min according to the manufacturer's instructions (Ventana). The slides were scanned using the Nanozoomer 2.0-HT slide imager (Hamamatsu).

RESULTS

Changes in serum miRs during pancreatic cancer progression in KPC mice

The *LSL-Kras*^G12D/+; *LSL-Trp53*^R172H/+; *P48-Cre* or KPC transgenic mouse model develops metastatic PDAC that recapitulates the human disease [23]. We investigated the serum miR expression in mice with PanIN lesions and mice with metastatic PDAC to assess whether serum miRs are altered during cancer progression. For this purpose we collected serum from KPC mice at 5 months of age and first evaluated the histology of the pancreas (Fig. 1a), lung and liver tissues (Fig. 1b). Serum from mice (n=3) with PanIN-3 as the highest grade component of lesions in the pancreas and from mice with metastatic PDAC (n=3) was combined into two pooled samples. The two pooled serum samples were analyzed for expression of 179 mature miRs by q-PCR. The 154 miRs that were detected in the serum of mice with metastases were then compared to those in mice with preinvasive PanIN-3 lesions (Supplementary Fig. 1). We found that fourteen serum miRs are downregulated more than 3-fold in mice with metastatic disease compared to age-matched mice with only preinvasive lesions, whereas thirteen miRs are upregulated >3-fold in the serum of mice with PDAC metastases (Table 1). Strikingly, the circulating miR that is upregulated the most in progressive cancer, miR-122-5p, is altered more than 22-fold. These findings indicate that serum miR expression is impacted during cancer progression which we further evaluate in human patients with PDAC.

a

PanIN-3

PDAC

b

Liver metastasis

Lung metastasis
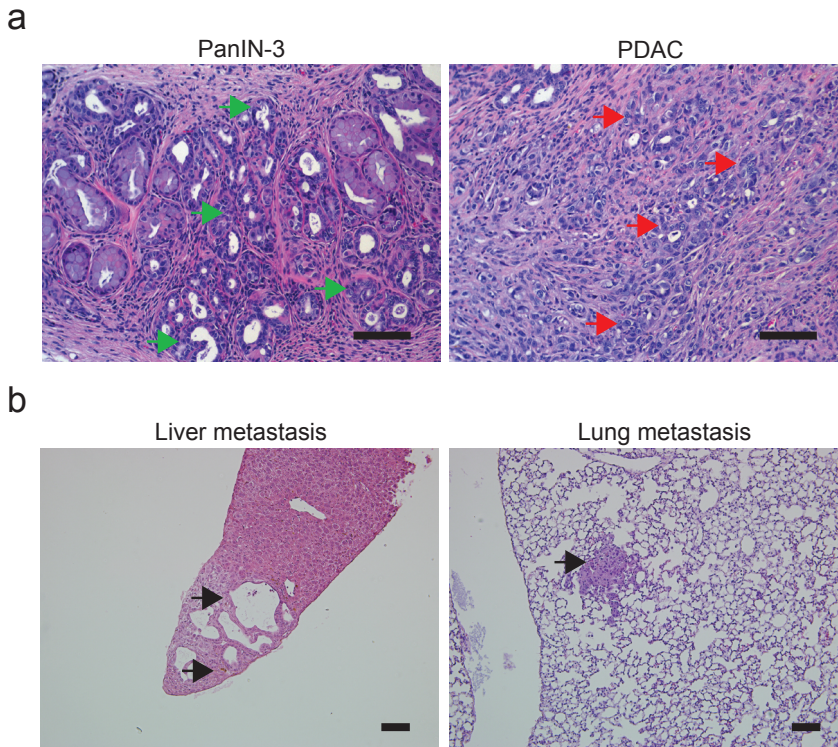
Figure 1. KPC mice with different stages of pancreatic neoplasia at the age of 5 months. (a) Images of formalin fixed, paraffin embedded (FFPE), H&E stained pancreatic tissues obtained from *LSL-Kras*[G12D/+]; *LSL-Trp53*[R172H/+]; *P48-Cre* (KPC) mice at the age of 5 months. PanIN-3 lesions are indicted by the green arrows, invasive pancreatic cancer is indicated by the red arrows. 20X magnification, scale bar = 100 μm. (b) Images of FFPE, H&E stained liver and lung tissues from KPC mice at the age of 5 months. Metastatic pancreatic cancer lesions are indicated by the black arrows. 10X magnification, scale bar = 100 μm.

Table 1. Differentially expressed serum miRs in KPC mice with pancreatic cancer metastases compared to mice with pre-invasive PanIN-3 lesions.

Serum miR	Fold down-regulation	Serum miR	Fold upregula-tion	Serum miR	Fold down-regulation	Serum miR	Fold upregula-tion
miR-15a-5p	-7.69	miR-122-5p	22.63	miR-25-3p	-3.45	miR-125a-5p	5.13
miR-451a	-7.69	miR-125b-5p	8.22	miR-93-5p	-3.33	miR-99a-5p	5.03
miR-15b-5p	-6.25	miR-133a	5.94	miR-16-5p	-3.23	Let-7b-3p	4.26
miR-142-3p	-5.88	miR-133b	5.82	miR-19a-3p	-3.23	miR-145-5p	3.86
miR-186-5p	-4.17	miR-10b-5p	5.28	miR-148b-3p	-3.13	miR-28-3p	3.46
miR-103a-3p	-3.85	miR-99b-5p	5.21	miR-20a-5p	-3.03	miR-143-3p	3.41
Let-7i-5p	-3.70	miR-365a-3p	5.17	miR-425-5p	-3.03		

Changes in serum miRs after tumor resection in patients with pancreatic cancer

Next, we analyzed pre- and post-pancreaticoduodenectomy serum from patients with resectable PDAC (n=28) who underwent surgery at the Erasmus Medical Center Rotterdam, in the Netherlands between 2013 and 2017. Patient characteristics are summarized in Table 2. Our aim was to assess the change in serum miR expression after surgery in patients with different progression free survival (PFS). In order to measure miR levels we used a novel technology that allows for exceptionally miR-specific and sensitive quantitative Real Time PCR [25]. The IDEAL assay from MiRXES is explained in Fig. 2a and utilizes miR-specific reverse transcription, as well as a combination of a miR-specific forward and reverse primer to detect and quantitate specific miRs. Details of the approach are shown in Fig. 2b. We initially profiled 250 miRs before and after primary tumor resection in 3 patients with PFS of 7, 11 or 18 months. The miRs that were measured in screen 1 are listed in Supplemental Table 1. From the 250 miRs, 190 were detected by qPCR and only 44 miRs were differentially altered after surgical tumor removal in the patients with different PFS. In a second cohort of PDAC patients (n=10), we measured the 44 informative miRs from screen 1, and an additional 12 miRs that were selected from the literature (Supplemental Table 2). We again compared the change in serum miR expression after surgery to the PFS. From this analysis, we found that 14 miRs can indicate disease progression after surgery. To test this in an indpendent third cohort of patients (n=15), we measured the levels of these 14 selected miRs (miR-122-5p, miR-125b-5p, miR-34a-5p, miR-99a-5p, miR-146b-5p, miR-154-5p, miR-379-5p, 193b-3p, miR-186-5p, miR-450a-5p, miR-301a-3p, miR-99b-5p, miR-181a-2-3p and miR-130a-3p) before and after surgery. When taking the miR measurements of all 28 pancreatic cancer patients together, we found that only miR-122-5p, miR-125b-5p and miR-99a-5p show a differential expression after surgery in patients with different PFS (Fig. 3a). Although the differential changes in expression of miR-122-5p, miR125b-5p and miR99a-5p did not reach statistical significance, these three miRs increase after tumor resection in patients who develop progressive cancer within 8 months, and decrease after tumor resection in patients who have a long PFS of more than 16 months (Fig. 3a). The Kaplan-Meier curves in Fig. 3b show post-surgery serum miR levels in relation to the progression free survival of the 28 patients that were analyzed. Despite the fact that miR-122-5p is upregulated 22-fold in KPC mice with metastatic disease, miR-122-5p is not differentially expressed in patients with short versus long PFS after surgery (Fig. 3b). On the other hand, patients with high serum levels of miR-125b-5p or miR-99a-5p after surgery have a significantly worse prognosis (Fig. 3b). In summary, we found that miR-125b-5p and miR-99a5p are prognostic circulating biomarkers in KPC mice and in patients with pancreatic cancer.

Table 2. Patient characteristics.

Patient ID	cohort	Disease stage	Serum time point [days]	PFS [months]	Progressive disease sites	OS [months]	Received therapy	Age [years]	Gender
001NT003 001NT005	1	resectable PDAC pT3N0 R0	pre surg post surg [11]	18.0	local; peritoneal	32.2	Whipple / adjuv gemcit / pall gemcit nab-paclitaxel	74	m
001PP011 001PP012	1	resectable PDAC pT3N1 R0	pre surg post surg [15]	6.5	local; lymph nodes	8.2	Whipple / adjuv gemcit	76	m
001NT017 001NT018	1	resectable PDAC pT3N1 R1	pre surg post surg [15]	10.9	local; osseous	14.5	Whipple / adjuv gemcit	73	f
001PP007 001PP008	2	resectable PDAC pT3N0 R0	pre surg post surg [15]	6.6	local; peritoneal	15.9	Whipple / adjuv gemcit	55	f
001PP009 001PP010	2	resectable PDAC pT3N1 R0	pre surg post surg [14]	7.1	peritoneal; lung	12.9	Whipple / adjuv gemcit	73	m
001PP036 001PP043	2	resectable PDAC pT3N1 R0	pre surg post surg [36]	5.0	liver	5.7	Whipple	71	f
001NT113 001NT118	2	resectable PDAC pT3N1 R0	pre surg post surg [27]	> 25.6		> 25.6	Whipple / adjuv gemcit	71	m
001PP048 001PP053	2	resectable PDAC pT3N1 R0	pre surg post surg [28]	29.6	local; lymph nodes; lung	>29.6	Whipple / adjuv gemcit	58	m
001NT115 001PP034	2	resectable PDAC pT3N1 R1	pre surg post surg [22]	5.23	local; liver	10.4	Whipple / adjuv gemcit	71	m
001PP041 001PP050	2	resectable PDAC pT3N1 R1	pre surg post surg [35]	> 30		> 30	Whipple / adjuv gemcit	74	m
001PP032 001PP039	2	resectable PDAC pT3N0 R0	pre surg post surg [30]	11.8	omental; liver; lung	31.5	Whipple / adjuv gemcit / pall FOLFIRINOX / IL1RAP inhibitor	60	m
001NT133 001NT137	2	resectable PDAC pT3N1 R1	pre surg post surg [25]	13.9	local; peritoneal; liver	16.6	Whipple / adjuv gemcit / pall FOLFIRINOX	59	m
001PP028 001PP030	2	resectable PDAC pT3N1 R0	pre surg post surg [22]	8.6	local; liver	15.1	Whipple / adjuv gemcit	78	f

Table 2. Patient characteristics. (continued)

Patient ID	cohort	Disease stage	Serum time point [days]	PFS [months]	Progressive disease sites	OS [months]	Received therapy	Age [years]	Gender
001PP072 001PP073	3	resectable PDAC pT3N0 R1	pre surg post surg [20]	12.1	liver	> 17	Whipple / adjuv gemcit	63	m
001PP077 001PP082	3	resectable PDAC pT3N1 R0	pre surg post surg [27]	> 16		> 16	Whipple / adjuv gemcit	51	m
001NT177 001NT183	3	resectable PDAC pT3N0 R1	pre surg post surg [22]	13.2	local; peritoneal; omental	15.1	Whipple / adjuv gemcit	69	m
001NT143 001NT148	3	resectable PDAC pT3N1 R1	pre surg post surg [27]	8.4	liver	16.9	Whipple / adjuv gemcit	72	m
001NT236 001NT245	3	resectable PDAC pT3N1 R1	pre surg post surg [26]	0.9	local; peritoneum; lungs; liver	2.1	Whipple / adjuv gemcit	72	f
001NT235 001NT246	3	resectable PDAC pT3N1 R1	pre surg post surg [29]	> 16		> 16	Whipple	84	m
001NT158 001NT161	3	resectable PDAC pT3N1 R1	pre surg post surg [48]	> 24		> 24	Whipple	87	f
001NT167 001NT173	3	resectable PDAC pT3N0 R1	pre surg post surg [27]	16.1	lungs; liver	> 23	Whipple / adjuv gemcit	73	m
001NT217 001NT223	3	resectable PDAC pT3N1 R0	pre surg post surg [26]	1.9	local; lymph node; liver	2.4	Whipple	68	m
001NT178 001NT187	3	resectable PDAC pT3N1 R0	pre surg post surg [22]	18.9	local; lymph node	> 18.9	Whipple / adjuv gemcit-capecit	70	m
001NT171 001NT175	3	resectable PDAC pT3N1 R1	pre surg post surg [31]	9.7	local; mesenteric; lungs; liver	> 9.7	Whipple / gemcit	73	m
001NT128 001NT134	3	resectable PDAC pT3N1 R1	pre surg post surg [34]	9.5	local; liver	16.2	Whipple / adjuv gemcit	55	m
001NT110 001NT121	3	resectable PDAC pT3N1 Rx	pre surg post surg [36]	16.0	local; liver	18.5	PPPD / adjuv gemcit	71	m

Table 2. Patient characteristics. (continued)

Patient ID	cohort	Disease stage	Serum time point [days]	PFS [months]	Progressive disease sites	OS [months]	Received therapy	Age [years]	Gender
001NT212 001NT221	3	resectable PDAC pT3N1 R1	pre surg post surg [36]	0.1	local; liver	4.3	PPPD / RT	84	m
001NT152 001NT156	3	resectable PDAC pT3N1 R1	pre surg post surg [34]	7.7	peritoneal; lymph node	8.2	Whipple	66	m

ID = identification; PDAC = pancreatic ductal adenocarcinoma; p = pathological; T = Tumor stage; No = lymph node metastases; N1= lymph node metastases; Ro = cancer free resection margins; R1 = cancer in resection margins; surg = surgery; PFS = progression free survival after surgery; OS = overall survival after surgery; RT = radiotherapy; Whipple = pancreaticoduodenectomy; PPPD = pylorus-preserving pancreaticoduodenectomy; adjuv = adjuvant; gemcit = gemcitabine; nab-paclitaxel = nanoparticle albumin-bound paclitaxel; IL1RAP = Interleukin 1 Receptor Accessory Protein; capecit = capecitabine; Age at time of surgery; m = male; f = female.
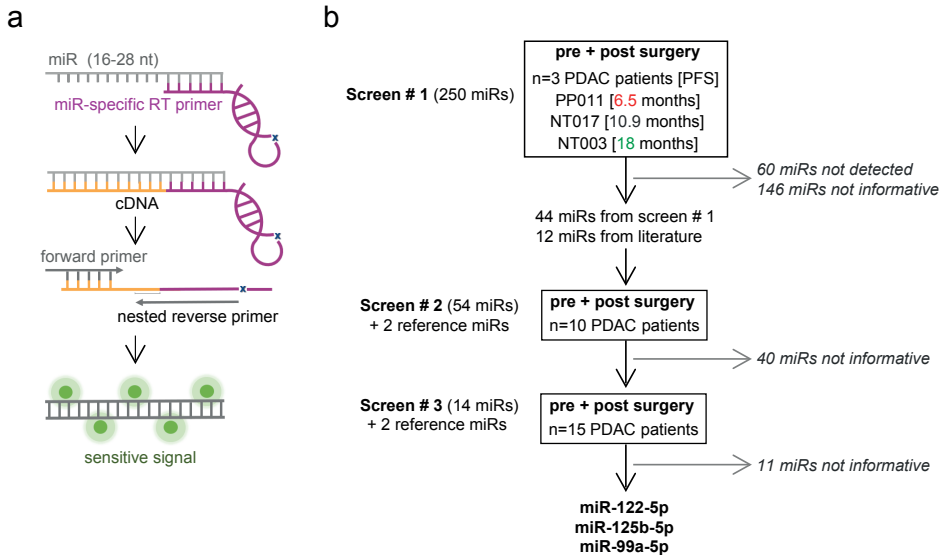
Figure 2. Analysis approach of prognostic miRs in the serum of patients with resectable pancreatic cancer. (a) Schematic of the IDEAL real time RT-PCR assay from MiRXES. MiR-specific reverse transcription (RT) and a miR-specific pair of forward and reverse primers lead to high specificity and sensitive PCR signals. miR = microRNA; nt = nucleotides; RT= reverse transcription; cDNA = complementary DNA. (b) Overview of performed serum miR analysis in patients with resectable pancreatic ductal adenocarcinoma (PDAC) to identify indicators of progression free survival (PFS) after surgical tumor removal.

MiR-125b-5p and miR-99a-5p are highly expressed in inflammatory cells in human resected pancreatic cancers

In order to assess the expression of miR-125b-5p and miR-99a-5p further, we analyzed the resected pancreatic cancer tissues by in situ hybridization (ISH) with DIG-labeled locked nucleic acid miR probes. The positive and negative controls for the ISH assays are shown in Supplemental Figure 2. MiR-125b-5p is expressed at low levels in the cytoplasm of normal acinar cells, as well as in a fraction of the PanIN cells (Fig. 4a). However, a small fraction of cells in the stroma surrounding the invasive cancer cells express high levels of miR-125b-5p (Fig. 4b). There is no difference in the number of miR-125b-5p-high stroma cells in tumors from patients with short versus long PFS. Insterestingly, the miR-125b-5p-high cells pertain in inflammatory cell aggregates in the tumor stroma and are located within clusters of CD79A positive cells (Fig. 4b), indicating that miR-125b-5p may play a role in B-lymphocyte/ plasma cell infiltration in pancreatic cancer stroma. MiR-99a-5p expressing cells are less abundant than miR-125b-5p positive cells in the pancreatic tumors. MiR-99a-5p positive cells are only present in limited regions of tumor stroma, specifically in muscular and connective tissue where pancreatic cancer cells invade into. Fig. 5 shows tumor regions with cells that express high levels of miR-99a-5p. In the centers of the pancreatic cancers
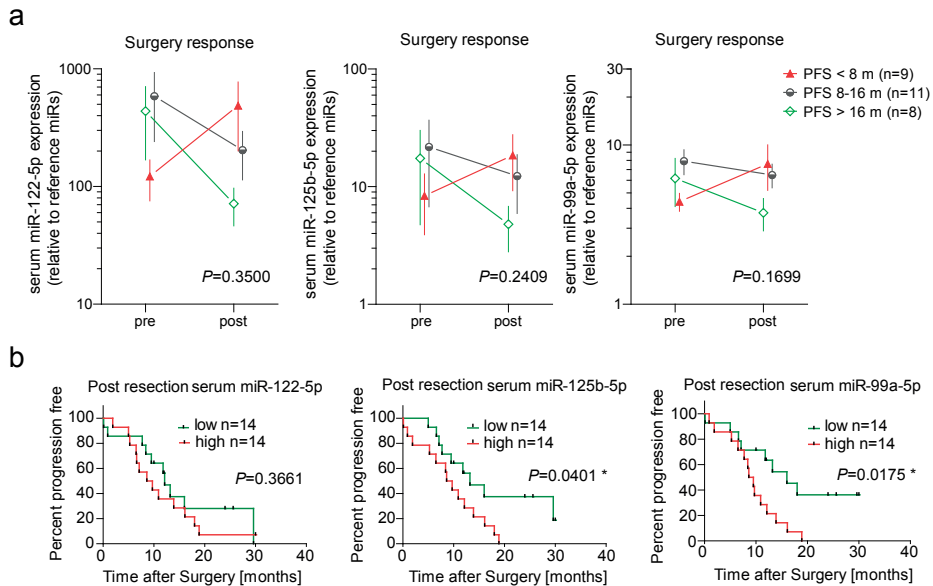
Figure 3. Expression levels of three serum miRs in pancreatic cancer patients with different outcomes. (a) Average expression levels of serum miRs 122-5p; 125b-5p or 99a-5p before and after surgery in 3 groups of patients with different progression free survival (PFS) duration. Serum miR values were normalized to the average expression of reference miR-29c-5p and miR-421 for each sample. Note the log scale of the Y-axis. Error bars are SEM, *P*-values by single factor ANOVA comparing the short (red) versus long (green) PFS patient groups. (b) Kaplan-Meier graphs of PFS for patients with increased or decreased serum miR-122-5p; 125b-5p or 99a-5p levels after surgical tumor removal. *P* values by Chi square (Logrank) test.

there are no cells that express miR-99a-5p. When comparing the location of CD79A positive cells in the adjacent tissue slides, we observed that the miR-99a-5p expressing inflammatory cells are in close proximity to cells of the B-cell lineage (Fig. 5).

In summary, we found that high expression of serum miR-125b-5p and miR-99a-5p is associated with pancreatic cancer progression in transgenic mice as well as in patients after surgical tumor removal. MiR-125b-5p as well as miR-99a-5p is highly expressed in a subset of inflammatory cells in the pancreatic tumor stroma, and are associated with cells from the B-lymphocyte lineage. The abundance of inflammatory cells expressing high levels of miR-125b-5p or miR-99a-5p in the tumor tissues was not different in patients with short versus long progression free survival.
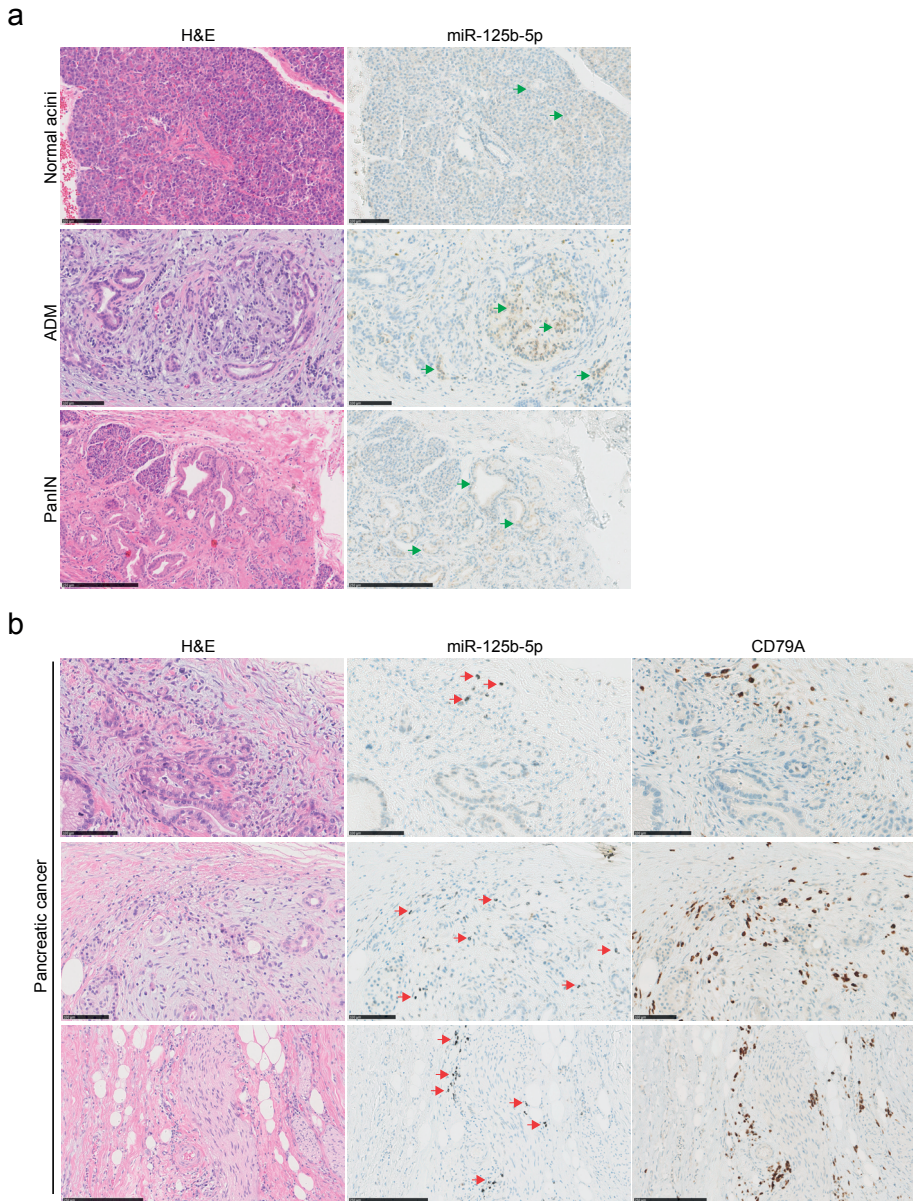
Figure 4. MiR-125b-5p detection by in situ hybridiation in pancreatic cancer tissues. Images of resected pancreas tissues from patients with pancreatic cancer. Consecutive FFPE tissue sections were stained with H&E or a DIG labeled miR-125b-5p probe. MiR-125b-5p expression is detected with silver resulting in brown/black staining, whereas nuclei are stained with Hematoxylin in blue. (a) Representative images of low expression of miR-125b-5p, (green arrows), in untransformed pancreatic acinar cells and cells that underwent acinar to ductal metaplasia (ADM) or pancreatic intraepithelial neoplasia (PanIN). (b) Representative images of cells in the tumor stroma with high expression of miR-125b-5p (red arrows). Corresponding tissue sections are stained with H&E and B-lymphocyte marker CD79A.
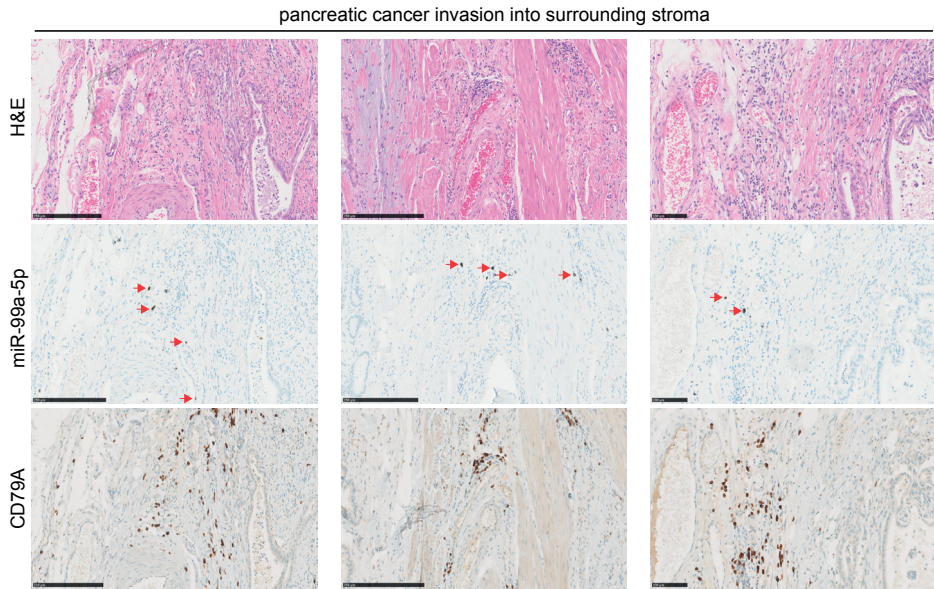
Figure 5. MiR-99a-5p detection by in situ hybridiation in pancreatic cancer tissues. Images of resected pancreas tissues from patients with pancreatic cancer. Consecutive FFPE tissue sections were stained with H&E or a DIG labeled miR-99a-5p probe, ora B-lymphocyte marker CD79A. Red arrows indicate miR-99a-5p expression, detected with silver resulting in brown/black staining, whereas cell nuclei are stained with Hematoxylin in blue.

DISCUSSION

Until now, approved non-invasive circulating biomarkers for the prognostication of patients with pancreatic cancer are lacking. Clinical follow up of pancreatic cancer patients in the Netherlands is not standardized [26] and currently consists of physical examination and at times radiographical imaging by CT scans which have a low performance in detecting early metastatic disease. Repeated blood draws followed by miR expression analysis that could stratify patients at higher risk for progressive disease and could prompt treatment adjustment would vastly improve patient care. MiRs are suitable candidates for the prediction of cancer progression due to their altered expression during tumorigenesis and their stability in the circulation[22].

Numerous studies have shown that circulating miRs are altered in early PDAC as well as in metastatic PDAC [27]. Zhou *et al.* showed that patients with early PDAC could be distinguished from healthy controls by the plasma upregulation of miR-122-5p; miR-125b-5p; miR-192-5p; miR 193b-3p; miR-122-3p and miR-27b-3p before treatment [14]. In contrast, they found that pre-treatment decreased miR-125b-5p was associated with worse OS. It was recently shown that increased serum expression of the miR-99 family is associated to

pancreatic cancer diagnosis [28]. Studies similar to these, which assess circulating miR levels for the diagnosis of PDAC are difficult to corroborate. Inconsistent results are due to interpatient diversity as well as technical differences in quantitation and data normalization [29].

Unfortunately, a subset of patients with PDAC that undergo primary tumor resection rapidly succumb to disease recurrence, whereas other patients have long progression free survival after surgery. Identifying the patients at risk for early disease recurrence could prompt adjustments in adjuvant treatment decisions and improve patient outcome. In the current study, we performed a prognostic miR biomarker analysis using serum samples of treatment-naïve, resectable PDAC patients. We profiled serum miR expression before and after surgery and compared the changes to the progression free survival of the patients. This comparison highlights the change in serum miR levels after removal of the primary cancer. The prognostic miRs identified in the patients were also indicative of PDAC metastases in the KPC mice, supporting their biologic importance for pancreatic cancer progression.

Genetically engineered mouse models of pancreatic cancer have led to major improvements in the understanding of PDAC development. Specifically, the *LSL-Kras*[G12D/+;] *LSL-Trp53*[R172H/+;] *P48-Cre* or KPC mice display progressive PDAC that mimics the features of the human disease [23]. KPC mice initially develop preinvasive acinar to ductal metaplasia (ADM) and pancreatic intraepithelial neoplasia (PanIN) lesions before widespread PDAC, all in the presence of an intact immune system. The median survival of KPC mice is 5 months and all mice succumb to the disease before the age of one year [23]. We performed a cross-species comparison of serum microRNA expression: the prognostic miRs we identified in the patients were also correlated to PDAC metastases in the KPC mice, confirming their importance in pancreatic cancer progression.

Circulating miRs that are associated with cancer presence often do not originate from cancer cells themselves. For example, miR-125b expression in colorectal liver and lung metastases is ~3 fold and ~7-fold higher in the stroma than in the cancer cells [30]. Indeed, the majority of circulating miRs are derived from blood cells and the endothelium [31,32]. PDAC progression goes hand in hand with alterations in systemic immune cell profiles [33] and this link between altered circulating miRs during cancer progression and immune cells was confirmed in our study. We found that miR-125b-5p and miR-99a-5p levels are soaring in cells that are closely associated to B-lymphocytes in the tumor stroma. Others have shown that miR-125b-5p is upregulated in B-lymphocytes [34] and can cause leukemia in mice [35,36]. In pancreatic tumors, high levels of infiltrating plasma cells are significantly correlated with worse prognosis in patients after surgery [37]. We found that after surgical tumor removal, patients with high levels of serum miR-125b-5p or miR-99a-5p

have shorter progression free survival. MiR-125b-5p and miR-99a-5p belong to the 20 most abundant miRs in human plasma exosomes [38], indicating that these miRs are actively packaged and released into the bloodstream. Circulating miRs are transferred from cell to cell and can elicit immune modulation [39]. MicroRNA-containing T-regulatory-cell-derived exosomes suppress pathogenic T helper 1 cells [40]. Serum miRs interact more with immune-related mRNA genes that with non-immune related genes [41]. A recent study showed that miR-125b-5p and miR-99a-5p both downregulate the activation of γδ T-lymphocytes and their cytotoxicity to lymphoma cells [42]. In humans and rats, treatment with methylprednisolone leads to increased plasma miR-99a-5p levels, suggesting miR-99a-5p is involved in systemic immune suppression [43]. Others have shown that miR-99a-5p inhibits the mammalian target of rapamycin (mTOR) signaling in bladder cancer cells [44], which was also described in gastric cancer tisues by Zhang et al. [45]. mTOR is not only an important cancer-related pathway, mTOR is also crucial for hematopoietic cell fate [46,47]. The differentiation of naïve T-cells into distinct effector T cells is promoted by mTOR [46]. In the absence of mTORC1 activity myeloid differentiation is impaired due to a block in glucose uptake and lipid metabolism [48]. Cell-free miR-99a-5p levels are high in the blood of patient with progressive pancreatic cancer, suggesting that the miR is produced at high levels by a subset of leukocytes, and can potentially be taken up by other cells, leading to the abrogation of mTOR among other pathways.

On the other hand, expression of miR-122-5p is liver specific and absent in most other tissues [49-51]. In the KPC mice with metastatic PDAC, miR-122-5p was upregulated 22-fold in comparison to mice with pre-invasive lesions. In the patients who underwent surgical tumor resection serum miR-122-5p levels went up after surgery in patients with early disease recurrence, however post-surgery serum miR-122-5p levels could not distinguish patients based on PFS, or based on the presence of liver metastases. This may suggest that liver damage is present at some level in all patients who undergo pancreaticoduodenectomy for pancreatic cancer.

There has been very little to no research that compares the levels of miRs after surgical removal of primary pancreatic cancers. In our study we compared serum miRs pre and post resection in treatment naïve patients that were operated at the Erasmus Medical Center between 2013 and 2017. Recently it became clear that patients with (borderline) resectable PDAC that undergo preoperative chemo/radiotherapy have a better survival [52,53]. From now on all patients with (borderline) resectable PDAC in the Netherlands will be offered to receive preoperative chemotherapy, if the performance status of the patient permits and the patient is willing to undergo systemic treatment. Chemotherapy has a vast impact on the immune landscape [54,55]. Whether serum miR-125b-5p and miR-99a-5p remains to be predictive of disease progression after surgery in pre-treated patients remains to be

evaluated. Therefore we are currently collecting blood samples to evaluate the changes in the serum miRs of patients with (borderline) resectable patients who undergo pre-operative FOLFIRINOX chemotherapy or gemcitabine/radiotherapy.

In summary, serum miR-125b-5p and miR-99a-5p levels are potential indicators of early disease recurrence after surgery in patients with pancreatic cancer and are likely originating from immune cells. Further dissection of the dynamics and functions of miR-125b-5p and miR-99a-5p in the immune response to pancreatic cancer will provide fundamental information to assist in the development of biomarkers and better immune therapies.

ACKNOWLEDGEMENTS

AUTHORS' CONTRIBUTIONS

AW, EEV. IP and CHJE conceived the project. IP and EEV performed the animal studies, MS led the patient care, blood collection and clinical data analyses, TPPB performed the in situ hybridization and immunohistochemistry. The histology was evaluated by pathologist JMK. IP analyzed the murine miR data, EEV analyzed the human miR data and EEV wrote the manuscript. IP, CHJE and MS contributed to edits of the manuscript. All authors reviewed and approved the manuscript.

DISCLOSURES

None of the authors have conflicts of interest to disclose.

Supplementary Table 1. List of miRs that were detected in screen # 1 in the serum of n=3 patients with resectable PDAC before and after surgical tumor resection.

let-7c-5p	let-7d-5p	miR-16-5p	miR-24-3p	miR-99a-5p	miR-150-5p
miR-196a-5p	miR-199a-5p	miR-199a-3p	miR-208a-3p	miR-215-5p	miR-223-3p
miR-200b-3p	miR-15b-5p	miR-27b-3p	miR-30b-5p	miR-125b-5p	miR-128-3p
miR-135a-5p	miR-152-3p	miR-153-3p	miR-191-5p	miR-23b-3p	miR-126-5p
miR-126-3p	miR-154-5p	miR-193a-3p	miR-194-5p	miR-302d-3p	miR-382-5p
miR-328-3p	miR-323a-3p	miR-326	miR-345-5p	miR-409-3p	miR-146b-5p
miR-495-3p	miR-497-5p	miR-518b	miR-92b-3p	miR-181a-2-3p	miR-144-5p
miR-29c-5p	miR-193b-5p	miR-532-3p	miR-885-5p	miR-301b-3p	miR-1246
miR-320d	miR-15a-5p	miR-19b-3p	miR-20a-5p	miR-26a-5p	miR-27a-3p
miR-28-5p	miR-98-5p	miR-29b-3p	miR-106a-5p	miR-192-5p	miR-129-5p
miR-30d-5p	miR-139-5p	miR-10a-5p	miR-181a-5p	miR-224-5p	miR-130a-3p
miR-142-3p	miR-9-3p	miR-125a-5p	miR-17-5p	miR-190a-5p	miR-195-5p
miR-200c-3p	miR-301a-3p	miR-99b-5p	miR-361-5p	miR-378a-5p	miR-330-3p
miR-337-3p	miR-324-3p	miR-338-3p	miR-425-3p	miR-429	miR-452-5p
miR-485-5p	miR-491-5p	miR-21-5p	miR-421	miR-181c-3p	miR-221-5p
miR-223-5p	miR-125a-3p	miR-219a-2-3p	miR-500a-5p	miR-374b-5p	miR-1271-5p
let-7f-5p	miR-19a-3p	miR-25-3p	miR-92a-3p	miR-95-3p	miR-96-5p
miR-10b-5p	miR-34a-5p	miR-103a-3p	miR-199b-5p	miR-122-5p	miR-132-3p
miR-133a-3p	miR-143-3p	miR-145-5p	miR-127-3p	miR-146a-5p	miR-185-5p
miR-186-5p	miR-188-5p	miR-29c-3p	miR-200a-3p	miR-130b-3p	miR-30e-5p
miR-30e-3p	miR-339-5p	miR-335-5p	miR-133b	miR-196b-5p	miR-20b-5p
miR-451a	miR-484	miR-486-5p	miR-193b-3p	miR-493-3p	miR-590-5p
miR-769-5p	miR-140-3p	miR-193a-5p	miR-34b-3p	miR-337-5p	miR-151a-5p
miR-423-5p	miR-616-3p	miR-628-5p	miR-874-3p	miR-1290	miR-1304-5p
let-7a-5p	let-7b-5p	miR-221-3p	miR-22-3p	miR-29a-3p	miR-30a-3p
miR-32-5p	miR-93-5p	miR-100-5p	miR-30c-5p	miR-183-5p	miR-204-5p
miR-205-5p	miR-219a-5p	miR-222-3p	miR-141-3p	miR-134-5p	miR-206
miR-320a	miR-106b-5p	miR-363-3p	miR-365a-3p	miR-370-3p	miR-375
miR-378a-3p	miR-379-5p	miR-151a-3p	miR-148b-3p	miR-324-5p	miR-450a-5p
miR-432-5p	miR-519c-3p	miR-503-5p	miR-539-5p	miR-487b-3p	miR-584-5p
miR-425-5p	miR-21-3p	miR-7-1-3p	miR-34a-3p	miR-106b-3p	miR-99b-3p
miR-362-3p	miR-342-5p	miR-589-5p	miR-1226-3p		

Supplementary Table 2. List of miRs that were measured in screen # 2 in the serum of n=10 patients with resectable PDAC before and after surgical tumor resection.

let-7d-5p	miR-144-5p	miR-28-5p	miR-375	miR-616-5p
let-7g-5p	miR-146b-5p	miR-29c-5p	miR-379-5p	miR-627-5p
let-7i-5p	miR-154-5p	miR-301a-3p	miR-421	miR-651-5p
miR-103a-3p	miR-154-5p	miR-302f	miR-450a-5p	miR-885-5p
miR-122-5p	miR-155-5p	miR-30e-3p	miR-454-3p	miR-9-3p
miR-1226-3p	miR-16-5p	miR-330-3p	miR-486-5p	miR-98-5p
miR-125b-5p	miR-181a-2-3p	miR-34a-3p	miR-491-5p	miR-99a-5p
miR-127-3p	miR-186-5p	miR-34a-5p	miR-493-3p	miR-99b-5p
miR-1285-3p	miR-18a-3p	miR-34b-3p	miR-495-3p	
miR-130a-3p	miR-191-5p	miR-363-3p	miR-584-5	
miR-135b-5p	miR-221-3p	miR-370-3p	miR-590-5p	
miR-140-3p	miR-22-3p	miR-374b-5p	miR-616-3p	

relative serum miR expression
[fold difference]

0.125 0.25 0.5 1 2 4 8 16 32

KPC mice with metastasis

serum miR

miR-122-5p — miR-125b-5p
miR-133a — miR-133b
miR-10b-5p — miR-99b-5p
miR-365a-3p — miR-125a-5p
miR-99a-5p — let-7b-3p
miR-145-5p
miR-28-3p
miR-143-3p
miR-1
miR-29c-3p
miR-126-3p
miR-200a-3p
miR-192-5p
miR-139-5p
miR-27b-3p
miR-215
miR-132-3p
miR-194-5p
miR-375
miR-150-5p
miR-574-3p
miR-152
miR-148a-3p
miR-342-3p
let-7d-3p
miR-193b-3p
miR-27a-3p
miR-324-5p
miR-30d-5p
miR-33a-5p
miR-29a-5p
miR-23b-3p
miR-195-5p
miR-29b-3p
miR-223-3p
miR-29a-3p
miR-24-3p
miR-532-5p
miR-378a-3p
miR-221-3p
miR-497-5p
miR-532-3p
miR-23a-3p
miR-30e-3p
miR-424-5p
miR-22-3p
miR-423-3p
miR-101-3p
miR-22-5p
miR-30a-5p
let-7b-5p
miR-21-5p
miR-146a-5p
miR-210
miR-141-3p
miR-151a-5p
miR-30b-5p
miR-181a-5p
miR-26a-5p
miR-320b
let-7a-5p
let-7c
miR-191-5p
miR-339-5p
miR-425-5p
miR-28-5p
miR-331
miR-130a-3p
miR-324-3p
miR-338-3p
miR-363-3p
miR-185-5p
miR-93-5p
miR-339-3p
let-7d-5p
let-7i-5p
miR-484
miR-652-3p
miR-326
miR-30c-5p
miR-320a
miR-205-5p
miR-20b-5p
miR-18a-5p
miR-92a-3p
miR-128
miR-130b-5p
miR-19b-3p
miR-200c-3p
miR-328
miR-142-5p
miR-423-5p
miR-18b-5p
miR-421
miR-26b-5p
miR-301a-3p
miR-106a-5p
miR-140-3p
miR-15b-3p
miR-140-5p
miR-222-3p
miR-486-5p
let-7g-5p
miR-296-5p
miR-30e-5p
miR-20a-5p — miR-425-5p
miR-148b-3p — miR-19a-3p
miR-16-5p — miR-93-5p
miR-25-3p — let-7i-5p
miR-103a-3p — miR-186-5p
miR-142-3p — miR-15b-5p
miR-15a-5p — miR-451a

Supplementary Figure 1. Relative expression levels of serum miRs in KPC mice with pancreatic cancer metastasis. Serum miRs from two groups of *LSL-Kras*[G12D/+]; *LSL-Trp53*[R172H/+]; *P48-Cre* (KPC) mice with different disease stage at the age of 5 months were analyzed. Serum from KPC animals with pancreatic cancer metastases (n=3 mice) was pooled and compared to pooled serum from n=3 mice with preinvasive PanIN-3 lesions. 155 microRNAs were detected by qPCR and expression levels were normalized to the median expression value per sample. MiRs that were differentially expressed > 3-fold are highlighted in red and green. Note the log scale for the Y-axis.
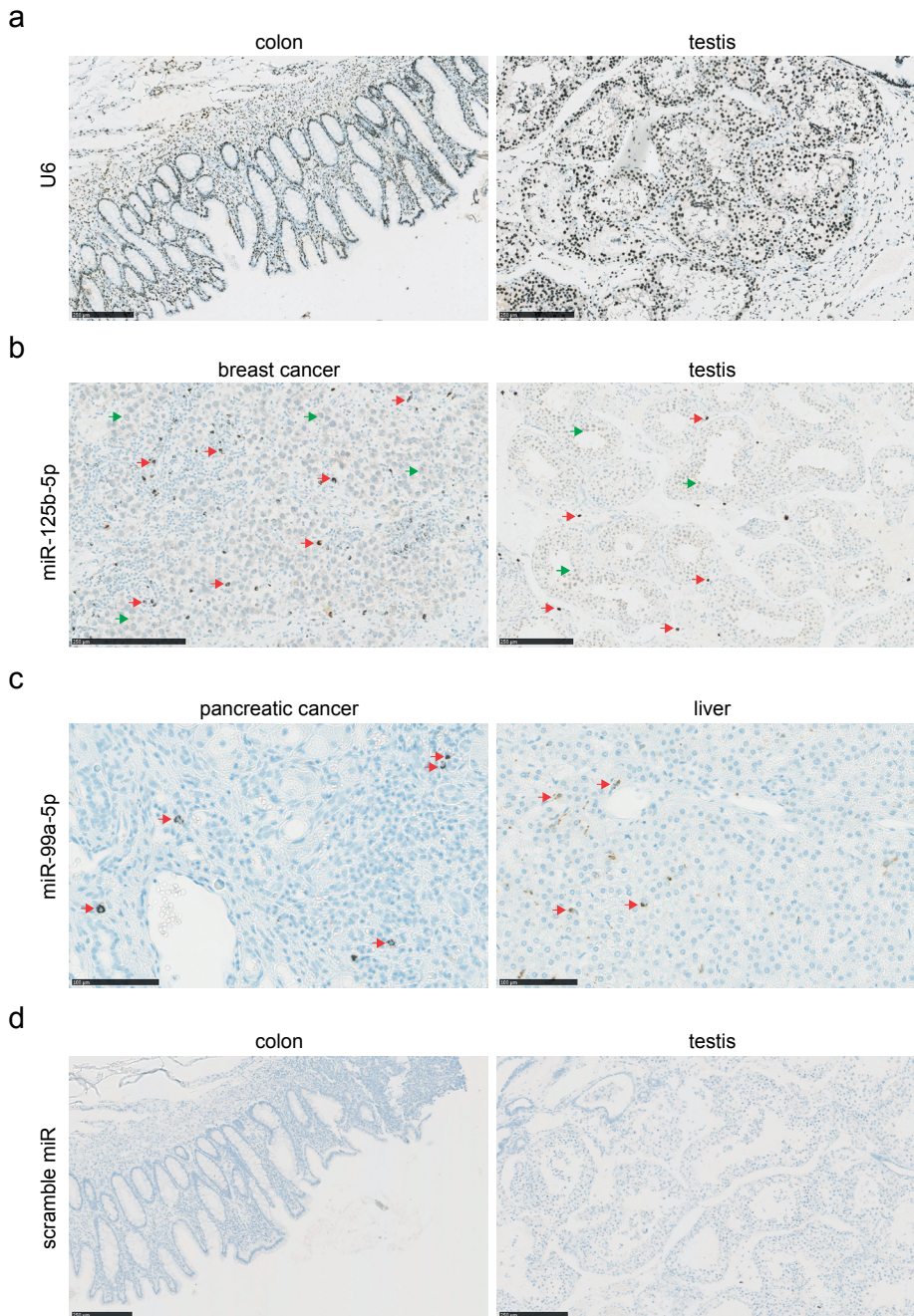
Supplementary Figure 2. MiR in situ hybridization (ISH) controls. Images of FFPE tissues that are stained with silver after in situ hybridization of dual-DIG labeled miR probes leading to brown/black staining. Nuclei are stained with Hematoxylin in blue. Scale bars = 250 μm. (a) U6 expression in human colon and testis tissue, serving as positive controls for the ISH assay. (b) MiR-125b-5p expression in

Her2Neu positive human breast cancer and human testis tissues. Note the distinct staining patterns in the breast cancer cells and Sertoli cells that have low miR-125b-5p expression (green arrows) versus the single cells in the stroma that have high expression (red arrows). (c) MiR-99a-5p expression in human pancreatic cancer and liver. Cells in the stroma with high levels of miR-99a-5p are indicated with the red arrows. (d) Scramble miR expression in human colon and testis tissues, which serves as a negative control for the ISH assay.

REFERENCES

1. Rahib, L., Smith, B. D., Aizenberg, R. et al. (2014) Projecting cancer incidence and deaths to 2030: the unexpected burden of thyroid, liver, and pancreas cancers in the United States. *Cancer Res* 74, 2913-2921

2. Stathis, A. & Moore, M. J. (2010) Advanced pancreatic carcinoma: current treatment and future challenges. *Nat Rev Clin Oncol* 7, 163-172

3. Luberice, K., Downs, D., Sadowitz, B. et al. (2017) Has survival improved following resection for pancreatic adenocarcinoma? *Am J Surg* 214, 341-346

4. van Rijssen, L. B., Koerkamp, B. G., Zwart, M. J. et al. (2017) Nationwide prospective audit of pancreatic surgery: design, accuracy, and outcomes of the Dutch Pancreatic Cancer Audit. *HPB* (Oxford) 19, 919-926

5. Conlon, K. C., Klimstra, D. S. & Brennan, M. F. (1996) Long-term survival after curative resection for pancreatic ductal adenocarcinoma. Clinicopathologic analysis of 5-year survivors. *Ann Surg* 223, 273-279

6. Mayo, S. C., Gilson, M. M., Herman, J. M. et al. (2012) Management of patients with pancreatic adenocarcinoma: national trends in patient selection, operative management, and use of adjuvant therapy. *J Am Coll Surg* 214, 33-45

7. Griffiths-Jones, S., Grocock, R. J., van Dongen, S. et al. (2006) miRBase: microRNA sequences, targets and gene nomenclature. *Nucleic Acids Res* 34, D140-144

8. Krol, J., Loedige, I. & Filipowicz, W. (2010) The widespread regulation of microRNA biogenesis, function and decay. *Nat Rev Genet* 11, 597-610

9. Chen, C. Z., Schaffert, S., Fragoso, R. et al. (2013) Regulation of immune responses and tolerance: the microRNA perspective. *Immunol Rev* 253, 112-128

10. Lu, L. F. & Liston, A. (2009) MicroRNA in the immune system, microRNA as an immune system. *Immunology* 127, 291-298

11. Lin, S. & Gregory, R. I. (2015) MicroRNA biogenesis pathways in cancer. *Nat Rev Cancer* 15, 321-333

12. Valadi, H., Ekstrom, K., Bossios, A. et al. (2007) Exosome-mediated transfer of mRNAs and microRNAs is a novel mechanism of genetic exchange between cells. *Nat Cell Biol* 9, 654-659

13. Kosaka, N., Iguchi, H., Yoshioka, Y. et al. (2010) Secretory mechanisms and intercellular transfer of microRNAs in living cells. *J Biol Chem* 285, 17442-17452

14. Zhou, X., Lu, Z., Wang, T. et al. (2018) Plasma miRNAs in diagnosis and prognosis of pancreatic cancer: A miRNA expression analysis. *Gene* 673, 181-193

15. Xu, J., Cao, Z., Liu, W. et al. (2016) Plasma miRNAs Effectively Distinguish Patients With Pancreatic Cancer From Controls: A Multicenter Study. *Ann Surg* 263, 1173-1179

16. Cao, Z., Liu, C., Xu, J. et al. (2016) Plasma microRNA panels to diagnose pancreatic cancer: Results from a multicenter study. *Oncotarget* 7, 41575-41583

17. Miyamae, M., Komatsu, S., Ichikawa, D. et al. (2015) Plasma microRNA profiles: identification of miR-744 as a novel diagnostic and prognostic biomarker in pancreatic cancer. *Br J Cancer* 113, 1467-1476

18. Ganepola, G. A., Rutledge, J. R., Suman, P. et al. (2014) Novel blood-based microRNA biomarker panel for early diagnosis of pancreatic cancer. *World J Gastrointest Oncol* 6, 22-33

19. Kawaguchi, T., Komatsu, S., Ichikawa, D. et al. (2016) Circulating MicroRNAs: A Next-Generation Clinical Biomarker for Digestive System Cancers. *Int J Mol Sci* 17

20. Schwarzenbach, H., Nishida, N., Calin, G. A. et al. (2014) Clinical relevance of circulating cell-free microRNAs in cancer. *Nat Rev Clin Oncol* 11, 145-156

21. Shivapurkar, N., Vietsch, E. E., Carney, E. et al. (2017) Circulating microRNAs in patients with hormone receptor-positive, metastatic breast cancer treated with dovitinib. *Clin Transl Med* 6, 37

22. Rapisuwon, S., Vietsch, E. E. & Wellstein, A. (2016) Circulating biomarkers to monitor cancer progression and treatment. *Comput Struct Biotechnol J* 14, 211-222

23. Hingorani, S. R., Wang, L., Multani, A. S. et al. (2005) Trp53R172H and KrasG12D cooperate to promote chromosomal instability and widely metastatic pancreatic ductal adenocarcinoma in mice. *Cancer Cell* 7, 469-483

24. Mestdagh, P., Van Vlierberghe, P., De Weer, A. et al. (2009) A novel and universal method for microRNA RT-qPCR data normalization. *Genome Biol* 10, R64

25. Wan, G., Lim, Q. E. & Too, H. P. (2010) High-performance quantification of mature microRNAs by real-time RT-PCR using deoxyuridine-incorporated oligonucleotides and hemi-nested primers. *Rna* 16, 1436-1445

26. Groot, V. P., Daamen, L. A., Hagendoorn, J. et al. (2017) Current Strategies for Detection and Treatment of Recurrence of Pancreatic Ductal Adenocarcinoma After Resection: A Nationwide Survey. *Pancreas* 46, e73-e75

27. Wei, L., Yao, K., Gan, S. et al. (2018) Clinical utilization of serum- or plasma-based miRNAs as early detection biomarkers for pancreatic cancer: A meta-analysis up to now. *Medicine* (Baltimore) 97, e12132

28. Stroese, A. J., Ullerich, H., Koehler, G. et al. (2018) Circulating microRNA-99 family as liquid biopsy marker in pancreatic adenocarcinoma. *J Cancer Res Clin Oncol* Sep 17

29. Jarry, J., Schadendorf, D., Greenwood, C. et al. (2014) The validity of circulating microRNAs in oncology: five years of challenges and contradictions. *Mol Oncol* 8, 819-829

30. Pecqueux, M., Liebetrau, I., Werft, W. et al. (2016) A Comprehensive MicroRNA Expression Profile of Liver and Lung Metastases of Colorectal Cancer with Their Corresponding Host Tissue and Its Prognostic Impact on Survival. *Int J Mol Sci* 17

31. Pritchard, C. C., Kroh, E., Wood, B. et al. (2012) Blood cell origin of circulating microRNAs: a cautionary note for cancer biomarker studies. *Cancer Prev Res (Phila)* 5, 492-497

32. Williams, Z., Ben-Dov, I. Z., Elias, R. et al. (2013) Comprehensive profiling of circulating microRNA via small RNA sequencing of cDNA libraries reveals biomarker potential and limitations. *Proc Natl Acad Sci U S A* 110, 4255-4260

33. Aziz, M. H., Sideras, K., Aziz, N. A. et al. (2018) The Systemic-Immune-Inflammation Index Independently Predicts Survival and Recurrence in Resectable Pancreatic Cancer and its Prognostic Value Depends on Bilirubin Levels: A Retrospective Multicenter Cohort Study. *Ann Surg* Jan 12

34. Malumbres, R., Sarosiek, K. A., Cubedo, E. et al. (2009) Differentiation stage-specific expression of microRNAs in B lymphocytes and diffuse large B-cell lymphomas. *Blood* 113, 3754-3764

35. Bousquet, M., Harris, M. H., Zhou, B. et al. (2010) MicroRNA miR-125b causes leukemia. *Proc Natl Acad Sci U S A* 107, 21558-21563

36. Ooi, A. G., Sahoo, D., Adorno, M. et al. (2010) MicroRNA-125b expands hematopoietic stem cells and enriches for the lymphoid-balanced and lymphoid-biased subsets. *Proc Natl Acad Sci U S A* 107, 21505-21510

37. Liu, Q., Niu, Z., Li, Y. et al. (2016) Immunoglobulin G4 (IgG4)-positive plasma cell infiltration is associated with the clinicopathologic traits and prognosis of pancreatic cancer after curative resection. *Cancer Immunol Immunother* 65, 931-940

38. Huang, X., Yuan, T., Tschannen, M. et al. (2013) Characterization of human plasma-derived exosomal RNAs by deep sequencing. *BMC Genomics* 14, 319

39.   Okoye, I. S., Coomes, S. M., Pelly, V. S. et al. (2014) MicroRNA-containing T-regulatory-cell-derived exosomes suppress pathogenic T helper 1 cells. *Immunity* 41, 89-103

40.   Mittelbrunn, M., Gutierrez-Vazquez, C., Villarroya-Beltri, C. et al. (2011) Unidirectional transfer of microRNA-loaded exosomes from T cells to antigen-presenting cells. *Nat Commun* 2, 282

41.   Nosirov, B., Billaud, J., Vandenbon, A. et al. (2017) Mapping circulating serum miRNAs to their immune-related target mRNAs. *Adv Appl Bioinform Chem* 10, 1-9

42.   Zhu, Y., Zhang, S., Li, Z. et al. (2018) miR-125b-5p and miR-99a-5p downregulate human gammad-elta T-cell activation and cytotoxicity. *Cell Mol Immunol* 2, 12

43.   Li, Z., Jiang, C., Ye, C. et al. (2018) miR-10a-5p, miR-99a-5p and miR-21-5p are steroid-responsive circulating microRNAs. *Am J Transl Res* 10, 1490-1497

44.   Tsai, T. F., Lin, J. F., Chou, K. Y. et al. (2018) miR-99a-5p acts as tumor suppressor via targeting to mTOR and enhances RAD001-induced apoptosis in human urinary bladder urothelial carcinoma cells. *Onco Targets Ther* 11, 239-252

45.   Zhang, C., Zhang, C. D., Ma, M. H. et al. (2018) Three-microRNA signature identified by bioinfor-matics analysis predicts prognosis of gastric cancer patients. *World J Gastroenterol* 24, 1206-1215

46.   Liu, Y., Zhang, D. T. & Liu, X. G. (2015) mTOR signaling in T cell immunity and autoimmunity. *Int Rev Immunol* 34, 50-66

47.   Malik, N., Sansom, O. J. & Michie, A. M. (2018) The role of mTOR-mediated signals during haemo-poiesis and lineage commitment. *Biochem Soc Trans* 8, 28

48.   Karmaus, P. W. F., Herrada, A. A., Guy, C. et al. (2017) Critical roles of mTORC1 signaling and metabolic reprogramming for M-CSF-mediated myelopoiesis. *J Exp Med* 214, 2629-2647

49.   Ward, J., Kanchagar, C., Veksler-Lublinsky, I. et al. (2014) Circulating microRNA profiles in human patients with acetaminophen hepatotoxicity or ischemic hepatitis. *Proc Natl Acad Sci U S A* 111, 12169-12174

50.   Jopling, C. (2012) Liver-specific microRNA-122: Biogenesis and function. *RNA Biol* 9, 137-142

51.   Ludwig, N., Leidinger, P., Becker, K. et al. (2016) Distribution of miRNA expression across human tissues. *Nucleic Acids Res* 44, 3865-3877

52.   Versteijne, E., Vogel, J. A., Besselink, M. G. et al. (2018) Meta-analysis comparing upfront surgery with neoadjuvant treatment in patients with resectable or borderline resectable pancreatic cancer. *Br J Surg* 105, 946-958

53.   Jang, J. Y., Han, Y., Lee, H. et al. (2018) Oncological Benefits of Neoadjuvant Chemoradiation With Gemcitabine Versus Upfront Surgery in Patients With Borderline Resectable Pancreatic Cancer: A Prospective, Randomized, Open-label, Multicenter Phase 2/3 Trial. *Ann Surg* 268, 215-222

54.   Liu, Q., Liao, Q. & Zhao, Y. (2017) Chemotherapy and tumor microenvironment of pancreatic cancer. *Cancer Cell Int* 17, 68

55.   Plate, J. M., Plate, A. E., Shott, S. et al. (2005) Effect of gemcitabine on immune cells in subjects with adenocarcinoma of the pancreas. *Cancer Immunol Immunother* 54, 915-925

CHAPTER 5

Circulating microRNAs in patients with hormone receptor-positive, metastatic breast cancer treated with dovitinib

Narayan Shivapurkar [1]*
Eveline E. Vietsch[1]*
Erin Carney[1]
Claudine Isaacs[1]
Anton Wellstein[1]

1 Department of Oncology, Lombardi Comprehensive Cancer Center, Georgetown University, 3970 Reservoir Road NW, Washington, DC, 20057, USA.

* these authors contributed equally to this work

ABSTRACT

Serial analysis of biomarkers in the circulation of patients undergoing treatment ("liquid biopsies") can provide new insights into drug effects. In particular the analysis of cell-free, circulating nucleic acids such as microRNAs (miRs) can reveal altered expression patterns indicative of mechanism of drug action, cancer growth, and tumor-stroma interactions. Here we analyzed plasma miRs in patients with hormone receptor positive, metastatic breast cancer with prior disease progression during aromatase inhibitor therapy (n = 8) in a phase I/II trial with the multiple tyrosine kinase inhibitor dovitinib (TKI258). Plasma miR levels were measured by quantitative RT-qPCR before and after treatment with dovitinib. A candidate miR signature of drug response was established from a 379 miR screen for detectable plasma miRs as well as from the published literature. Changes in miR expression patterns and tumor sizes were compared. In this analysis we identified miR-21-5p, miR-100-5p, miR-125b-5p, miR-126-3p, miR-375 and miR-424-5p as potential indicators of a response to dovitinib. The altered expression patterns observed for the six circulating miRs separated patients with resistant disease from those with drug responsive disease. There was no relationship between adverse effects of dovitinib treatment and identifiable changes in miR patterns. We conclude that changes in the expression patterns of circulating miRs can be indicators of drug responses that merit prospective studies for validation.

INTRODUCTION

One of the hallmarks of cancer is the oncogenic activation of receptor tyrosine kinases (RTKs) that control cell growth and survival [1-3]. In addition to the autocrine cancer cell-autonomous effects, RTKs mediate the paracrine crosstalk between tumor cells and host stroma that controls fibrosis, tumor angiogenesis and the immune environment [4-8]. Thus, small molecule kinase inhibitors or antibodies that target ligands or receptors have become a mainstay of RTK targeted cancer therapy.

A recently added kinase inhibitor is dovitinib (TKI258 or CHIR-258), an orally available inhibitor of multiple RTKs that include FGFR1, FGFR3, VEGFR, KIT, and PDGFRβ with IC50 values < 30 nmol/L [9]. Integrated analysis of clinical and preclinical studies indicates that inhibition of FGFR signaling by dovitinib disrupts the paracrine interaction between prostate cancer and stromal cells and thus mediates the antitumor effect [10]. In some men with metastatic prostate cancer, dovitinib treatment led to improvements in bone scans and lymphadenopathy [10]. Furthermore, in pretreated patients with metastatic renal cell carcinoma, dovitinib showed significant antitumor activity in a phase-I study [11]. More-over, in patients with metastatic renal cell carcinoma that were previously treated with a VEGFR tyrosine kinase inhibitor and an mTOR inhibitor, dovitinib treatment resulted in two partial responses (3.6%) and 29 stable diseases (52.7%) in a phase-II setting [12]. In a phase I/II and pharmacodynamic study in patients with advanced melanoma dovitinib was found to decrease levels of soluble VEGFR2 in plasma, consistent with FGFR and VEGFR inhibition [13]. Additionally, melanoma patients showed dose dependent changes in the vascularity of liver metastases after 2 days of dovitinib treatment [13]. Finally, in patients with breast cancer dovitinib showed more antitumor activity in tumors with high levels of FGFR1 amplification. In the FGFR1-amplified breast cancer group, a 20.2% reduction in tumor size was found after dovitinib but no reduction in tumors with less than six copies of FGFR1 [14].

Blood based molecular analyses ("liquid biopsies") are used for serial monitoring of cancer progression as well as the response to treatment [15]. Here we focus on the analysis of microRNAs (miRs) in the circulation, which are transcribed, processed, packaged and released from cells in normal and in diseased tissues as part of the local and at-a-distance cellular crosstalk [16,17]. Distinct alterations in circulating miRs can reflect dysregulation of cell proliferation, immunity and stromal interactions. As shown in numerous studies, circulating miRs can serve as predictors of cancer outcome [18-22] and may allow for a real-time assessment of treatment responses after surgical resection [23], chemotherapy [24-27] or pathway targeted therapy [28]. Drug treatment impacts both cancerous lesions and the host tissues. Therefore, changing patterns of miRs in the circulation should reflect the impact of

the treatment on the cancer lesion as well as the host organism and makes circulating miRs suitable biomarkers [15].

Here we analyzed cell-free miRs in the plasma of breast cancer patients in a phase I/II trial of dovitinib. We hypothesized that changes in circulating miR patterns can indicate dovitinib treatment responses, resistance to treatment, or adverse effects.

MATERIAL AND METHODS

Patient eligibility

Post-menopausal women with hormone receptor positive, HER2 negative metastatic breast cancer 18 years or older were included in this phase I/II open-label single arm trial evaluated dovitinib in combination with an aromatase inhibitor (AI), i.e. anastrozole, exemestane or letrozole. Index tumors had to be 10 mm or greater on a CT scan and had previously been sensitive to endocrine therapy followed by disease progression after > 2 years of adjuvant endocrine therapy. At entry into the study evidence of disease resistance to an AI, defined as documented disease progression while receiving an AI, or development of disease recurrence < 6 months after completing adjuvant therapy with an AI. Patients had to have a good performance status (eastern Cooperative Group 0–1), adequate organ function and had to have life expectancy of > 3 months. All patients gave written consent for the clinical trial protocol that had been approved by the IRB at Medstar Georgetown University Hospital (IRB #2010-535). The trial is registered at clinicaltrials.gov as NCT01484041.

Study design and treatment

Dovitinib was given at an oral dose of 500 mg daily 5 days on/2 days off in combination with the standard dose of AI (either anastrozole 1 mg daily, exemestane 25 mg daily, or letrozole 2.5 mg daily). One treatment cycle was defined as 4 weeks. After each cycle, peripheral venous blood samples were collected and after removal of personal identifiers plasma was separated and stored at – 80 °C until further processing. For the phase I portion of the study, if more than 2 dose-limiting-toxicities (DLT) were seen in the first 6 subjects, the dose of dovitinib was reduced to 400 mg daily 5 days on/2 days off in combination with the fixed dose of AI. Eventually 3 subjects remained on the initial dose of 500 mg and dose de-escalation was performed for 9 patients that were treated at 400 mg after the first cycle. Tumor responses to treatment with dovitinib were evaluated every 2 cycles (8 weeks) as determined by CT scans of patients' index lesions. The trial was stopped after 12 patients had enrolled when the decision was made to discontinue development of dovitinib. Plasma samples before and after treatment were collected for only 8 out of 12 patients due to early exit from the study by 2 patients, and logistical difficulties.

Circulating miR analysis

Plasma miR extraction and RT-qPCR analysis was conducted as previously reported [22,29]. Briefly, two replicates of 170 μL of plasma were thawed, mixed with 5 volumes of Qiazol lysis reagent and vortexed. For one patient, 500 μL plasma pre and post treatment was used to extract miRs for a broader analysis of 379 miRs in an array format. The miRs were extracted with chloroform and the aqueous phase was further processed using the miRNeasy Mini kit (Qiagen, Valencia, CA). MiRs were converted to cDNA using the miScript II RT kit (Qiagen Valencia, CA, cat. # 218160). This kit contains a miScript HiSpec buffer MiR to enable either mature miRNA profiling (using miScript miRNA PCR Arrays) or mature miRNA quantification using individual miScript Primer Assays. In this reverse transcription reaction with miScript HiSpec Buffer, mature miRNAs are polyadenylated by poly(A) polymerase and converted into cDNA by reverse transcriptase with oligo-dT priming. The cDNA is then used for real-time PCR quantification of mature miRNA expression. MiR expression was quantified by qRT-PCR, using the SYBR green PCR Master mixture (Qiagen cat. # 218073) in an ABI7900HT Real-Time PCR system using (Applied Biosystems, Foster City, CA) with 95 °C for 15 min followed by 40 cycles (94 °C for 15 s, 55 °C for 30 s and 72 °C for 30 s) followed by a melting curve step to evaluate specificity of amplification. A broad miR expression array (379 miRs + U6) was performed for global miR profiling using one randomly selected patient (# 101) that required 500 μL plasma at baseline and post dovitinib treatment (Qiagen Valencia, CA). The miR expression values from the array were normalized to the mean expression level of all miRs in the respective sample, to adjust for the different quality of RNA preservation and extraction. MiR specific primers were used for the panel of six miRs selected for further study (Qiagen Valencia, CA). Expression values were calculated using the comparative Ct method. Levels of a panel of six selected signature of miRs were measured in the plasma of eight patients before and after treatment and normalized to U6 levels [30,31]. The data was processed with Prism 5.0 Graphpad software for t test analysis and the display of data. Reproducibility of the miRNA assays within and across studies supports that these assays are specific for mature miRNAs, as also claimed by the manufacturer.

Statistical analysis

Principal component analysis (PCA) and the agglomerative hierarchical clustering were performed with the miR measurements from all 8 patients and included the levels of the selected six miRs before and after treatment. The XLSTAT Version 2014.6.01 from Addinsoft was used for these analyses. From the PCA and clustering of the miR measurements, distinct patterns of patients' responses to the drug treatment were visualized and patients were assigned to distinct response groups. The investigators performing the miR panel selection, and the PCA-based assignment of patients to treatment response groups were blinded to the clinical outcomes and the measurements of tumor sizes during the trial.

Expression level changes of the six selected miRs between groups of patients based on their response to dovitinib were compared to baseline levels in Prism Graphpad Version 5.03 by using unpaired Student *t*-test.

RESULTS

Patients undergoing dovitinib treatment

Out of the 12 patients enrolled in the trial, 6 patients came off study for disease progression, 4 patients for toxicity, and 2 patients chose to discontinue treatment. Patient enrollment stopped after the 12th patient due to limited clinical benefits and the company's strategic decision not to develop the drug further. Sufficient amounts and quality of pre- and post-treatment plasma samples for miR analysis were available from 8 of 12 patients. The comparative miR analysis was done with the pre-treatment and the earliest available plasma sample after initiation of dovitinib treatment. For 2 out of 8 patients blood samples were not collected after the first cycle of dovitinib (patients 101, 301), therefore miRs were analyzed after the second cycle of dovitinib for these patients.

The clinical characteristics of the 8 patients studied as well as their treatments and adverse effects are compiled in Table 1. Baseline index tumor size of target lesions before dovitinib treatment, obtained from the computerized tomography (CT) measurements are shown in Fig. 1a. The change in tumor sizes over the course of dovitinib treatment is shown in Fig. 1b. Tumor responses after 8 weeks of treatment were not correlated with tumor sizes at baseline. The change in index tumor size based on the CT measurements after 8 weeks of treatment were used to separate patients into subgroups, i.e. tumors that had increased in size by more than 8% (n = 3; red symbols), decreased in size by more than 8% (n = 3; green symbols), and those that were not changed (n = 2; grey symbols) relative to baseline.

Selection of circulating microRNAs impacted by dovitinib treatment

We followed the approach and rationale of our recent study on the selection of a panel of circulating miRs in patient samples [22]: Six miRs were selected based on the following criteria in order of priority: (a) abundance of the miR: Measurable levels in the plasma before and after treatment; (b) references in the published literature that relate the respective miR to breast cancer and/or to FGF, VEGF or PDGF signaling, i.e. the pathways targeted by dovitinib; (c) detectable change relative to dovitinib treatment by at least threefold up or down. The workflow of the miR analysis is shown in Fig. 1c. To support the selection of a small panel of miRs, a screen for 379 miRs and U6 was run on paired plasma samples that were obtained before and after treatment of a patient that was randomly selected and also contained sufficient amounts of U6 for the assay. In this qRT-PCR based miR expression array, 135 of 379 miRs were detectable above the threshold expression level in samples

Table 1. Patients with hormone positive metastatic breast cancer treated with dovitinib.

pt #	age	index lesion tumor size at baseline	aromatase inhibitor	total # cycles of dovitinib	dovitinib dose	AE after first cycle	change in tumor size after 8 w dovitinib	sites of metastases
001	61	6.5 cm	Exemestane	6	500 mg	fatigue GI: nausea, dry mouth Neuromusc: myalgia, dizziness	- 9.23%	lymph nodes, bone, skin/soft tissue
002	32	15 cm	Anastrozole	1	500 mg	fatigue GI: nausea, vomiting, diarrhea, dehydration, poor appetite, Neuromusc: headaches, blurred vision, lightheadedness, Liver: ALP↑	+ 6.0%	lymph nodes, lung, bone
004	65	2.9 cm	Letrozole	2	400 mg	fatigue, hypertension, bone pain, GI: anorexia, nausea, dyspepsia	+ 24.14%	lung, liver
005	58	5.7 cm	Exemestane	3	400 mg	fatigue, GI:, nausea, vomiting, anorexia, dysgeusia, Neuromusc: muscle weakness Liver: ALP↑ , AST↑	+ 24.56%	lymph nodes, soft tissue, liver
101	64	1 cm	Anastrozole	4	500 mg	serum amylase↑, creatine↑, magnesium↑ Liver: GGT↑	- 30.0%	lymph nodes, bone
102	57	4.8 cm	Letrozole	2	400 mg	GI: nausea, Liver: GGT↑	0%	lymph nodes, bone
103	52	13.1 cm	Anastrozole	7	400 mg	GI: diarrhea, Neuromusc: backpain, Liver: GGT↑, ALT↑, ALP↑	- 21.37%	lymph nodes, bone, pleura, liver
301	51	1 cm	Letrozole	3	400 mg	hypokalemia GI: diarrhea, dyspepsia Neuromusc: arthralgia, Liver: triglycerides↑, ALT↑, ALP↑, GGT↑ Anemia, Cholesterol↑	+ 10%	lung

pt, patient; cm, centimeter; mg, milligram; AE, adverse events; GI, gastro-intestinal; Neuromusc, neu-romuscular; PD, progressive disease;
ALP, alkaline phosphatase; ALT, alanine aminotransferase; GGT, gamma-glutamyl transpeptidase; AST, aspartate aminotransferase; w, weeks.

collected before and after dovitinib treatment (Additional file 1: Table S1). After data nor-malization using the mean expression value of all miRs detectable in the respective samples, 60 miRs showed a down-regulation and 33 miRs an upregulation of at least threefold after

the treatment. Six circulating miRs i.e. miR-21-5p, miR-100-5p, miR-125b-5p, miR-126-3p, miR-375 and miR-424-5p were selected based on the three criteria that were outlined above. The expression of the 6 miRs was then measured by qRT-PCR before and after dovitinib in all patients. The change in expression after treatment relative to baseline is shown in Fig. 2. A > 100-fold concentration range of these six miRs was found in the circulation of the patients. The response to dovitinib was distinct amongst patients indicating differential drug effects between patients.
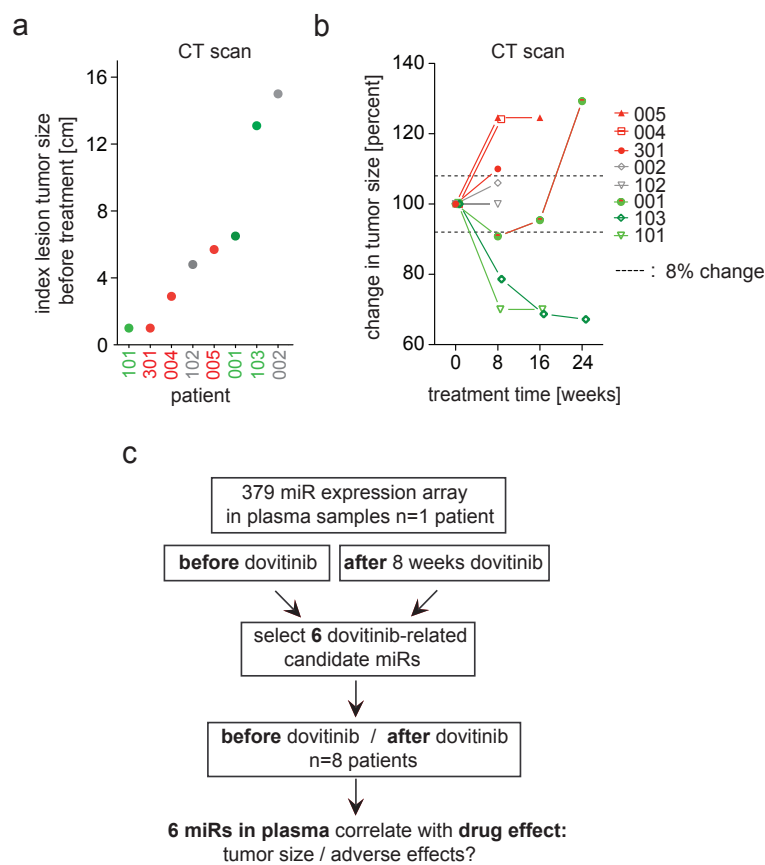
Figure 1. Breast cancer lesion sizes, treatment responses and design of the miR analysis.
a. Patient numbers are color coded to indicate changes in tumor sizes after 8 weeks of treatment (red = increase, green = decrease, grey = no change). The sizes of the index lesions were measured by CT before treatment with dovitinib (baseline).
b. Change in tumor size of the index lesion during the course of dovitinib treatment.
c. Flow chart of plasma miR analysis design. From a genome wide miR expression array with samples collected before and after dovitinib treatment in a single patient, 6 signature miRs were selected and tested for their indication of a dovitinib response in 8 patients. Further criteria for selection of the miRs are provided in the 'Results' section.
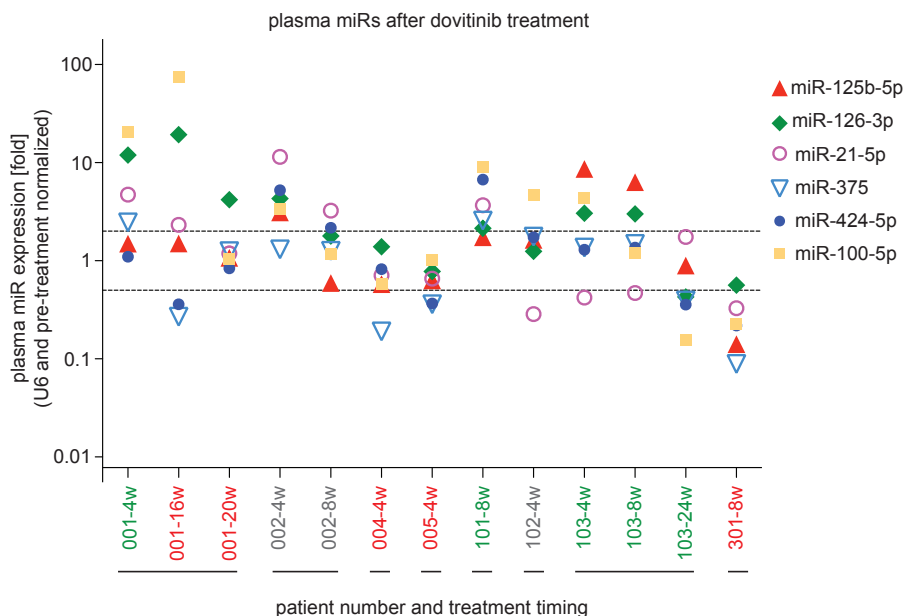
Figure 2. Effect of dovitinib treatment on plasma miR levels of patients with metastatic breast cancer. MiRs were measured in plasma samples of patients collected before and after dovitinib treatment. The change in expression levels of six miRs relative to U6 in eight patients at different treatment times (in weeks; w) is shown. The dashed lines indicate two fold up- or down-regulation of miR expression levels after treatment. The numbers on the x-axis indicate the patients. The color code of patients indicates changes in tumor sizes during treatment (red = increase, green = decrease, grey = no change).

Plasma miR levels as indicators of response to dovitinib treatment

To evaluate whether the circulating miRs could indicate patient's responses based on the change in expression after dovitinib, we used principal component analyses (PCA) and clustering analysis. The PCA in Fig. 3a indicates the pattern changes per patient changes based on the miR levels before and after the initial dovitinib treatment (4–8 weeks). The closed circles in the PCA (Fig. 3a) indicate the expression signature of six miRs at baseline per patient. We found three categories of patients based on the change in miR levels after the initial dovitinib treatment as indicated by the direction of the arrows pointing from baseline to post treatment. A cluster analysis of miR patterns (Fig. 3b) separated the patients into two major

groups with one group split further into two subgroups ($P < 0.05$). PCA and cluster analyses of miR expression patterns were carried out by investigators that were blinded to the disease outcome. After completion of these analyses, the patient treatment responses were matched to the miR response data and are shown with a color code indicative of treatment responses (see Fig. 1b). The three patients with tumors that were resistant to dovitinib treatment

showed distinct changes of plasma miR expression in the PCA and in the cluster analysis relative to patients with stable disease or tumor regression in the first 8 weeks. Interestingly, the baseline miR signatures did not separate responding from non-responding patients (closed circles in Fig. 3a). Moreover, no relationship was found between the adverse effects of dovitinib listed in Table 1 and the changes in miR patterns after dovitinib.
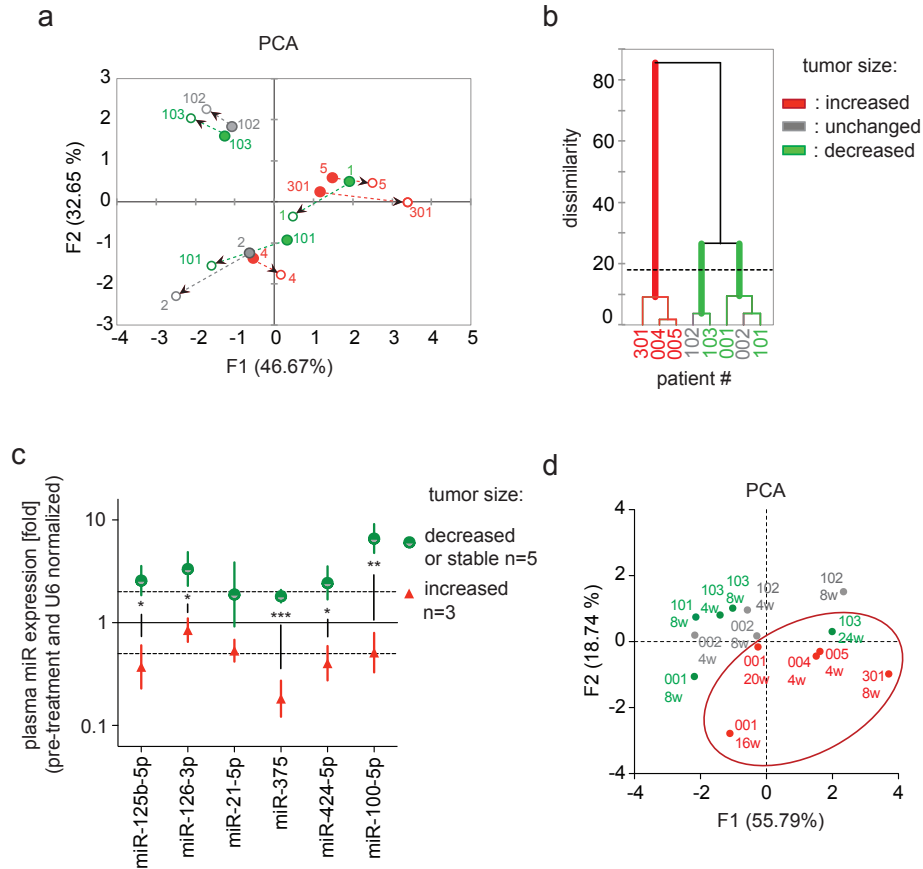
Figure 3. Expression patterns of circulating miRs separate patients based on the response to dovitinib treatment. a. Principal component analysis of the expression of six miRs before treatment (closed circles) and after treatment (open circles): patients 001, 002, 004, 005, 102, 103: 4 weeks; patients 101, 301: 8 weeks. The arrows indicate the before-to-after direction of the change. Patients that are separated by color code to indicate changes in tumor sizes after 8 weeks treatment (red = increase, green = decrease, grey = no change). b. Cluster analysis of the miR expression changes after 4 or 8 weeks treatment with dovitinib. The dashed line indicates significant differences (Euclidian distance) between 3 patient groups. c. Changes in six circulating miRs early after dovitinib treatment (4 weeks, except patient 101 and 103 at 8 weeks) based on tumor responses. The fold change in expression after treatment relative to U6 is indicated. Error bars = SEM, $*P < 0.05$; $**P = 0.0032$; $***P = 0.0006$ by unpaired t-test. d. Principal Component Analysis of the changes in expression of six miRs after dovitinib at multiple time points. The red circle includes patients with dovitinib resistant tumors. Patient 103 at 24 weeks is the exception in this group.

A comparison of the changes in miR expression after initial treatment in patients with tumor progression (n = 3) versus patients with stable disease or tumor regression (n = 5) shows that 5 out of 6 miRs were differentially expressed. In patients with treatment-resistant tumors relative to patients with stable disease or sensitive tumors miR-125b-5p, -126-3p, -375, 424-5p, and -100-5p were significantly down-regulated after the initial dovitinib treatment (Fig. 3c). This suggests that miR patterns after initial treatment can serve as response indicators. This could then support a decision to continue or terminate a planned treatment. For example, patient 001 showed a 9.23% reduction in tumor size after 2 cycles of dovitinib. However, acquired resistance became evident on the CT measurements at 24 weeks (see Fig. 1b). The lack of a response based on CT measurements is obvious at 24 weeks but was already evident based on the circulating miR patterns at 16 weeks, as seen in the PCA (Fig. 3d). Additionally, patient 103 had a long-term anti-tumor response to dovitinib (Fig. 1b). However, when this anti-tumor response began to diminish at 24 weeks, the circulating miR pattern was already similar to that of the resistant group of patients (Fig. 3d). Thus, the change in expression levels of six miRs selected here may serve as biomarkers of anti-tumor responses during treatment with a TKI in patients with metastatic breast cancer.

DISCUSSION

Here we report that distinctly altered patterns of circulating miR expression are observed in patients after treatment with dovitinib. Plasma miRs have a major potential as cancer biomarkers [30,32-34]. MiRs are deregulated as a result of the uncontrolled cell proliferation, stromal remodeling and immune regulation that define cancer and are stably exported into the circulation. Distinct alteration in circulating miRs reflects dysregulation of cell growth and stroma recruitment and the impact of therapy. Generally speaking, the six miRs selected as potentially informative miRs for a dovitinib effect will reflect the effects of the drug on the host as well as on the tumor and serial blood sampling relative to treatments may capture the dynamics of these events.

The function of the five miRs that show a significant change in dovitinib-responsive tumors (Fig. 3c) and a possible relation with drug efficacy is discussed next. Recent work indicates that elevated miR-125b expression predicts poor prognosis in breast cancer and is a candidate therapeutic target in AI-resistant breast cancers [35]. Interestingly, miR-125b expression is transiently induced in endothelial cells upon stimulation with VEGF or by ischemia [36]. Also, miR-125b inhibits translation of vascular endothelial (VE)-cadherin mRNA, in vitro tube formation by endothelial cells, and induced nonfunctional blood vessel formation in vivo resulting in inhibition of xenograft tumor growth [36]. This matches with an antiangiogenic effect of dovitinib treatment expected from an inhibitor that targets FGF and VEGF pathways.

MiR-126 is considered the prototype of an endothelial-specific miRNA. VEGF-A is a target for miR-126 and studies suggested that miR-126 could suppress tumor growth and tumor angiogenesis through VEGF-A signaling [37,38]. Others described miR-126 as an independent suppressor of the sequential recruitment of mesenchymal stem cells and inflammatory monocytes into breast cancer stroma to inhibit lung metastasis [39]. This study also demonstrated a correlation between miR-126 downregulation and poor metastasis-free survival of breast cancer patients [39]. The expression of miR-126 has been shown to be downregulated in breast metastases [40], as well as different cancers acting as a tumor suppressor by inhibiting tumor growth [41,42]. The treatment related upregulation in patients with dovitinib-responsive tumors fits with this role of miR-126.

Circulating miR-375 is negatively correlated with disease relapse and resistance to neoadjuvant chemotherapy in stage II–III breast cancer patients [43]. Wu et al. also identified miR-375 as the most significantly different miRNA, whose prevalence in the circulation appeared to reflect better clinical outcome of breast cancer [43]. miR-424 was reported to directly control the expression of FGFR1 and MAP2K1 in the human trophoblast through a discrete 3'UTR site [44]. Thus, the increase observed in patients with dovitinib-responsive tumors suggests a relationship between the altered circulating miR-424 levels and the efficacy of dovitinib towards one of its known targets, the FGF receptor pathway.

MiR-100 was the most differentially upregulated miR in patients with dovitinib-responsive tumors (Fig. 3c). It has been shown that miR-100 inhibits the maintenance and expansion of breast cancer stem cells in basal-like cancer and plays a role in cancer free-survival, as confirmed by a cohort analysis of patient tumors implicating low expression of miR-100 as a negative prognostic factor [45]. Thus, the upregulation in patients with treatment responsive tumors matches with the role ascribed to this miR.

Given the complex interplay of cancer and stroma that includes distinct drivers in different cancers as well as genetic and environmental differences in the patient, analysis of patterns of miRs can provide a more reliable read-out than individual miRs and will compensate for this heterogeneity. Also, rather than evaluating absolute levels of single miRs in patients with different genetic backgrounds, co-morbidities and lifestyle, our study suggests that it is more informative to evaluate changes in the expression patterns of a set of miRs due to therapy and during the course of the disease. Here, we assessed miR expression pattern changes in response to therapy, and evaluated whether this differs amongst patients with different courses of their disease.

As a caveat, the small size of the current study limits the potential for general conclusions. However, we have attempted to follow the guidelines of McShane *et al.* [46] and were sur-

prised by the robustness of the relationship between the change in tumor size and circulating miR pattern changes. Rather than trying to find a correlation between miR pattern changes and cancer lesion treatment responses we opted to use the miR pattern changes to assign patients to different response groups in an analysis of miRs that was blinded to the patient outcome. This blinded assignment of patients to distinct response groups also strengthens the conclusions one can draw from the findings.

In conclusion, altered patterns of serially analyzed circulating miR expression patterns can indicate the impact of treatment on the whole organism as well as cancer lesion. Changes in the pattern changes after treatment will be informative on the potential long-term benefit of the therapy and thus can provide an early decision point for continuation of a given treatment [15]. The current study suggests that the use of circulating miRs for treatment monitoring could be useful in treatment decisions though a prospective trial will be necessary to unanimously confirm the utility of the approach described here.

Authors' contributions
EEV, NS and AW wrote the manuscript. EEV, NS and AW analyzed the data. NS measured the microRNAs. EC and CI compiled and analyzed the clinical data. All authors edited and commented on the manuscript. All authors read and approved the final manuscript.

Acknowledgements

Competing interests
The authors are employees of Georgetown University. The authors generated and analyzed the data and wrote the manuscript independent of influence by the funding agencies. The authors declare that they have no competing interests.

Ethics approval and consent to participate
All patients gave written consent for the clinical trial protocol. The protocol was approved by the IRB at Medstar Georgetown University Hospital (IRB #2010-535). The registration at clinicaltrials.gov is under NCT01484041.

Funding

Supplemental Table 1. Genome wide miR expression screen before and after dovitinib treatment. An RT-qPCR assay was performed on a paired set of one patient's (#101) plasma samples. Abundant miRs with cycle numbers (Ct) below 32 are listed.

	Ct before treatment	Ct after treatment
mean Ct value	26.08	28.76
miR		
hsa-let-7a-5p	21.18	28.84
hsa-let-7b-5p	21.13	29.23
hsa-let-7c	24	27.32
hsa-let-7d-3p	24.98	30.29
hsa-let-7d-5p	23.88	28.66
hsa-let-7e-5p	23.34	30.57
hsa-let-7f-5p	22.39	28.14
hsa-let-7g-5p	23.18	28
hsa-let-7i-5p	24.69	30.52
hsa-miR-1	26.26	29.68
hsa-miR-100-5p	25.84	25.96
hsa-miR-101-3p	28.89	31.75
hsa-miR-105-5p	23.97	28.92
hsa-miR-106b-5p	25.34	29.53
hsa-miR-107	28.24	31.2
hsa-miR-1180	28.44	30.7
hsa-miR-122-5p	24.41	29.22
hsa-miR-124-3p	30.76	29.45
hsa-miR-125a-5p	24.19	30.75
hsa-miR-126-3p	22.06	28.27
hsa-miR-126-5p	21.01	25.53
hsa-miR-127-3p	26.79	24.73
hsa-miR-128	27.53	30.96
hsa-miR-1290	27.65	30.44
hsa-miR-130a-3p	26.20	29.52
hsa-miR-130b-3p	30.16	28.34
hsa-miR-132-3p	28.72	30.42
hsa-miR-132-5p	18.40	22.68
hsa-miR-134	28.10	25.74
hsa-miR-135a-5p	26.52	28.35
hsa-miR-142-3p	26.69	26.95
hsa-miR-142-5p	29.40	30.56
hsa-miR-144-3p	23.24	28.89
hsa-miR-144-5p	28.05	30.54
hsa-miR-146a-5p	23.17	28.52

Supplemental Table 1. Genome wide miR expression screen before and after dovitinib treatment. An RT-qPCR assay was performed on a paired set of one patient's (#101) plasma samples. Abundant miRs with cycle numbers (Ct) below 32 are listed. (continued)

	Ct before treatment	Ct after treatment
hsa-miR-146b-5p	25.78	30.07
hsa-miR-148a-3p	25.57	28.82
hsa-miR-148b-3p	25.73	30.86
hsa-miR-150-5p	23.16	24.2
hsa-miR-151a-3p	24.99	30.77
hsa-miR-151a-5p	26.59	30.68
hsa-miR-152	27.94	31.8
hsa-miR-155-5p	27.62	30.84
hsa-miR-15b-3p	26.59	30.58
hsa-miR-15b-5p	30	28.89
hsa-miR-16-5p	20.35	25.82
hsa-miR-17-5p	25.37	30.13
hsa-miR-181a-5p	30.10	28.25
hsa-miR-181c-3p	27.52	26.2
hsa-miR-183-3p	29.46	24.87
hsa-miR-185-5p	24.96	29.12
hsa-miR-186-5p	23.05	26.68
hsa-miR-187-5p	29.66	28.44
hsa-miR-18a-3p	27.53	30.61
hsa-miR-18a-5p	25.86	29.3
hsa-miR-18b-5p	26.56	30
hsa-miR-191-5p	22.90	26.49
hsa-miR-192-5p	28.10	30.63
hsa-miR-193a-5p	28.23	31.38
hsa-miR-194-5p	28.82	31.82
hsa-miR-195-5p	20.69	25.43
hsa-miR-197-3p	24.89	30.34
hsa-miR-199a-3p	23.43	29.72
hsa-miR-19a-3p	24.67	30.01
hsa-miR-19b-3p	24.57	28.62
hsa-miR-200b-3p	29.35	28.78
hsa-miR-200c-3p	29.95	29.95
hsa-miR-200c-5p	28.11	28.87
hsa-miR-205-3p	31.50	28.2
hsa-miR-20a-5p	24.31	30.28
hsa-miR-20b-5p	25.46	31.56
hsa-miR-21-5p	20.53	22.91

Supplemental Table 1. Genome wide miR expression screen before and after dovitinib treatment. An RT-qPCR assay was performed on a paired set of one patient's (#101) plasma samples. Abundant miRs with cycle numbers (Ct) below 32 are listed. (continued)

	Ct before treatment	Ct after treatment
hsa-miR-210	31.13	30.21
hsa-miR-22-3p	23.56	18
hsa-miR-22-5p	28.9	30.72
hsa-miR-221-3p	20.89	25.28
hsa-miR-221-5p	31.13	31.18
hsa-miR-222-3p	26.92	30.08
hsa-miR-223-3p	20.93	25.44
hsa-miR-223-5p	27.47	30.39
hsa-miR-23b-3p	24.68	30.7
hsa-miR-24-3p	22.73	28.22
hsa-miR-25-3p	22.19	25.1
hsa-miR-25-5p	28.73	30.21
hsa-miR-26a-5p	22.54	28.48
hsa-miR-26b-5p	23.99	30.02
hsa-miR-27a-3p	24.28	30.39
hsa-miR-27b-3p	23.96	31.57
hsa-miR-28-3p	28.58	28.57
hsa-miR-29a-3p	27.09	28.32
hsa-miR-30a-5p	25.49	30.78
hsa-miR-30c-5p	24.43	30.2
hsa-miR-30d-5p	24.70	29.46
hsa-miR-30e-3p	26.54	31.72
hsa-miR-30e-5p	25.31	28.94
hsa-miR-31-5p	31.75	30.52
hsa-miR-320a	22.70	27.08
hsa-miR-320b	26.99	28.49
hsa-miR-324-5p	28.80	30.8
hsa-miR-328	27.10	25.24
hsa-miR-330-3p	30.11	28.12
hsa-miR-342-3p	24.57	26
hsa-miR-34c-3p	30.18	31.46
hsa-miR-34c-5p	30.76	32
hsa-miR-361-5p	26.24	31.96
hsa-miR-370	28.46	27.48
hsa-miR-373-5p	28.32	31.92
hsa-miR-374b-5p	24.95	30.92
hsa-miR-375	28.81	28.46

Supplemental Table 1. Genome wide miR expression screen before and after dovitinib treatment. An RT-qPCR assay was performed on a paired set of one patient's (#101) plasma samples. Abundant miRs with cycle numbers (Ct) below 32 are listed. (continued)

	Ct before treatment	Ct after treatment
hsa-miR-382-5p	26.41	31.61
hsa-miR-411-5p	30.34	24.96
hsa-miR-421	28.64	26.86
hsa-miR-423-3p	27.85	31.73
hsa-miR-424-5p	27.03	27
hsa-miR-431-5p	28.45	25.94
hsa-miR-433	27.18	23.85
hsa-miR-451a	20.63	25.1
hsa-miR-484	24.07	28.61
hsa-miR-486-5p	19.30	24.83
hsa-miR-489	25.67	20.59
hsa-miR-495-3p	26.41	24.73
hsa-miR-497-5p	30.11	30.95
hsa-miR-539-5p	29.31	21.08
hsa-miR-551b-3p	31.74	30.66
hsa-miR-652-3p	24.95	31.68
hsa-miR-661	28.82	27.68
hsa-miR-7-5p	25.79	30
hsa-miR-720	23.97	31.37
hsa-miR-744-5p	24.12	30.61
hsa-miR-92a-3p	21.04	27.99
hsa-miR-92b-3p	27.24	30.67
hsa-miR-93-5p	25.75	28.65
hsa-miR-99b-5p	28.62	31.29
RNU6-2	27.26	30.76

REFERENCES

1   Krause, D. S. & Van Etten, R. A. (2005) Tyrosine kinases as targets for cancer therapy. *N Engl J Med* 353, 172-187

2   Hojjat-Farsangi, M. (2014) Small-molecule inhibitors of the receptor tyrosine kinases: promising tools for targeted cancer therapies. *Int J Mol Sci* 15, 13768-13801

3   Weinstein, I. B. & Joe, A. K. (2006) Mechanisms of disease: Oncogene addiction--a rationale for molecular targeting in cancer therapy. *Nat Clin Pract Oncol* 3, 448-457

4   Turner, N. & Grose, R. (2010) Fibroblast growth factor signalling: from development to cancer. *Nat Rev Cancer* 10, 116-129

5   Park, C. K., Jung, W. H. & Koo, J. S. (2016) Expression of cancer-associated fibroblast-related proteins differs between invasive lobular carcinoma and invasive ductal carcinoma. *Breast Cancer Res Treat* 159(1):55-69

6   Katoh, M. (2016) FGFR inhibitors: Effects on cancer cells, tumor microenvironment and whole-body homeostasis (Review). *Int J Mol Med* 38, 3-15

7   Holdman, X. B. et al. (2015) Upregulation of EGFR signaling is correlated with tumor stroma remodeling and tumor recurrence in FGFR1-driven breast cancer. *Breast Cancer Res* 17, 141

8   Brown, W., Tan, L., Smith, A., Gray, N. S. & Wendt, M. (2016) Covalent targeting of fibroblast growth factor receptor inhibits metastatic breast cancer. *Mol Cancer Ther* 15(9):2096-106

9   Lee, S. H. et al. (2005) In vivo target modulation and biological activity of CHIR-258, a multitargeted growth factor receptor kinase inhibitor, in colon cancer models. *Clin Cancer Res* 11, 3633-3641

10 Wan, X. (2014) Prostate cancer cell–stromal cell crosstalk via FGFR1 mediates antitumor activity of dovitinib in bone metastases. *Science Translational Medicine*, 1-14

11 Angevin, E. et al. (2013) Phase I study of dovitinib (TKI258), an oral FGFR, VEGFR, and PDGFR inhibitor, in advanced or metastatic renal cell carcinoma. Clinical cancer research : an official journal of the American Association for *Cancer Research* 19, 1257-1268

12 Escudier, B. et al. (2014) Phase II results of Dovitinib (TKI258) in patients with metastatic renal cell cancer. *Clin Cancer Res* 20, 3012-3022

13 Kim, K. B. et al. (2011) Phase I/II and Pharmacodynamic Study of Dovitinib (TKI258), an Inhibitor of Fibroblast Growth Factor Receptors and VEGF Receptors, in Patients with Advanced Melanoma. Clinical cancer research : an official journal of the American Association for *Cancer Research* 17, 7451-7461

14 André, F. et al. (2013) Targeting FGFR with Dovitinib (TKI258): Preclinical and Clinical Data in Breast Cancer. Clinical cancer research : an official journal of the American Association for *Cancer Research* 19, 3693-3702

15 Rapisuwon, S., Vietsch, E. E. & Wellstein, A. (2016) Circulating biomarkers to monitor cancer progression and treatment. *Comput Struct Biotechnol J* 14, 211-222

16 Kosaka, N. et al. (2010) Secretory mechanisms and intercellular transfer of microRNAs in living cells. *J Biol Chem* 285, 17442-17452

17 Cortez, M. A. et al. (2011) MicroRNAs in body fluids--the mix of hormones and biomarkers. *Nat Rev Clin Oncol* 8, 467-477

18 Kleivi Sahlberg, K. et al. (2015) A serum microRNA signature predicts tumor relapse and survival in triple-negative breast cancer patients. *Clin Cancer Res* 21, 1207-1214

19 Stuckrath, I. et al. (2015) Aberrant plasma levels of circulating miR-16, miR-107, miR-130a and miR-146a are associated with lymph node metastasis and receptor status of breast cancer patients. *Oncotarget* 6, 13387-13401

20   Eichelser, C., Flesch-Janys, D., Chang-Claude, J., Pantel, K. & Schwarzenbach, H. (2013) Deregulated serum concentrations of circulating cell-free microRNAs miR-17, miR-34a, miR-155, and miR-373 in human breast cancer development and progression. *Clin Chem* 59, 1489-1496

21   Madhavan, D. et al. (2012) Circulating miRNAs as surrogate markers for circulating tumor cells and prognostic markers in metastatic breast cancer. *Clin Cancer Res* 18, 5972-5982

22   Shivapurkar, N. et al. (2014) Recurrence of early stage colon cancer predicted by expression pattern of circulating microRNAs. *PLoS One* 9, e84686

23   Kodahl, A. R., Zeuthen, P., Binder, H., Knoop, A. S. & Ditzel, H. J. (2014) Alterations in circulating miRNA levels following early-stage estrogen receptor-positive breast cancer resection in post-menopausal women. *PLoS One* 9, e101950

24   Muller, V. et al. (2014) Changes in serum levels of miR-21, miR-210, and miR-373 in HER2-positive breast cancer patients undergoing neoadjuvant therapy: a translational research project within the Geparquinto trial. *Breast Cancer Res Treat* 147, 61-68

25   Li, Q. et al. (2014) Circulating miR-19a and miR-205 in serum may predict the sensitivity of luminal A subtype of breast cancer patients to neoadjuvant chemotherapy with epirubicin plus paclitaxel. *PLoS One* 9, e104870

26   Bovy, N. et al. (2015) Endothelial exosomes contribute to the antitumor response during breast cancer neoadjuvant chemotherapy via microRNA transfer. *Oncotarget* 6, 10253-10266

27   Wang, H. et al. (2012) Circulating MiR-125b as a marker predicting chemoresistance in breast cancer. *PLoS One* 7, e34210

28   Jung, E. J. et al. (2012) Plasma microRNA 210 levels correlate with sensitivity to trastuzumab and tumor presence in breast cancer patients. *Cancer* 118, 2603-2614

29   LaConti, J. J. et al. (2011) Tissue and serum microRNAs in the Kras(G12D) transgenic animal model and in patients with pancreatic cancer. *PLoS One* 6, e20687

30   Zheng, G. et al. (2013) Identification and validation of reference genes for qPCR detection of serum microRNAs in colorectal adenocarcinoma patients. *PLoS One* 8, e83025

31   Rice, J., Roberts, H., Rai, S. N. & Galandiuk, S. (2015) Housekeeping genes for studies of plasma microRNA: A need for more precise standardization. *Surgery* 158, 1345-1351

32   Huo, D., Clayton, W. M., Yoshimatsu, T. F., Chen, J. & Olopade, O. I. (2016) Identification of a circulating MicroRNA signature to distinguish recurrence in breast cancer patients. *Oncotarget* 7(34):55231-55248

33   Casey, M. C., Sweeney, K. J., Brown, J. A. & Kerin, M. J. (2016) Exploring circulating micro-RNA in the neoadjuvant treatment of breast cancer. *Int J Cancer* 139, 12-22

34   Schwarzenbach, H., Nishida, N., Calin, G. A. & Pantel, K. (2014) Clinical relevance of circulating cell-free microRNAs in cancer. *Nat Rev Clin Oncol* 11, 145-156

35   Vilquin, P. et al. (2015) MicroRNA-125b upregulation confers aromatase inhibitor resistance and is a novel marker of poor prognosis in breast cancer. *Breast Cancer Res* 17, 13

36   Muramatsu, F., Kidoya, H., Naito, H., Sakimoto, S. & Takakura, N. (2013) microRNA-125b inhibits tube formation of blood vessels through translational suppression of VE-cadherin. *Oncogene* 32, 414-421

37   Chen, H. et al. (2014) Reduced miR-126 expression facilitates angiogenesis of gastric cancer through its regulation on VEGF-A. *Oncotarget* 5, 11873-11885

38   Kong, R. et al. (2016) The crucial role of miR-126 on suppressing progression of esophageal cancer by targeting VEGF-A. *Cell Mol Biol Lett* 21, 3

39   Zhang, Y. et al. (2013) miR-126 and miR-126* repress recruitment of mesenchymal stem cells and inflammatory monocytes to inhibit breast cancer metastasis. *Nat Cell Biol* 15, 284-294

40   Tavazoie, S. F. et al. (2008) Endogenous human microRNAs that suppress breast cancer metastasis. *Nature* 451, 147-152

41   Saito, Y. et al. (2009) Epigenetic therapy upregulates the tumor suppressor microRNA-126 and its host gene EGFL7 in human cancer cells. *Biochem Biophys Res Commun* 379, 726-731

42   Yanaihara, N. et al. (2006) Unique microRNA molecular profiles in lung cancer diagnosis and prognosis. *Cancer Cell* 9, 189-198

43   Wu, X. et al. (2012) De novo sequencing of circulating miRNAs identifies novel markers predicting clinical outcome of locally advanced breast cancer. *J Transl Med* 10, 42

44   Mouillet, J. F. et al. (2013) The unique expression and function of miR-424 in human placental trophoblasts. *Biol Reprod* 89, 25

45   Petrelli, A. et al. (2015) By promoting cell differentiation, miR-100 sensitizes basal-like breast cancer stem cells to hormonal therapy. *Oncotarget* 6, 2315-2330

46   McShane, L. M. et al. (2006) REporting recommendations for tumor MARKer prognostic studies (REMARK). *Breast Cancer Res Treat* 100, 229-235

CHAPTER 6

Summary and Discussion

SUMMARY AND DISCUSSION

As early as 1976 scientists noted that genomic instability of a proliferating cancer population is followed by additional genetic diversity under the selection pressures in the tumor environment, resulting in multiple heterogeneous subpopulations [1]. Cancer heterogeneity is the main cause of drug therapy resistance. Therefore, we conducted a study that could provide insights for the improvement of effective cancer therapies, described in **chapter 2**. We generated a model of cancer heterogeneity by isolating and characterizing clonal cancer cell lines from a transgenic *LSL-Kras*^{G12D/+;} *LSL-Trp53*^{R172H/+;} *P48*-Cre (KPC) mouse pancreatic cancer (PDAC). We found that the clonal cell lines from the same tumor harbor common ancestor mutations and more importantly, each have a set of unique signature mutations. Not only do these clonal cell lines grow at different rates in vitro, their sensitivity to anti-cancer drugs of various mechanisms of action was distinct.

The novelty of our study lies in the fact that we can mix the clones back together and study their drug sensitivity in the context of a heterogeneous population where paracrine crosstalk is possible. The unique clonal mutations are used for the measurement of clone abundance in the mixed tumors by next generation sequencing (NGS). Although each clone is driven by the RAS-RAF-MEK-ERK signaling pathway due to the *Kras* G12D mutation, the clones are differentially sensitive to the MEK inhibitor trametinib on their own. What was even more striking is that the clonal sensitivity to trametinib in vitro was altered when clones were mixed back together and thus subjected to paracrine signaling. This finding was confirmed when using the conditioned media from the clone mixture, and shows that pharmacological screenings in vitro using cell lines such as the NCI-60 panel should rather be performed in heterogeneous mixtures of cell lines to improve the predictive validity.

We studied the clone mixture as allograft tumors in immune competent syngeneic mice, and noticed a difference in growth rate amongst the clones. Moreover, gemcitabine treatment had a stimulating effect on the slow growing clones C5 and D10 that were underrepresented in control tumors. Gemcitabine treatment allowed these clones to gain a 4-5 fold increase in growth as compared to the control conditions. Others reported similar findings in minor dormant human colorectal cancer clones that can become dominant and reinitiate tumor growth after chemotherapy [2]. Strikingly, two other clones that were sensitive to gemcitabine in vitro, were not responding to gemcitabine in the mixed tumors in presence of tumor stroma. This suggests that the crosstalk with the tumor stroma offers paracrine factors that protect these clones from the chemotherapy.

A comparison of clonal effects of MEK inhibitor in the mixed culture in vitro and in the tumors showed a discordant result for clone G9 that moved from sensitive in vitro to resistant

in the tumors and clone C8 that moved in the opposite direction. Others have also described that the tumor environment alters the drug sensitivity of cancer cells [3,4]. Yet, until now, most cancer drug screens are performed in vitro, or in xenograft tumors with homogeneous cancer cell lines in immune compromised animals.

The beauty of our clonal allograft model lies in the fact that it allows for analyses of heterogeneous tumors in the context of an intact immune system. The striking differences in α-PD-1 efficacy towards clones present in the heterogeneous tumor mix which we observed in our study provides some interesting insights that may allow to overcome resistance to checkpoint blockade. One of the clones, C8 is highly sensitive to α-PD-1 treatment and on its own attracts the highest number of CD8+ PD-1+ T-lymphocytes towards the tumors. We conducted a co-culture experiment in vitro with primed mouse T-lymphocytes and the clonal PDAC cell lines to corroborate this finding. In order to generate enough vital T-cells we used the caecal patches of tumor bearing mice as source of tumor-reactive T-cells, instead of the commonly used tumor infiltrating lymphocytes which are often exhausted [5]. We observed that the pancreatic cancer clones elicit different levels of T-cell activation, measured by Interferon-γ secretion. Strikingly, growth of one clone, D10 was stimulated in vivo by anti-PD-1 treatment and we are currently exploring this further. Moreover, we found that that the caecal patch, the equivalent of the human vermiform appendix [6,7], contains pancreatic cancer reactive T-cells. We are the first to have shown this and we are currently exploring the reactivity of T-cells from the vermiform appendix of patients with locally advanced pancreatic cancer.

To conclude chapter 2, we found that the composition of heterogeneous cancers is affected by crosstalk amongst the cancer subpopulations as well as the host environment that includes the immune system as a major player. We developed an in vivo model that allows for the quantitation of clonal cancer subpopulations in heterogeneous tumors, growing in immune competent. Our model is suited for the assessment of stromal and immune modulators and their impact on growth of heterogeneous cancer cells.

Cancer is a heterogeneous and dynamic disease. Yet, until today, molecular analyses of cancer are still performed using small tissue biopsies. In **chapter 3** we sought to assess the changes in the mutational makeup of colon and pancreatic adenocarcinoma between the time of primary tumor surgery and detection of metastatic disease using circulating cell free DNA. In this study we also provide a direct comparison of mutation detection in primary tumor DNA and plasma DNA at diagnosis. For this, amplicons covering 263 mutations in 56 cancer-associated genes were analyzed by next generation sequencing. We found that on average less than half of colon tumor mutations were detected in the plasma at time of diagnosis. For pancreatic cancer this percentage was even lower: less than 30% of pancreatic

tumor mutations were detected in the circulating DNA. Whether ctDNA can fully replace or complement tissue analyses in all cancer types remains controversial, especially in early stage diseases.

Disadvantages of circulating tumor DNA (ctDNA) include the fact that high background levels of wildtype DNA can lead to missed ctDNA detection. Also, the genetic make-up of dying cells is dominant in ctDNA, and that of vital tumor cells may be underrepresented. Others have shown that in formalin fixed-paraffin-embedded cancer tissues and plasma from patients with different types of cancer an overall concordance of 60% in mutations of 19 genes analyzed was found [8]. Another prospective study with matched plasma and tissue samples of 75 cancer patients with different tumor types (61 metastatic and 14 clinical stage II patients) looked at 54 genes with digital deep sequencing technology. In the tumor tissues, at least one somatic mutation in 44 of 61 samples (72.1%) was found. From those 44 tissue samples with mutations, ~66 % of the matched patients had detectable mutations in the plasma DNA [9]. The sensitivity of ctDNA mutation detection improves as the tumor load increases. An extensive study including different cancer types showed that the fraction of patients with mutant ctDNA increases with cancer stages: 47% of patients with stage I cancers of any type had detectable ctDNA, whereas the fraction of patients with detectable ctDNA was 55%, 69%, and 82% for patients with stage II, III, and IV cancers, respectively [10].

On the other hand, we detected 71-78% of mutations in the plasma DNA of patients at time of diagnosis that were not detected in the tumor tissue. One reason for the discordance is the small size of the tumor biopsy. The tumor biopsies are merely a tiny fraction of the entire heterogeneous tumor. Moreover, the patients may already have micrometastases that are not detected on the CT scans, but already release mutant DNA in the circulation. Overall the presence of ctDNA in patients with progressive cancer provides a median lead-time of detection of 8-9 months over computed tomography (CT) scans [11,12]. A recent study in patients with non-small cell lung cancer patients revealed that 18 patients had detectable *EGFR* T790M ctDNA in their plasma, while the tumor DNA was negative for *EGFR* T790M genotyping [13]. This demonstrates that tissue biopsies may not represent the entire cancer cell population, or result in false negative mutation results due to low abundance of cancer cells in the specimen. One of the caveats is that circulating DNA mutations may not originate from cancer cells. It is worth noting that somatic mutations found in skin biopsies from healthy individuals can approach the mutation levels seen in cancers [14], however, mutant DNA from healthy tissues is typically below detection in the circulation. This is likely due to the induction of senescence in normal cells with mutant DNA rather than cell death and shedding of their DNA, and the low frequency of mutations at a variety of random sites in the genome. Cancer cells on the other hand are highly abundant, and often

have non-synonymous mutations. More importantly, cancer cells have a high turnover rate and thus a high death rate.

We assessed the change in mutations from the time of primary resectable cancer diagnosis to the recurrence of cancer after surgical tumor removal and adjuvant therapy in patients with colon and pancreatic cancer. This analysis reflects the evolution of primary to recurrent cancer. After metastasis, new ctDNA mutations are gained both in colon (33.8%) and pancreatic cancer (62.6%) and were not detected at the time of diagnosis of the primary cancer. Complementary to the gain of mutations after metastasis, we also observed a loss of approximately half of the ctDNA mutations. The analysis of a relatively broad panel of cancer-related genes is feasible for ctDNA and would allow monitoring of changes in the molecular makeup over time and under therapy.

Summarizing chapter 3, we found that circulating tumor DNA appears to represent the heterogeneity of colon and pancreatic cancer more extensively than tumor tissue DNA. By comparing the evolution of mutant ctDNA over the course of treatment, emergence of mutations that are associated with therapy-resistant cancer can be studied easily by collecting repeated patient blood samples. It is highly likely that liquid biopsies will become essential in cancer patient diagnostics and follow-up in the very near future.

Until now, the clinical follow up of patients with pancreatic cancer after surgery is not standardized in the Netherlands and consists mainly of clinical physical examination and at times radiographical imaging by CT-scans [15]. Simple repeated blood draws followed by biomarker analyses could vastly improve patient monitoring and prediction of outcome. Circulating microRNAs (miRs) are suitable candidates due to their high stability in the circulation and their importance in pathophysiology. In **chapter 4** we measured serum miRs in patients with treatment-naïve resectable PDAC before and after surgical tumor removal and compared the changes of miR levels to the progression free survival of the patients. Importantly, we performed a cross-species comparison of serum miR expression: we analyzed the serum miR levels in KPC mice that develop metastatic pancreatic cancer. The prognostic miRs we identified in the patients were also correlated to PDAC metastases in the KPC mice, confirming their importance in pancreatic cancer progression. From the 250 miRs we profiled, the expression levels of only miR-125b-5p and miR-99a-5p could significantly separate patients based on progression free survival after surgery.

Next, we assessed whether miR-125b and miR-99a-5p are expressed in the resected pancreatic cancer tissues by using in situ hybridization. To our surprise, the cells that express the miRs are very low abundant, and are only present in the pancreatic stroma. It is becoming increasingly clear that circulating miRs represent a rich source of information about the

status of the immune system. MiRs in the serum originate mainly from endothelium and blood cells [17,18]. The circulating miRs are transferred from cell to cell and can elicit immune modulation [19,20]. Serum miRs interact more with immune-related mRNA genes that with non-immune related genes [21]. We found that the high miR-125b-5p and miR-99a-5p expressing cells are limited to inflammatory infiltrates in the connective tissue of the pancreatic tumors. After staining the consecutive tumor sections for CD79A we found that the high miR-125b-5p and miR-99a-5p expressing cells are in very close proximity to CD79A positive cells which are part of the B-lymphocyte lineage. This underlines the importance of circulating microRNAs in the host response to cancer. Our future aim is to conduct a histopathological validation to study the co-localization of miR-125b-5p and miR-99a-5p in various subtypes of immune cells to gain understanding in the immune cell function alterations in patients with cancer.

Although there are a multitude of studies comparing circulating miR levels in pancreatic cancer patients to healthy controls [22,23], there has been very little to no research that compares the levels of miRs after surgical removal of primary pancreatic cancers. In our study we compared serum miRs pre and post-surgery from treatment-naïve patients that were operated at the Erasmus Medical Center between 2013 and 2017. Recently it became clear that patients with (borderline) resectable PDAC that undergo preoperative chemo/radiotherapy have a better survival [24,25]. From now on all patients with (borderline) resectable PDAC in the Netherlands will be offered to receive preoperative chemotherapy, if the performance status of the patient permits the therapy, and the patient is willing to undergo systemic treatment. Chemotherapy has a vast impact on the immune landscape [26,27]. Whether serum miR-125b-5p and miR-99a-5p are also predictive of disease progression after surgery in pre-treated patients remains to be evaluated. Therefore we are currently collecting blood samples to evaluate the changes in the serum miRs of patients with (borderline) resectable patients who undergo pre-operative FOLFIRINOX chemotherapy or gemcitabine/radiotherapy.

In **Chapter 5** we analyzed plasma miRs in patients with hormone receptor positive, metastatic breast cancer with prior disease progression during aromatase inhibitor therapy in a phase I/II trial with the multiple tyrosine kinase inhibitor dovitinib. The dual inhibition of FGF and VEGF signaling by dovitinib enhances the antitumor effects through the targeting of immune evasion and angiogenesis in the tumor microenvironment [28]. We hypothesized that expression of circulating miRs can provide an accurate read-out of these effects of dovitinib. Changes in plasma miR levels were measured by quantitative RT-qPCR before and after treatment with dovitinib and compared to changes in tumor sizes. The altered expression patterns observed for the six circulating miRs (miR-21-5p, miR-100-5p, miR-125b-5p, miR-126-3p, miR-375 and miR-424-5p) separated patients with resistant disease

from those with drug responsive disease. What was striking is that in a patient with long term response to dovitinib we observed a change in the circulating miR signature before the CT scan showed a reduced effect of the treatment at 24 weeks. Although this study consisted of a low number of patients, we conclude that changes in the expression patterns of circulating miRs can be indicators of dovitinib response, and this research merits the understanding of the host response to metastatic cancer.

CONCLUSIONS

The research in this thesis provides rationale for the implementation of circulating nucleic acid analyses into the standard of care of patients with cancer. Until now, cancer tissue specimens are used for molecular analyses of cancer, and clinical follow-up consists mainly of radiographical imaging. Cancer is a heterogeneous, dynamic disease that constantly changes over time and across different locations in the body. To improve our understanding in the molecular features of this disease as well as the response to cancer therapy, blood samples need to be taken repeatedly and analyzed for changes in circulating nucleic acids. Changes in circulating DNA mutations indicate clonal evolution of cancer populations and altered abundance of mutant circulating DNA suggests a change in disease burden. Moreover, changes in circulating DNA mutations reflect the emergence of resistant clones and prompt changes in treatment. In contrast to mutant DNA, circulating microRNAs take part in the extracellular crosstalk between cells and provide a readout of the organism's physiologic or disease state. Furthermore, changes in circulating miR patterns can reflect the immune landscape, treatment efficacy or resistance as well as adverse effects associated with the respective intervention. Thus, the combined serial analysis of mutant DNA and microRNAs in the circulation has the potential to provide a molecular footprint of cancer and can be used to monitor cancer progression as well as treatment responses in real time with a minimally invasive procedure.

REFERENCES

1   Nowell, P. C. (1976) The clonal evolution of tumor cell populations. *Science* 194, 23-28

2   Kreso, A. et al. (2013) Variable clonal repopulation dynamics influence chemotherapy response in colorectal cancer. *Science* 339, 543-548

3   McMillin, D. W. et al. (2010) Tumor cell-specific bioluminescence platform to identify stroma-induced changes to anticancer drug activity. *Nat Med* 16, 483-489

4   Straussman, R. et al. (2012) Tumour micro-environment elicits innate resistance to RAF inhibitors through HGF secretion. *Nature* 487, 500-504

5   Jiang, Y., Li, Y. & Zhu, B. (2015) T-cell exhaustion in the tumor microenvironment. *Cell Death Dis* 6, e1792

6   Alkadhi, S., Kunde, D., Cheluvappa, R., Randall-Demllo, S. & Eri, R. (2014) The murine appendiceal microbiome is altered in spontaneous colitis and its pathological progression. *Gut Pathog* 6, 25

7   Watson Ng, W. S., Hampartzoumian, T., Lloyd, A. R. & Grimm, M. C. (2007) A murine model of appendicitis and the impact of inflammation on appendiceal lymphocyte constituents. *Clin Exp Immunol* 150, 169-178

8   Perkins, G. et al. (2012) Multi-purpose utility of circulating plasma DNA testing in patients with advanced cancers. *PLoS One* 7, e47020

9   Kim, S. T. et al. (2015) Prospective blinded study of somatic mutation detection in cell-free DNA utilizing a targeted 54-gene next generation sequencing panel in metastatic solid tumor patients. *Oncotarget* 6, 40360-40369

10   Bettegowda, C. et al. (2014) Detection of circulating tumor DNA in early- and late-stage human malignancies. *Sci Transl Med* 6, 224ra224

11   Garcia-Murillas, I. et al. (2015) Mutation tracking in circulating tumor DNA predicts relapse in early breast cancer. *Sci Transl Med* 7, 302ra133

12   Scholer, L. V. et al. (2017) Clinical Implications of Monitoring Circulating Tumor DNA in Patients with Colorectal Cancer. *Clin Cancer Res* 23, 5437-5445

13   Oxnard, G. R. et al. (2016) Association Between Plasma Genotyping and Outcomes of Treatment With Osimertinib (AZD9291) in Advanced Non-Small-Cell Lung Cancer. *J Clin Oncol* 34, 3375-3382

14   Martincorena, I. et al. (2015) Tumor evolution. High burden and pervasive positive selection of somatic mutations in normal human skin. *Science* 348, 880-886

15   Groot, V. P. et al. (2017) Current Strategies for Detection and Treatment of Recurrence of Pancreatic Ductal Adenocarcinoma After Resection: A Nationwide Survey. *Pancreas* 46, e73-e75

16   Groot, V. P. et al. (2018) Patterns, Timing, and Predictors of Recurrence Following Pancreatectomy for Pancreatic Ductal Adenocarcinoma. *Ann Surg* 267, 936-945

17   Pritchard, C. C. et al. (2012) Blood cell origin of circulating microRNAs: a cautionary note for cancer biomarker studies. *Cancer Prev Res (Phila)* 5, 492-497

18   Williams, Z. et al. (2013) Comprehensive profiling of circulating microRNA via small RNA sequencing of cDNA libraries reveals biomarker potential and limitations. *Proc Natl Acad Sci U S A* 110, 4255-4260

19   Okoye, I. S. et al. (2014) MicroRNA-containing T-regulatory-cell-derived exosomes suppress pathogenic T helper 1 cells. *Immunity* 41, 89-103

20   Mittelbrunn, M. et al. (2011) Unidirectional transfer of microRNA-loaded exosomes from T cells to antigen-presenting cells. *Nat Commun* 2, 282

21   Nosirov, B. et al. (2017) Mapping circulating serum miRNAs to their immune-related target mRNAs. *Adv Appl Bioinform Chem* 10, 1-9

22   Li, Y. & Sarkar, F. H. (2016) MicroRNA Targeted Therapeutic Approach for Pancreatic Cancer. *Int J Biol Sci* 12, 326-337

23   Vietsch, E. E., van Eijck, C. H. & Wellstein, A. (2015) Circulating DNA and Micro-RNA in Patients with Pancreatic Cancer. *Pancreat Disord Ther* 5,2

24   Versteijne, E. et al. (2018) Meta-analysis comparing upfront surgery with neoadjuvant treatment in patients with resectable or borderline resectable pancreatic cancer. *Br J Surg* 105, 946-958

25   Jang, J. Y. et al. (2018) Oncological Benefits of Neoadjuvant Chemoradiation With Gemcitabine Versus Upfront Surgery in Patients With Borderline Resectable Pancreatic Cancer: A Prospective, Randomized, Open-label, Multicenter Phase 2/3 Trial. *Ann Surg* 268, 215-222

26   Liu, Q., Liao, Q. & Zhao, Y. (2017) Chemotherapy and tumor microenvironment of pancreatic cancer. *Cancer Cell Int* 17, 68

27   Plate, J. M., Plate, A. E., Shott, S., Bograd, S. & Harris, J. E. (2005) Effect of gemcitabine on immune cells in subjects with adenocarcinoma of the pancreas. *Cancer Immunol Immunother* 54, 915-925

28   Katoh, M. (2016) FGFR inhibitors: Effects on cancer cells, tumor microenvironment and whole-body homeostasis (Review). *Int J Mol Med* 38, 3-15

CHAPTER 7

Nederlandse samenvatting

Kanker bestaat uit een groot aantal cellen met een verschillende genetische en fenotypische eigenschappen. De cellen vermenigvuldigen zich snel en er komen steeds nieuwe DNA mutaties bij doordat de tumor omgeving cellen selecteert met een gunstigere set eigenschappen voor overleving. Als kanker cellen zich verspreiden over het lichaam zijn er nieuwe omgevingsfactoren waardoor er weer andere kanker cellen overleven. De diversiteit aan kanker cellen binnen een patient heet tumor heterogeniteit.

Tumor heterogeniteit is de grootste oorzaak van kanker therapie falen. In **hoofdstuk 2** hebben we een muismodel van tumor heterogeniteit ontwikkeld om de invloed van tumo heterogeniteit op therapie resistentie te bestuderen. Hiervoor hebben we klonale kanker cellijnen uit een alvleesklier tumor gegenereerd van een transgene *LSL-Kras*^G12D/+; *LSL-Trp53*^R172H/+; *P48*-Cre (KPC) muis die alvleesklier kanker ontwikkeld heeft. We hebben ontdekt dat deze klonale cellijnen in cel kweek elk een unieke set aan DNA mutaties hebben, verschillende groeisnelheden vertonen en verschillend reageren op kanker medicijnen.

De innovatie in onze studie ligt in het feit dat we de klonale cellen weer bij elkaar kunnen mengen en in de heterogene groep kunnen volgen door hun unieke DNA mutaties te meten met next generation sequencing. De klonale cellijnen reageren verschillend op een medicijn dat de belangrijke kanker-geassocieerde MEK pathway remt. Maar als de klonale cellijnen samen bij elkaar groeien, verandert de gevoeligheid van de klonale cellen voor de MEK remmer. Dit betekent dat de kanker cellen signalen met elkaar uitwisselen waardoor ze anders reageren op medicijnen. Daarom is het belangrijk dat medicijn screenings uitgevoerd worden op mengsels van verschillende kanker cellen, zodat een tumor beter word nagebootst.

Als we de klonale cellijnen gemengde tumoren laten vormen in de omgeving van fibrotisch bindweefsel en een intact immuun systeem in syngenetische muizen, vinden we dat de klonale cellijnen niet even snel groeien. Bovendien reageren de klonale cellijnen heel anders op de kanker medicijnen in vergelijking met de resultaten in celkweek. Dit betekent dat de tumoromgeving de gevoeligheid van kankercellen op medicijnen beinvloedt en we de resultaten van medicijn respons in celkweek niet goed kunnen vertalen naar de resultaten in een levend organisme.

Op immuun therapie reageren de klonale cellijnen heel verschillend, ondanks dat ze allemaal uit dezelfde ene tumor afkomstig zijn. We ontdekten dat er een klonale cellijn is die heel gevoelig is voor een anti-PD-1 medicijn en deze cellijn is ook beter in staat om T-lymphocyten te activeren in vergelijking met de andere klonale cellen. Hiervoor hebben we T-lymphocyten geisoleerd uit de blinde darmen van muizen met kanker. Wij zijn de eerste onderzoekers die hebben waargenomen dat de blinde darm van muizen met kanker

tumor-reactieve T-cellen bevat. Dit gaan wij ook onderzoeken in patienten met inoperabele alvleesklier kanker om zo betere immuun therapie opties te ontwikkelen. Samengevat kunnen we door ons muismodel belangrijke inzichten vergaren op het gebied van kanker medicijn resistentie en de effectiviteit van immuun therapie.

In **hoofdstuk 3** bestuderen wij de mutaties in circulerend DNA van patienten met alvleesklier en dikke darm kanker. Door middel van next generation sequencing van plasma DNA vergelijken we de mutaties ten tijde van de diagnose met de mutaties ten tijde van uitgezaaide ziekte. Zo kunnen we de evolutie van de kankercellen bestuderen. Bovendien hebben we de mutaties in het circulerende DNA ten tijde van de diagnose vergeleken met de mutaties in de tumor weefsels zelf. We hebben ontdekt dat slechts een deel van de tumor mutaties in het bloed gemeten konden worden. Dit kan zijn doordat in een vroeg kanker stadium de kanker mutaties in het bloed te sterk verdund zijn en dat met de huidige sequencing technieken deze nog niet meetbaar zijn. Daarnaast werden er in het bloed ook een groot percentage mutaties gemeten die in de tumor niet meetbaar waren. Dit betekent dat het kleine tumor weefsel niet voldoende de gehele kanker populatie kan representeren. Ook kan het zijn dat er al kleine uitzaaiingen elders in het lichaam aanwezig waren. Vervolgens hebben we de circulerende DNA mutaties vergeleken ten tijde van de diagnose met die van de uitgezaaide ziekte. Hieruit bleek dat er een flink percentage nieuwe mutaties zijn ontstaan en er ook sommige mutaties zijn verloren. We kunnen hieruit concluderen dat kanker constant veranderd en dat het bepalen van een behandelings strategie gebaseerd op een enkele tumor biopsie niet goed van toepassing is op uitgezaaide kanker. Bovendien weerspiegelt circulerend DNA de tumor heterogeniteit beter dan een het DNA van een weefsel biopsie.

MicroRNAs (miRs) zijn korte strengen genetisch materiaal die door cellen kunnen worden uitgescheiden om vervolgens gen expressie te beinvloeden in andere cellen. MiRs in het bloed zijn met name afkomstig van endotheel, bloed en immuun cellen. Veranderingen in hoeveelheden van circulerende miRs kunnen verstoringen in het lichaam weergeven en daarom zijn circulerende miRs goede kanker biomarker kandidaten. In **hoofdstuk 4** hebben we de circulerende miRs bestudeerd in het bloed van patienten met alvleesklier kanker voor en na operatie. Het doel van de studie was om te onderzoeken of specifieke circulerende miRs geassocieerd zijn met progressieve ziekte. Daarnaast hebben we in het KPC muismodel van alvleesklier kanker serum miRs vergeleken in muizen met voorstadium van kanker en in muizen met uitgezaaide ziekte. Het bleek dat serum miR-125b-5p en miR-99a-5p geassocieerd zijn met progressie van alvleesklier kanker in zowel muizen als patienten. Vervolgens hebben we onderzocht in welke cellen deze miRs tot expressie komen in de patienten tumoren door middel van in situ hybridizatie. We vonden dat er enkele ontstekings cellen in het bindweefsel van de tumoren zijn die deze miR-125b-5p en

miR-99a-5p tot expressie brengen. In het specifiek, zijn de miR-positieve cellen in nauw verband met B-lymfocyten zichtbaar. Uit ons onderzoek blijkt dat er specifieke circulerende miRs geassocieerd zijn met progressieve alvleesklierkanker en dat deze afkomstig zijn van immuun cellen. Nader onderzoek moet uitwijzen welke immuun cellen dit zijn en in welk stadium van activering de miR-positieve zich bevinden.

In **hoofdstuk 5** onderzochten wij of circulerende miRs de effectiviteit van een multi-kinase remmer kunnen aantonen in patienten met uitgezaaide borstkanker. Dovitinib remt zowel FGFR als VEGR, belangrijke eiwitten in de vorming van bloedvaten en tumor bindweefsel. Wij onderzochten of veraderingen in plasma miRs konden aantonen of dovitinib een effectieve remming geeft op de groei van borstkanker tumoren. Hiervoor onderzochten wij de expressie van miRs in het bloed van patienten voor en na gebruik van dovitinib. We vonden dat expressie van 6 miRs patienten konden scheiden op basis van hun respons op de therapie. Hieruit concluderen we dat circulerende miRs potentiele biomarkers zijn voor de effectiviteit van kanker medicijnen.

Deze dissertatie bevat wetenschappelijke onderbouwingen voor de implementatie van circulerende biomarker analyses in de klinische zorg van patienten met kanker. Tot op heden worden tumor weefsels gebruikt om de moleculaire eigenschappen van kanker te onderzoeken. Kanker is een dynamische, heterogene ziekte die continue verandert onder de druk van omgevingsfactoren in het tumor weefsel en anti-kanker behandelingen. Kanker cellen in uitzaaiingen bevatten andere genetische en fenotypische kenmerken dan de cellen in de primaire tumor. Om deze ziekte beter te bestuderen is het nodig om genetisch materiaal in herhaalde bloed monsters te analyzeren. Circulerend DNA kan het genetische landschap van de kankercellen in het hele lichaam bloot geven en circulerende miRs lenen zich voor het onderzoeken van de staat van het lichaam in reactie op de kanker cellen. Door middel van de bovengenoemde circulerende biomarkers kunnen we betere inzichten verkrijgen in het ontstaan van kanker progressie en in het verbeteren van therapie.

APPENDICES

Curriculum vitae auctoris

List of Publications

PhD portfolio

Acknowledgements

CURRICULUM VITAE AUCTORIS

Eveline Emma Vietsch was born on the 31st of January 1986 in Seria, Brunei. She graduated from Atheneum in Goes, the Netherlands in 2004. The same year she started medical school at the Erasmus University in Rotterdam. During her study she worked as a student assistant in the dissecting room and was a mentor for the ErasmusMC Anatomy Research Program, EARP. She performed her final clinical rotation at the Department of Clinical Pathology of the Erasmus Medical Center. For her research project under supervision of Prof. Casper van Eijck, she visited the lab of Prof. Anton Wellstein at the Lombardi Comprehensive Cancer Center at Georgetown University in Washington DC, USA for 10 months. After obtaining her medical degree in 2011, she returned to the lab of Prof. Anton Wellstein in Washington DC to work as a research fellow in molecular oncology until 2017, in close collaboration with Prof. Casper van Eijck. She returned to the Erasmus Medical Center in 2017 to continue her research in the field of pancreatic cancer.

LIST OF PUBLICATIONS

This thesis

Vietsch EE, van Eijck CH, Wellstein A. Circulating DNA and Micro-RNA in Patients with Pancreatic Cancer. *Pancreat Disord Ther. 2015 Jun;5(2). pii: 156.*

Rapisuwon S, **Vietsch EE**, Wellstein A. Circulating biomarkers to monitor cancer progression and treatment. *Comput Struct Biotechnol J. 2016 Jun 1;14:211-22.*

Shivapurkar N *, **Vietsch EE** *, Carney E, Isaacs C, Wellstein A.Circulating microRNAs in patients with hormone receptor-positive metastatic breast cancer treated with dovitinib. *Clin Transl Med. 2017 Oct 4;6(1):37.* * **The authors contributed equally to this work**

Vietsch EE, Graham GT, McCutcheon JN, Javaid A, Giaccone G, Marshall JL, Wellstein A. Circulating cell-free DNA mutation patterns in early and late stage colon and pancreatic cancer *Cancer Genet. 2017 Dec;218-219:39-50.*

Vietsch EE, Martinez Roth S, Simmons JK, Javaid A, Park MD, Stenstra MHBC, McCutcheon JN, Berens EB, Peran P, Moussa M, Catalfamo M, Mock BA, Giaccone G, Schmidt MO, Riegel AT, Wellstein A. Impact of drug therapy and the immune system on intratumoral subpopulations in a pancreatic cancer model. Impact of drug therapy and the immune system on intratumoral subpopulations in a pancreatic cancer model. *Submitted*

Vietsch EE, Peran I, Suker M, van den Bosch TPP, Kros JM, Wellstein A and Van Eijck CHJ. Circulating miR-125b-5p and miR-99a-5p are associated with pancreatic cancer progression in patients after surgery. *Submitted*

Other publications

Zhang W, Nandakumar N, Shi Y, Manzano M, Smith A, Graham G, Gupta S, **Vietsch EE**, Laughlin SZ, Wadhwa M, Chetram M, Joshi M, Wang F, Kallakury B, Toretsky J, Wellstein A, Yi C. Downstream of mutant KRAS, the transcription regulator YAP is essential for neoplastic progression to pancreatic ductal adenocarcinoma. *Sci Signal. 2014 May 6;7(324):ra42.*

Rodriguez OC, Choudhury S, Kolukula V, **Vietsch EE**, Catania J, Preet A, Reynoso K, Bargonetti J, Wellstein A, Albanese C, Avantaggiati ML. Dietary downregulation of mutant p53 levels via glucose restriction: mechanisms and implications for tumor therapy. *Cell Cycle. 2012 Dec 1;11(23):4436-46.*

PHD PORTFOLIO

Name PhD student	Eveline Emma Vietsch, MD
Erasmus MC Department	Surgery
Promotors	Prof. Dr. C.H.J. van Eijck
	Prof. Dr. A. Wellstein

Courses

Scientific Paper Writing Class at Georgetown University	2012
Animal Care and Use in Research Education trainings from the Institutional Animal Care and Use Committee (IACUC) Georgetown University	2012
Environment and Health trainings in Lab, biological and fire safety, Blood borne pathogens, basic radiation safety at Georgetown University	2012
Signal Transduction Journal Club Presentations, at the weekly Tumor Biology Journal Club at Georgetown University	2012-2017
Research Data Meeting Presentations, weekly at Georgetown University	2012-2017
Weekly Seminar Series with top-tier visiting international cancer scientists presenting their research at Georgetown University	2012-2017

Oral Presentations

De-convoluting therapeutic resistance in a pancreatic cancer model: Pharmacogenomic evaluation of intratumoral clonal heterogeneity. At the International Targeted Anticancer Therapies (TAT) Congress, Washington DC, USA.	2014
Intratumoral heterogeneity in a mutant KRAS driven pancreatic cancer model: Relevance of clonal dynamics in drug response. At the RAS Initiative Symposium, Frederick, MD, USA.	2016
MicroRNA analysis in liquid biopsies. At the Circulating Biomarkers World Congress, Boston, MA, USA.	2016
Circulating cell-free DNA mutation patterns in early and late stage colon	2018

and pancreatic cancer. At the Arts-Assistenten Vereniging (AAV) Wetenschapsmiddag, Erasmus MC, Rotterdam, the Netherlands.

Circulating microRNAs as treatment response markers of surgery and FOLFIRINOX in patients with pancreatic cancer. At the Pancreas Club Meeting, Washington, DC, USA.   2018

Poster presentations

De-convoluting therapeutic resistance in a pancreatic cancer model: Pharmacogenomic evaluation of intratumoral clonal heterogeneity. At the AACR Pancreatic Cancer Conference Innovations in Research and Treatment, New Orleans, LA, USA   2014

Circulating MicroRNAs as response indicators for the treatment of patients with pancreatic cancer. At The Pancreas Club Annual Meeting, Washington DC, USA   2015

Impact of intratumoral clonal heterogeneity on checkpoint inhibitor response. At The Society for Immunotherapy of Cancer (SITC) Annual Meeting, National Harbor, MD, USA   2016

Circulating MicroRNAs as response indicators for the treatment of patients with pancreato-biliary cancer. At The National Cancer Institute (NCI) Symposium of RNA Biology, Bethesda, MD, USA   2017

Teaching

Mentored and trained a medical student from the Erasmus MC in the lab at Georgetown University   2013-2014

Mentored and trained medical student from the Erasmus MC in the lab at Georgetown University   2014-2015

Mentored and trained a Pre-Med Undergraduate student in the lab at Georgetown University   2014-2017

Mentored and trained a Tumor Biology PhD student in the lab at Georgetown University   2014

Mentored and trained a Tumor Biology PhD student in the lab   2016-2017
at Georgetown University

Mentored and trained oncology master student from the Dutch   2016-2017
Cancer Institute (NKI) in the lab at Georgetown University

Examiner of the Basic Life Support course for medical students at the   2018
Erasmus MC

Teaching assistant for: Pathology: diagnosis and staging   2018
of cancer course for medical students at the Erasmus MC

Awards
Research Grant from the Lisa Waller Hayes Foundation, the Netherlands   2012-2013
Topic: Serum microRNA response pattern in treatment of pancreatic cancers

Research Grant from The Ruesch Center for the Cure of   2016-2017
Gastrointestinal Cancers, USA. Topic: Assessment of the mutation
patterns of colon and pancreatic cancers from the analysis of
circulating, cell-free tumor DNA.

Erasmus Trustfonds Travel Grant to for the attendance of the Pancreas   2018
Club Meeting in Washington DC, USA

ACKNOWLEDGEMENTS